A DIAGNOSTIC ANALYSIS OF THE 30 MAY 1967 SQUALL LINE IN CENTRAL OKLAHOMA

by

Randy J. Coleman

United States
Naval Postgraduate School

THESIS

A DIAGNOSTIC ANALYSIS OF THE 30 MAY 1967
SQUALL LINE IN CENTRAL OKLAHOMA

by

Randy J. Coleman

October 1969

A Diagnostic Analysis of the 30 May 1967 Squall Line in Central Oklahoma

by

Randy J. Coleman
Lieutenant, United States Navy
B.S., Texas A&M University, 1964

Submitted in partial fulfillment of
requirements for the degree of

MASTER OF SCIENCE IN METEOROLOGY

from the

NAVAL POSTGRADUATE SCHOOL
October 1969

ABSTRACT

A squall line is investigated during a 3-hour period of its mature life. Upper air data from the mesonetwork in Oklahoma at 1700, 1830, and 2000 GMT is used to determine vorticity, divergence, and vertical motion at 50 mb intervals. These and other fields are computed and investigated in detail, and possible problems associated with them are discussed. Two methods of computing vertical motion are described in detail.

A mesoscale wave with a wavelength of approximately 90 n.m. is found at 700 mb. It moves faster than the wind at 700 mb but slower than the squall line. This wave is investigated in detail and is hypothesized to be the cause and the terminator of the squall line.

The kinematic vertical motion technique presented appears to give realistic fields. Appendix B describes the problems found in the vorticity method and how it can be used on the synoptic scale.

TABLE OF CONTENTS

LIST OF TABLES

LIST OF FIGURES

TABLE OF SYMBOLS AND ABBREVIATIONS

c_p	Specific heat at constant pressure
$\overline{D}^{w}$	Vertically averaged isobaric divergence
f	Coriolis parameter
GMT	Greenwich Meridian time
h	Heat per unit mass
K_s	Curvature of streamline
p	Pressure in millibars
P	Potential vorticity
q	Specific humidity
S.I.	Showalter Index
T	Temperature
u	Component of $\mathbb{V}$ in y direction $\left(\frac{dy}{dt}\right)$
v	Component of $\mathbb{V}$ in x direction $\left(\frac{dx}{dt}\right)$
V_s	Velocity component along a streamline
$\mathbb{V}$	Horizontal wind velocity
w	Vertical component of wind (x, y, z, t) system = $\frac{dz}{dt}$
α	Specific volume
γ	Lapse rate = $-\frac{\partial T}{\partial z}$
γ_d	Dry adiabatic lapse rate = $\frac{g}{c_p}$
$(\gamma_d - \gamma)$	Proportional to static stability
ζ_a	Vertical component of the absolute vorticity: referred to as "absolute vorticity"
ζ_r	Vertical component of the relative vorticity: referred to as "relative vorticity"

θ	Potential temperature
$\left(-\frac{\partial\theta}{\partial p}\right)$	Static stability
ω	Vertical component of wind (x, y, p, t) system = $\frac{dp}{dt}$
∇_p	Del operator in pressure coordinates
$\nabla\cdot W$	Velocity divergence

ACKNOWLEDGEMENTS

The author wishes to express his appreciation to his main advisor, Dr. J. D. Mahlman, for his considerable technical assistance, and his moral support during the "black days" of this thesis. His extra efforts, in such things as working with the vorticity method on the synoptic scale, are greatly appreciated.

Thanks is also expressed to Dr. R. L. Alberty for his initial efforts in making possible this study and supplying the necessary data, his availability and help throughout, and his comments and suggestions as second reader.

Appreciation is expressed to the National Severe Storms Laboratory (NSSL) for providing the data in computerized format, to the Computer Facility at the U. S. Naval Postgraduate School for providing free computer time and programming assistance, and to Messrs. K. J. Roberts, M. B. McDermet, and P. R. Adler of the Meteorology Department for their help in producing the figures.

To the one person without whose typing and moral support this study might have never obtained fruitful completion, my wife, I am forever indebted.

I. INTRODUCTION

The severe convective storm, which produces death and destruction in the form of tornadoes, hail, and violent winds, has plagued man since the beginning of time. With the advance of the science of meteorology in the last century, man has attempted to increase his knowledge of these interesting yet deadly storms. House (1963) has stated that attempts were being made as early as the 1880's to anticipate the development of such storms. However, most of the work on the possible causes and structure of these phenomena has been done, as has most of the advances in meteorology, in the last twenty-five years.

To date a considerable gap remains in man's understanding of the severe storm. A major problem has been his inability to measure the atmospheric parameters such as wind and temperature on the scale necessary to represent the severe storm. Within the last decade significant progress has been made with the introduction of observations on the scale of these phenomena. This is the scale of motion (10 to 500 km) in which convective storms appear.

The studies that have been made to date are at times contradictory, yet they all add to our general knowledge. Carlson and Ludlum (1968) point out that either a band of strong wind in the middle troposphere or strong vertical wind shear is necessary for the development of severe convective storms. Also, Koscielski (1965) found that the lack of an upper level jet was generally associated with no activity or less intense activity than that associated with such a jet. However, Byers and Braham (1949) in the report of the Thunderstorm Project

in Florida and lately Asai (1964) have determined that the presence of vertical wind shear acts as a deterrent to convective growth of the "air mass" variety.

Newton (1966) has noted this different effect on severe storms and "air mass" cells, and proposes that the conflicting area is the intermediate zone where the two possibly intermingle or overlap.

Takedo (1965) studied downdrafts and updrafts in storms. He noted that vertical wind shear seems to organize the release of energy in a convective system. When significant vertical wind shear was present, stronger upcurrents formed in front of the convective region than when they were absent. He indicates that vertical wind shear is very important for continuation of the system if the lower layer of the troposphere is very stable. Therefore, he concludes that vertical wind shear is necessary for continuance of a squall-type system.

Newton (1966) and Alberty (1969) both note that the disposal of warm air in upper levels through the action of anvil blow-off, caused by vertical shear, is an important revitalizing mechanism of the severe storm. Alberty (1969) points out that although the strong vertical shear would be expected to force the convective system to lean in a down shear direction, the strong shear simultaneously yields an effect that enhances vertical motion near the strong updraft core. This increased vertical motion tends to overpower any leaning in the down shear direction since the environmental flow has less time to impart its horizontal momentum upon the vertically moving air parcels.

Senshu (1961), in a study of a mesoscale disturbance in western Japan in 1955, proposed that the initial activity is caused by strong

convergence in the lower levels causing an upward current. Condensation aloft causes precipitation which falls, because of the rapidly moving system, slightly behind the convergence maximum. Some rain evaporates as it falls, cooling the air and causing the downdraft and a mesohigh to form. This increases the wind, and the local time change of wind velocity balances with the large pressure gradients preceding the system. This wind system then maintains the strong convergence in front of the high cell, thus maintaining the moving system. This mesoscale disturbance studied by Senshu (1961) moved at a speed of 45 kts.

Much of the work done in the United States on mesoscale systems can be attributed to T. Fujita of the University of Chicago. Fujita (1955) made a detailed study of two systems of squall lines in the central United States. Since only synoptic data was available in the area, Fujita developed a technique for converting time cross sections to space cross sections. By assuming that the local change of an element is small over an interval of an hour (using barograph traces, etc.), time sections were converted to space sections. This technique made available a much more detailed data network over the area covered by only synoptic-scale reports. Only surface data is used by Fujita. The assumption that the local change of an element is negligible over an hourly interval is reasonable in the middle and upper troposphere for synoptic-scale motions, but it seems somewhat debatable near the surface for sub-synoptic motions. Nevertheless, the scheme used by Fujita would seem to be a relatively good approach in areas where no other data is available. This directly points out the need for meso-scale networks, as noted by Fujita (1955, 1957). Fujita (1955) found

large surface divergences of 10 to 60 x 10^{-5} sec^{-1} over areas from 100 to 10,000 square miles in the vicinity of the squalls. He found that the storms develop as a small mesohigh and dissipate as a meso-depression after going through five stages. The movement of the squall lines was associated with a "pressure-surge" line, caused by the mesohigh. However, in one case, he noted that the system was initiated before a pressure-surge line was formed, suggesting the futility of seeking a "trigger" mechanism in the surface pressure field at the initial stage. A similar study by Fujita and Brown (1958) again noted the mesosystem and its associated convective cells and stressed the above technique for tracking it (when a mesonetwork is not available), fortified by a dense raingauge network and continuous radar pictures. Fujita (1957) noted the direct relationship between mesosystems of 10 to 100 miles in size to severe storms, and proposed that similar features are found in other parts of the world, particularly in Japan.

Considerable work has been done in Japan in recent years on mesoscale disturbances, some of which has already been mentioned. Matsumoto (1967) and Matsumoto et al (1967a, b) have worked with data obtained from the surface mesonetwork set up in Japan for the Japanese Heavy Snow Storm Project. The results of these studies will be noted in more detail later, but they indicated that squall lines and severe convective activity in general are initiated and controlled by the surface area of convergence. This same conclusion is found by Doroshenko (1960). However, he indicates that this convergence may be caused by a trough or other causes; therefore, it is still unclear if this surface convergence is the cause of the squall formation, only one

of a series of events triggered by the cause of the squall line, or possibly even a direct effect of the squall line itself.

The possibility of quasi-stationary mesoscale waves of wavelength 500 to 600 km setting off squall activity in the central United States has been proposed by Dirks, Mahlman, and Reiter (1967). They assumed constant static stability and vertical wind shear over the area and found that a stationary wave of varying wavelength (dependent on several factors) could be postulated which would account for the seasonal maximum of squall line formations which are initiated three-fourths of a wavelength downstream from the ridge over the Rocky Mountains. Considerable use was made of satellite pictures in this study to fill in the gaps left by the synoptic upper air network and special pilot balloon observations in the area. A major recommendation of this study was again the call for an operational upper air mesonetwork so that the possibility of such mesoscale waves might further be investigated. Because of the great expense of such a network, very few will likely be made available in the United States or elsewhere for years to come.

An experiment by Tepper (1959) showed the importance of mesoscale data. Using nine experienced Weather Bureau forecasters, three were given good surface mesoanalyses and the other six provided the regular analyses available at regional forecast centers. The three given mesoanalyses completely outperformed the other six in all phases of the forecast. So, it was evident that a definite increase in forecasting ability and understanding the weather would result if a sufficiently dense and financially practical surface mesonetwork could be employed. Such a network (called a Beta network) was set

up in central Oklahoma in the spring of 1960 by the National Severe Storms Project (NSSP). It was used in the spring of 1960 and 1961 by the NSSP staff (1961) to gather data on severe storms and their environment. This Beta network contained 36 stations 10 to 15 miles apart. A similar network was used in Japan in conjunction with the Japanese Heavy Snow Storm Project previously mentioned. Since no upper air mesonetwork existed in the area, aircraft were used in an effort to determine the middle and upper features of the severe weather which occurred. Computations from the data recorded by the aircraft indicated an area of convergence of magnitude 15×10^{-5} sec^{-1} near 800 mb in the vicinity of the activity. Again, because of the lack of conventional upper air data throughout the area and the problems associated with aircraft reconnaissance, it was strongly recommended that a mesonetwork of upper air stations be formed in the area.

Because 1) central Oklahoma is a hotbed for convective activity, 2) the Beta surface network was already established there, and 3) of the previously stated numerous appeals for an upper air mesonetwork somewhere in the United States, the National Severe Storms Laboratory (NSSL) of ESSA initiated a program of mesoscale upper air soundings in 1966 covering the south central Oklahoma area. This network consisted of nine upper air stations operating in the spring and early summer (maximum severe weather) which were to take soundings every one-and-a-half hours beginning at 1700 GMT on days when severe weather was expected (see Fig. 1). These stations are approximately 40 to 50 n.m. apart. It was hoped that this data, combined with the Beta surface network and radar pictures from the WSR-57 radar located at Norman,

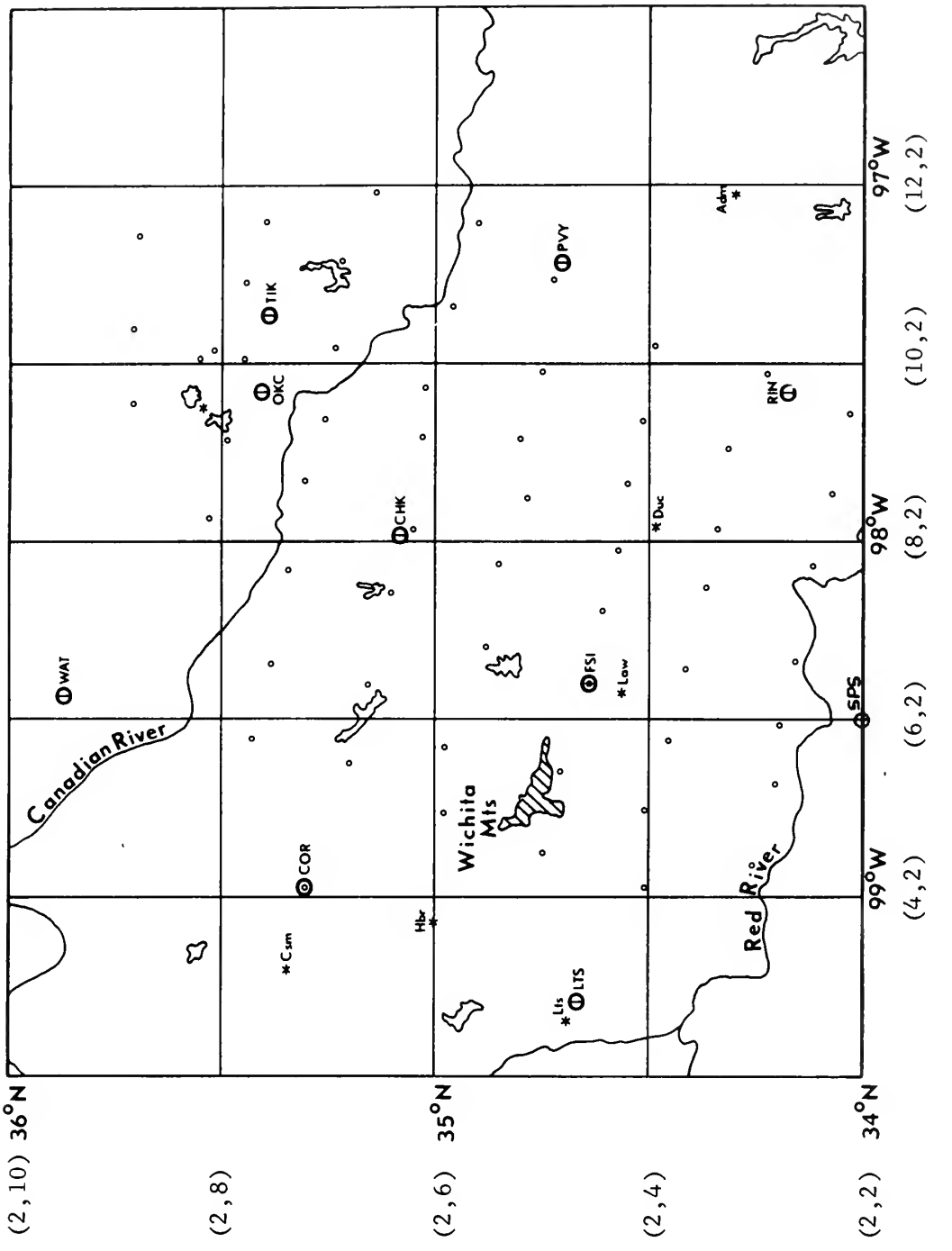

FIG. 1. NSSL mesoscale area and networks.

- Rawinsonde network (except OKC which is the only synoptic rawinsonde station in the area).
- Surface network.
- Lakes.

Oklahoma, would open new doors in the study of severe storms and their interactions with the environment.

Considerable use of the data obtained on 28 May 1967 by this network (a case of isolated activity) has been made, most notably by J. C. Fankhauser (1968, 1969) of the National Center for Atmospheric Research (NCAR). He investigated the thunderstorm which occurred that day using five consecutive sets of soundings covering the lifetime of the storm, and described it using divergence, vertical motion, and other computed parameters. He finds in general that the resultant picture of the storm area using the above parameters shows strong surface convergence and upward motion aloft (average of 72 mb hr^{-1} in the vicinity of the storm). His figures indicate a strong convergence region near 500 mb which is of great interest, but he does not postulate any ideas as to the cause or significance of this occurrence. His research shows that although the sounding system alone is not complete enough to make possible an intense study of singular thunderstorm dynamics, it does provide a reliable framework within which the possible cause and effect of thunderstorm systems can be studied.

With the above conclusion in mind, this study was initiated using the data obtained by the NSSL mesonetwork on 30 May 1967. On this day an active squall line and numerous other cells occurred within the area. In order to obtain as much detail as possible, a 13 x 11 grid was used for obtaining data used in computations. This grid covers the area from $96^{\circ}45'$ to $99^{\circ}45'$ West and from $33^{\circ}45'$ to $36^{\circ}15'$ North, cutting grid sections of 15' of longitude and 15' of latitude, and encompassing the mesonetwork. Fig. 1 shows the majority of the grid area (the boundary points are dropped as they are lost in most of the

differencing schemes used in making computations). Wichita Falls (SPS) is noted in Fig. 1 but not noted in proceeding figures; however, SPS data is used at all times unless otherwise noted. Grid points (I, J) are referenced in later sections and are shown in part in Fig. 1.

The objectives of this study are as follows:

(1) describe the convective system and its relation to the mesoscale environment,

(2) develop a method for obtaining the vertical motion field,

(3) seek an explanation for the squall line which occurs during the period.

It is necessary to be able to fulfill the above requirements in this and similar cases in order to understand the development and life cycle of destructive severe storms.

II. GENERAL SYNOPTIC SITUATION AND INDICATION OF SEVERE WEATHER PRODUCTION

Since more information has been compiled on the synoptic scale concerning conditions necessary for severe weather production than on the mesoscale, it seems appropriate to look at the general synoptic situation present in the central United States on 30 May 1967. The times of interest here are centered around 1830 GMT (1230 CST), but since complete soundings on the synoptic scale are taken only twice daily at 0000 GMT and 1200 GMT, the general picture at 1200 GMT will provide a preview of the conditions associated with the mesosystem which developed later in the mesonetwork area.

Synoptic conditions necessary for the occurrence of severe weather have been noted by many authors. However, these vary and many are only general in nature. The Weather Bureau is presently in the process of publishing a new guideline for severe weather criteria. The general criteria used by the Weather Bureau were noted in an unpublished study by Koscielski (1965). He found that severe weather generally occurs when the following parameters are relatively strong: instability, 500 mb positive vorticity advection, upper jet, low level moisture, and 850 mb temperature and moisture advection. Endlich and Mancuso (1968), using a computer objective analysis technique, have proposed that a combination of the above synoptic indicators and numerous kinematic quantities available through computer use by dynamical techniques will improve synoptic severe weather forecasting. But much work has yet to be done here. Probably the simpliest and best summary of severe weather indicators to date is that made by Dirks

(1969). He has noted that synoptic-scale upper level divergence and lower level convergence are sometimes associated with severe weather, however, such occurrences are not frequent enough to account for the general formation of mesoscale convective systems. He lists the following as conditions for the production of severe weather:

(1) a warm, moist tongue at low levels;

(2) general convective instability (S.I. $\leq$ 4);

(3) possible presence of an upper level short wave;

(4) a low and/or upper level jet;

(5) cold air advection aloft;

(6) mid-tropospheric stable layer;

(7) a cold or "dry front" is often present.

Fig. 2 indicates the synoptic conditions prevalent in the central United States in the early morning hours on 30 May 1967. Fig. 2a shows that a cold front dipped southward into Oklahoma and Texas from a wave in east central Kansas and then trailed off northwestward as a stationary front. A "dry front", or Marfa front as it is often called, was located in far west Texas and eastern New Mexico. Southerly flow is indicated across east and central Texas converging into the mesonetwork area. A dying squall line is present just southeast of the mesonetwork over north central Texas, indicating the instability over the area of the previous night and evening. Fig. 2b shows the surface conditions at 1800 GMT. Fig. 2c shows the frontal configuration at 850 mb. Considerable thermal gradient is indicated behind the front in central Kansas. A warm, moist tongue is evident from west and south Texas across the mesonetwork to Kansas. The small cool pocket over north central Texas appears a direct result of the decaying squall line

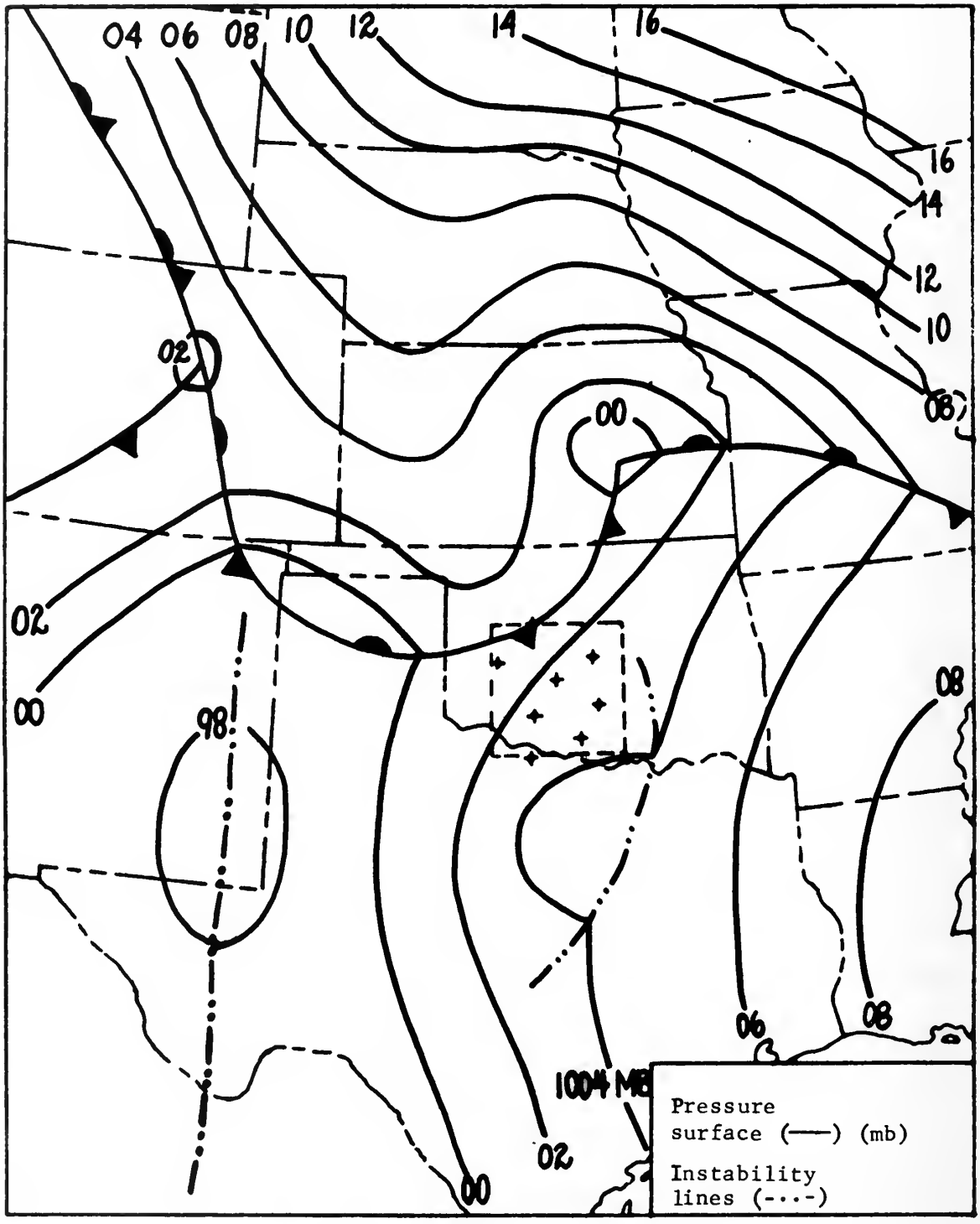

FIG. 2a. Surface analysis for 1200 GMT on 30 May 1967 with fronts and instability lines. Mesonetwork is small square in Oklahoma.

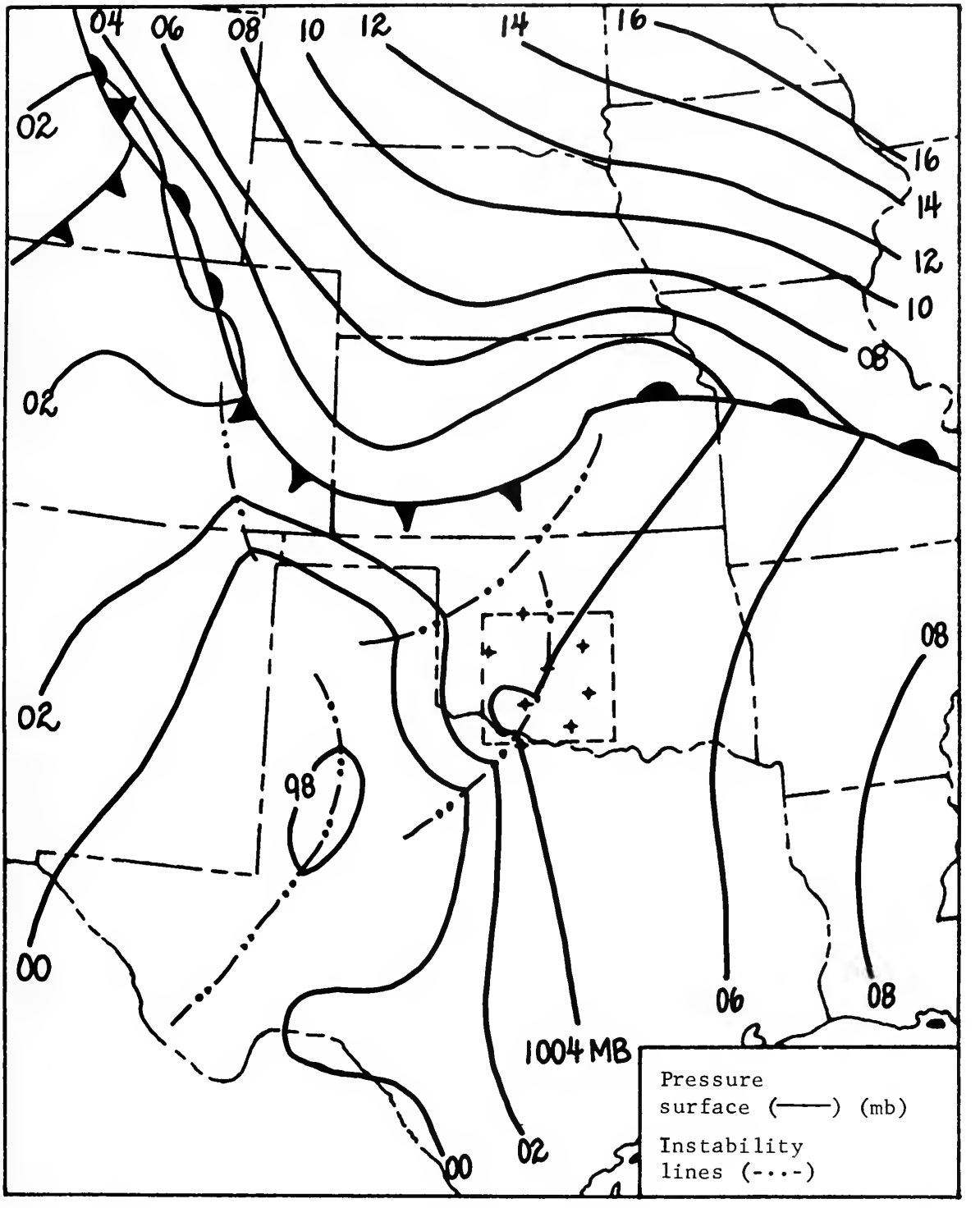

FIG. 2b. Surface analysis for 1800 GMT on 30 May 1967 with fronts and instability lines.

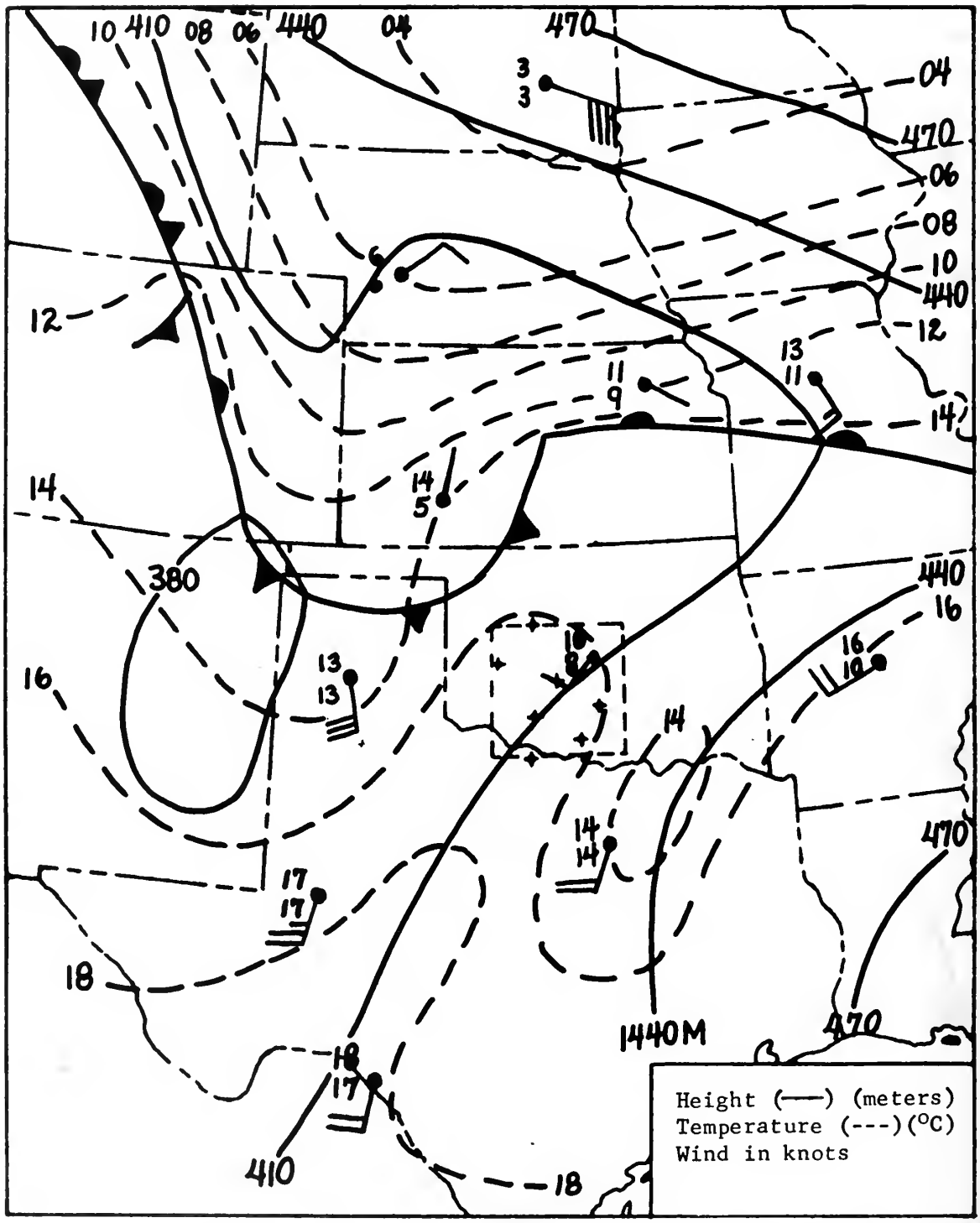

FIG. 2c. 850 mb height and temperature analysis for 1200 GMT on 30 May 1967 with fronts and dewpoints (°C).

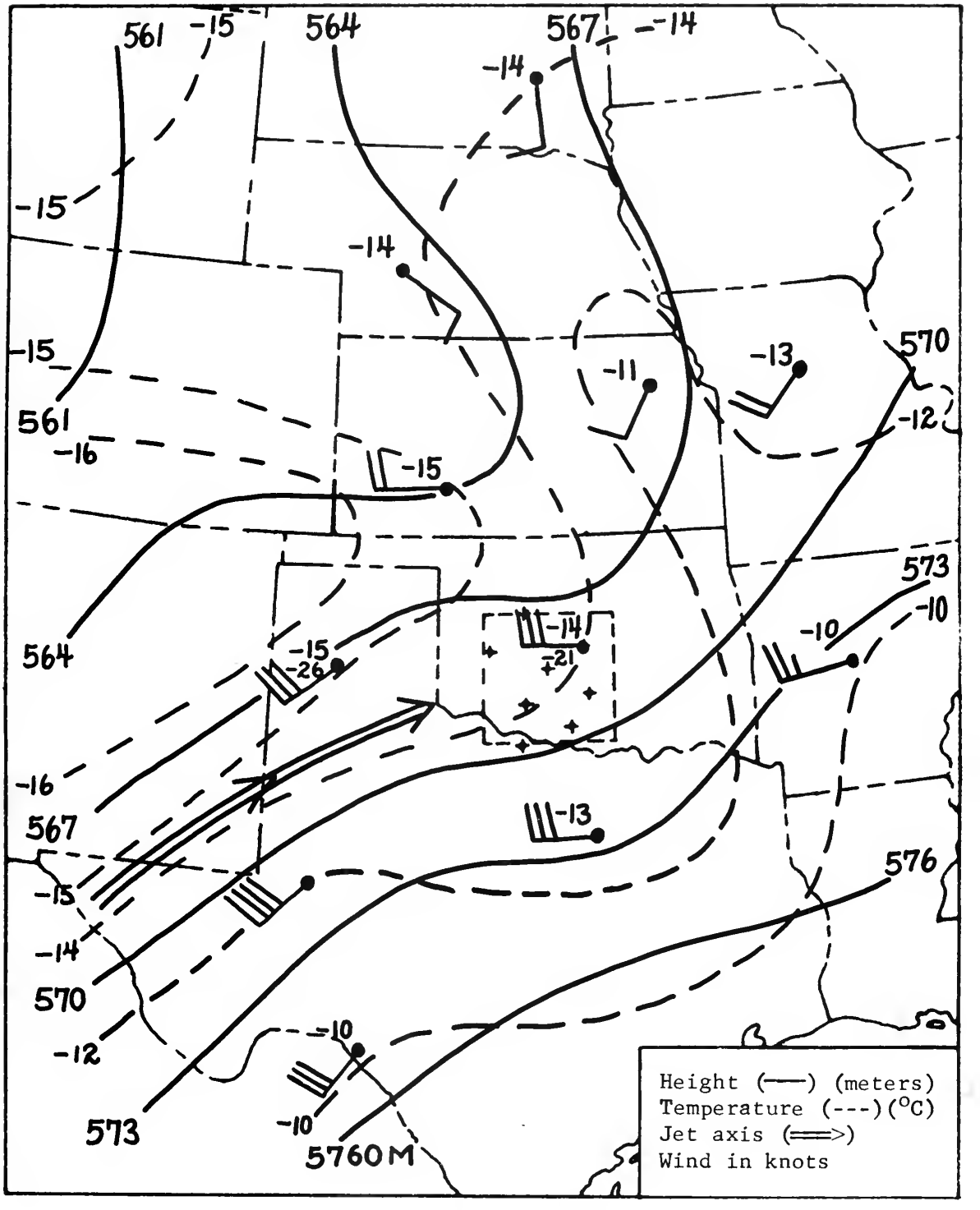

FIG. 2d. 500 mb height and temperature analysis for 1200 GMT on 30 May 1967 with jet axis.

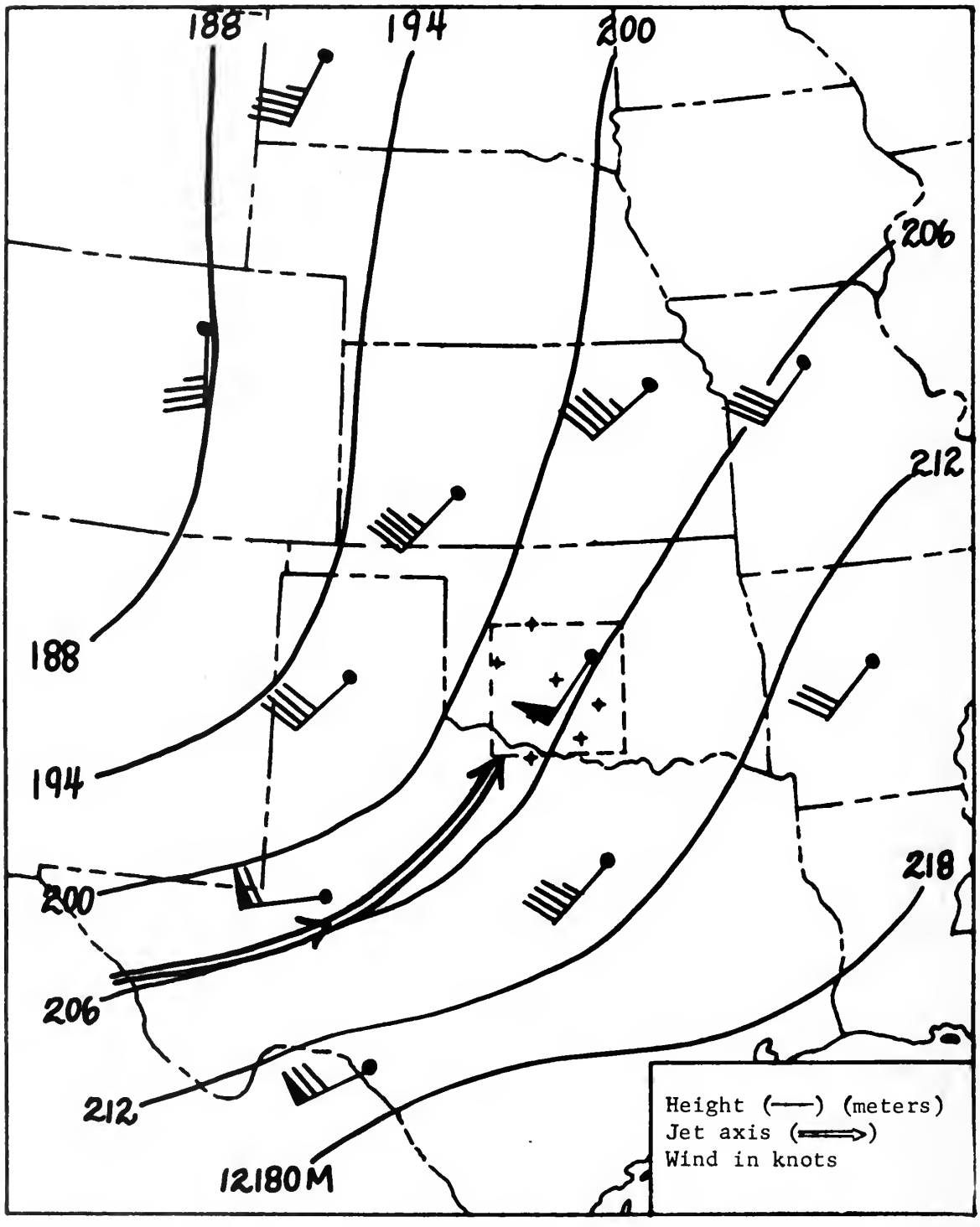

FIG. 2e. 200 mb height analysis for 1200 GMT on 30 May 1967 with jet axis.

there. Also, both Amarillo and Midland, reporting 30 and 25 knot winds respectively, indicate a moderate wind maximum over the eastern Texas Panhandle and possible western Oklahoma, between the depression in eastern New Mexico and the warm ridge to the east.

Fig. 2d shows a short wave trough at 500 mb with a wavelength of approximately 600 n.m. extending from northwest Kansas to northeast Texas. The double shafted arrow extending northeastward over the high plains of Texas represents the jet stream. Also notice the cold advection occurring over Oklahoma.

Finally, Fig. 2e shows the same short wave trough at 200 mb located over Texas, indicating a well developed trough. The double shafted arrow again represents the jet stream with an apparent moderate maximum of 65 or 70 knots.

Cold advection at 500 mb (Fig. 2d) over warm advection at 850 mb (Fig. 2c) indicates decreasing stability. To gain an understanding of whether or not this is significant, write the first law of thermodynamics in the form

$$\frac{1}{c_p}\frac{dh}{dt} = \frac{dT}{dt} - \frac{\alpha\omega}{c_p}.$$

Expanding and rearranging the above gives

$$\frac{\partial T}{\partial t} = \frac{1}{c_p}\frac{dh}{dt} + \frac{\alpha\omega}{c_p} - \mathbb{V}\cdot\nabla_p T - \omega\frac{\partial T}{\partial p}.$$

Taking $\frac{\partial}{\partial z}$ of the above and interchanging the derivatives on the left side gives

$$\frac{\partial}{\partial t}\left(\frac{\partial T}{\partial z}\right) = \frac{\partial}{\partial z}\left(\frac{1}{c_p}\frac{dh}{dt}\right) + \frac{\partial}{\partial z}\left(\frac{\alpha\omega}{c_p}\right) - \frac{\partial}{\partial z}\left(\mathbb{V}\cdot\nabla_p T\right) - \frac{\partial}{\partial z}\left(\omega\frac{\partial T}{\partial p}\right).$$

(1) (2) (3) (4) (5)

To determine the effects of advection on stability, analyze how (4) affects (1). For simplicity, measure $\mathbb{W}\cdot\nabla_p T$ along a streamline (natural coordinates) over the mesonetwork area at 850 mb (Fig. 2c) and subtract the value found at 500 mb (Fig. 2d) to get an estimate of the rate of change of stability over the mesonetwork area previous to the outbreak of squall line activity.

Fig. 2c indicates a maximum of 10 knots diagonally across the area and a temperature gradient of $-2^{o}C/150$ n.m. Fig. 2d indicates a wind of 30 knots and a temperature gradient of $+1.5^{o}C/100$ n.m. Using these values one obtains a rate of change of stability (or an increase in lapse rate) of $\frac{\partial}{\partial t}\left(\frac{\partial T}{\partial z}\right) \approx -\ 0.2^{o}C\ km^{-1}\ hr^{-1}$ over the layer 850 to 500 mb. OKC (only synoptic station in mesonetwork area on Figs. 2c and 2d) shows approximately a standard atmospheric lapse rate at 1200 GMT (0600 CST). Therefore, as the day progresses, slow destabilization takes place on the synoptic scale over the area, due to differential temperature advection alone. This would indicate a probable drop of $-0.5^{o}C\ km^{-1}\ hr^{-1}$ or slightly more as low level solar heating adds to the advective destabilization. However, this destabilization on the synoptic scale seems rather weak and, by itself, would seem to indicate possibly only weak showers.

From Figs. 2a, 2c, 2d, and 2e it is apparent that most of the conditions necessary for severe weather development indicated previously are present over the mesonetwork area at 1200 GMT. By 1600 GMT, a squall line was developing over the western part of the mesonetwork, and considerable instability was present on the synoptic scale by 1800 GMT as is shown in Fig. 2b.

III. DATA AND ANALYSIS PROBLEMS

Data has been taken for three time periods (1700, 1830, and 2000 GMT) from the NSSL mesonetwork in Oklahoma for 30 May 1967. The data was plotted (wind only) and analyzed (both for streamlines and isotachs) for 17 levels in the vertical (surface to 150 mb at 50 mb intervals). Only the winds are used for calculations in this study. Clark (1969) and Van Sickle (1969) have indicated that wind information is the most accurate data returned by the radiosonde for use in mesoscale studies. These winds have been smoothed by a (1, 2, 1) process over a 600 meter vertical layer in order to make them even more representative. Analysis on the mesoscale presents some problems which must be tackled with other than conventional synoptic thinking, as has been shown in detail by Fujita (1963). Basically, of course, time and space continuity is maintained to a good extent; however, at 50 mb intervals the exact analysis of the transition zones between low level systems and the general upper level jet flow are open to question and any of several answers may apply. However, even though analysis might be easier, a true picture of the atmospheric motion present during the period, complex as it is, would probably be obscured if more than a 50 mb increment was used. Time continuity was almost impossible in the low levels, even though only a seemingly small 90 minute interval occurs between soundings. It appears that mesoscale features in the low levels can change considerably within this time period, as indicated by Fujita (1963).

Surface data used for the three hour period (1700 - 2000 GMT) was obtained from the Beta network explained in Section I. Surface pressure tendency and rainfall were analyzed for 1-1/2 hour intervals. All radar presentations used in the study are from the WSR-57 radar at Norman, Oklahoma. All presentations utilized are at 0^{o} elevation. Unfortunately, the Sensitivity Time Control (STC) component was in use at all times because of ground return, so no return is available within 25 n.m. of Norman. This is a drawback, especially at 1830 GMT, when it is apparent that cells are present in this area.

All of the preceding analyses were done using the data from the NSSL computer output. The data was plotted on station and considered to be representative of the time of the sounding. As noted by Fankhauser (1969), the displacement of the balloon with altitude from the launch station, time lag of the different pressure levels from launch time, varying launch times, and differing ascent rates may all present problems on the mesoscale. A detailed investigation into these four possible problems showed that the latter two were not fundamental difficulties because of the close adherance to the rules set up for this mesoscale network. The former two were found to produce problems only under a very few critical situations. Appendix A describes in detail the investigation made. In general, it was determined that the data could be used in the conventional, synoptic manner, but corrections were made in the few critical situations mentioned.

IV. DESCRIPTION OF VORTICITY, DIVERGENCE, AND VERTICAL MOTION CALCULATIONS

A. VORTICITY AND DIVERGENCE

In order to best represent the mesoscale environment in southwestern Oklahoma on 30 May 1967, the patterns of relative vorticity and divergence, which are well understood and described on the synoptic scale but much less understood or described on the mesoscale, were deemed necessary quantities.

The definition of relative vorticity is

$$\zeta_r \equiv \frac{\partial v}{\partial x} - \frac{\partial u}{\partial y},$$

with all indicated differentiations to be performed on a surface of constant pressure.

Relative vorticity was determined using a centered difference scheme. Non-centered differencing was used at the boundaries. Absolute vorticity was also calculated.

The definition of divergence is

$$DIV = \nabla \cdot \mathbf{V} \equiv \frac{\partial u}{\partial x} + \frac{\partial v}{\partial y}.$$

Both relative vorticity and divergence fields were smoothed in the vertical by a .2-.6-.2 smoother, and in the horizontal by a Laplacian .15-.15-.4-.15-.15 smoother.

B. DESCRIPTIONS OF POSSIBLE VERTICAL MOTION SCHEMES

The determination of reliable vertical motions in the atmosphere is of fundamental importance in a number of meteorological problems. Because there is no generally accurate method of computing vertical

motion, no method can be tested completely. However, qualitative methods such as comparing computed vertical motions to radar pictures, rainfall records, and local pressure change fields can give acceptable verification to a system. Also, such principles as conservation of potential vorticity can be used for verification purposes. It therefore is possible to verify areas of upward motion where precipitation occurs to some degree of success, but areas of downward motion are difficult if not impossible to substantiate. However, the upward motion areas are the weather producing areas, and therefore one can conscientiously concentrate on obtaining accuracy in these regions.

Many techniques and methods have been developed and used on the synoptic scale. Ballenzweig (1955) reviewed many of these, noting that they can generally be broken down into three categories: adiabatic, kinematic, and vorticity methods. All have their disadvantages and advantages, but particular ones seem more suited for use on the mesoscale.

Panofsky et al (1959) compared several methods of determining vertical motions on the synoptic scale and concluded that the kinematic and omega equation techniques were best. However, a necessary condition for the validity of any omega equation method is that the balance equation be valid, and it is only valid if the Rossby number (R_o) is less than 1. Using appropriate mesoscale motions such as $V \sim 20$ m sec^{-1}, $f \sim 10^{-4}$ sec^{-1}, and L (wavelength) $\sim$ 100 km = 10^5 meters, one sees that

$$R_o \equiv \frac{V}{fL} = 2.$$

Therefore, the balance equation is not valid, so no omega equation method is valid on the mesoscale.

The use of an adiabatic or thermal equation technique would appear less desirable because 1) of the frequently observed weak thermal gradients on the mesoscale, 2) most of these techniques give time averaged vertical motions whereas instantaneous values would be of greater interest for mesoscale studies, and 3) in general, the mass field is difficult to measure accurately on this scale of motion. Van Sickle (1969) used this type of technique and noted that the problems associated with such an approach made it undesirable.

The above critiques lead to an initial choice of a kinematic type technique. But it is desirable to have two methods for computing vertical motion for cross checking. The previously indicated reliability of wind data and the inapplicability of other techniques lead to a choice of a vorticity method. Although the twisting term is generally considered negligible on the synoptic scale, it apparently must be retained on the mesoscale (Matsumoto et al (1967a)), so the entire vorticity equation was chosen. A scheme similar to the one used here was used by Yanai and Nitta (1967) in a synoptic study of a Caribbean easterly wave. They retained the troublesome twisting term, as it was found not to be negligible in the upper troposphere. They obtained a convergent scheme, which gave hope that the important twisting term could also be included successfully on the mesoscale.

C. THE ADJUSTED KINEMATIC TECHNIQUE

The major problem with the kinematic method is that errors are additive and as successive omegas are determined, as one integrates from the surface up, the method tends to "blow up" near the top of the atmosphere. The scheme used here, similar to the one suggested by Mahlman (1968), is to force the average divergence between two levels

(generally a 50 mb increment except for the first layer - surface to 900 mb) to conform to the vertically averaged divergence determined previously by an integral constraint. This must be the case if the computed vertical motions are to agree with the upper and lower boundary conditions.

The kinematic technique used here was developed in the following manner. First, the divergence is found at all interior points of the grid area and smoothed. Then the average divergence for each vertical column is found by mass-weighting the 17 levels of divergence and averaging.

Integration of the continuity equation between the surface and 150 mb gives

$$\omega_{sfc} - \omega_{150} = - \overset{ww}{D} (p_{sfc} - 150), \qquad (1)$$

where sfc = surface and $\overset{ww}{D}$ = vertically averaged isobaric divergence.

Surface pressures were determined from topography and the standard atmosphere, and surface winds were taken to be those at 950 mb. This was done in an attempt to get a representative surface omega at any time.

Assuming that the vertical motion at 150 mb is zero, or approximately so (this seems a good assumption since examination of all soundings indicated that the 150 mb level was above or at the tropopause for all cases), one can rewrite (1) solving for $\overset{ww}{D}$ as

$$\overset{ww}{D} = \frac{-\omega_{sfc}}{p_{sfc} - 150}, \qquad (2)$$

where ω_{sfc} is determined by the terrain effect, or

$$\omega_{sfc} = u \frac{\partial p}{\partial x} + v \frac{\partial p}{\partial y} = \mathbb{W} \cdot \nabla p_{sfc}.$$

This surface omega is used in both the adjusted kinematic and complete vorticity methods.

Equation (2) then defines the vertically averaged divergence for a column of air to be that determined by the surface omega and the depth of the column in millibars. One may average all the divergences computed over the column, but this average must equal that value determined by (2). Therefore, (2) acts as a "constraint" on the divergence fields, and will hereafter be referred to as the integral constraint. It is well known that divergence in itself is difficult to obtain accurately on the synoptic scale, since $\frac{\partial u}{\partial x}$ and $\frac{\partial v}{\partial y}$ are often nearly equal and of opposite sign. Therefore, a slight error in either term can cause a relatively large error in the divergence. This problem may not be as great on the mesoscale, since average divergences appear to be an order of magnitude larger than those on the synoptic scale (noted earlier), but it still exists. Therefore, since the integral constraint is determined from accurately measured quantities, forcing individual divergences (through the use of $\overset{ww}{D}$) to meet this criteria by correcting them in some manner would seem to give divergence fields with less error that more accurately represent the state of the atmosphere.

Reiter (1963) and Clark (1969) have shown that radiosonde errors tend to increase linearly with height. This assertion indicates that vertical velocities determined from the computed divergence patterns decrease in accuracy as one proceeds upward, so a normalized scheme for a smaller correction to the lower level divergences and a greater correction to the upper fields was developed. This method is similar to the one used by Fankhauser (1969) which was developed by O'Brien (1969). Since 17 levels have been used here, a mid-level (level 9

or 550 mb) was chosen as the level to which the total correction was applied to the divergence field. This total correction (CORK) is the difference between the integral constraint and the vertical average of the mass-weighted divergences of all 17 levels. By using a vertical indicator K, the divergence fields in the vertical were corrected by the following:

$$\text{DIV (NEW)} = \text{DIV (OLD)} + \frac{K}{9} \text{ (CORK)}$$

where K ranges from 1 at the surface to 17 at 150 mb,

and CORK = D - computed vertically averaged divergence.

(NOTE: Abbreviations such as CORK are the ones used in the computer program at the end of this text and are used here to maintain continuity.)

The final corrected divergence fields were then used to calculate the omega fields at all levels.

Calculation of vertical motions by the adjusted kinematic technique was done in five steps in order to compare the preference of one answer to the other. These steps were:

(1) no corrections to divergence (true kinematic);

(2) total correction;

(3) K/9 times total correction;

(4) K/9 times total correction with horizontal divergence smoother;

(5) K/9 times total correction with horizontal and vertical divergence smoothers.

The above steps correspond to Figs. 3 - 7 for time 1700 GMT at point (5, 5) (the Wichita Mountains). This was the vicinity of the squall line at 1700 GMT. Examination of Figs. 3 - 7 shows that a general improvement in vertical consistency occurs as one progresses through the figures. The extremely large values of divergence near

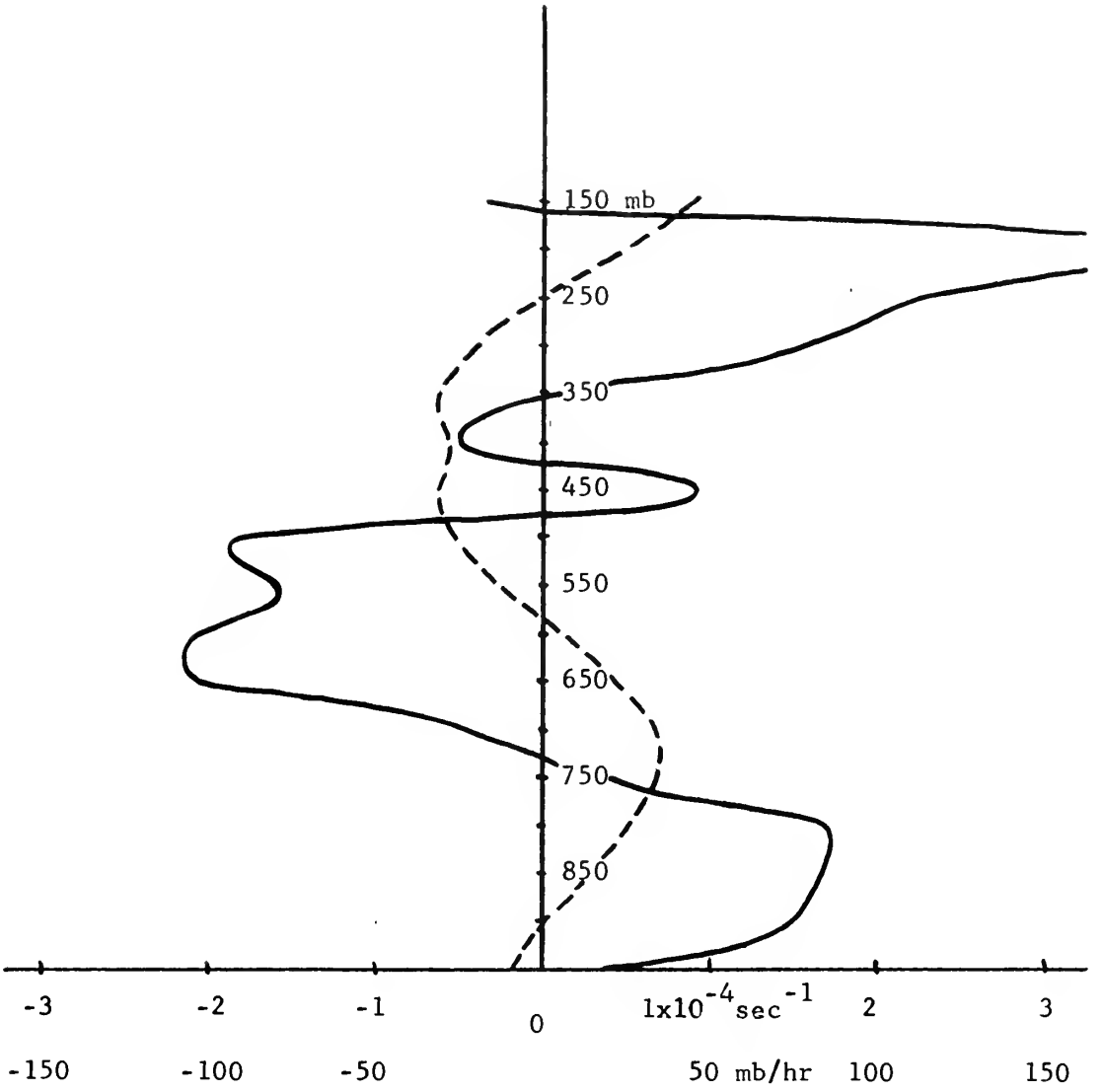

FIG. 3. Vertical profiles of divergence (——) and vertical motion (---), determined by the true kinematic method with no corrections, for grid point (5, 5) (Wichita Mountains) at 1700 GMT on 30 May 1967.

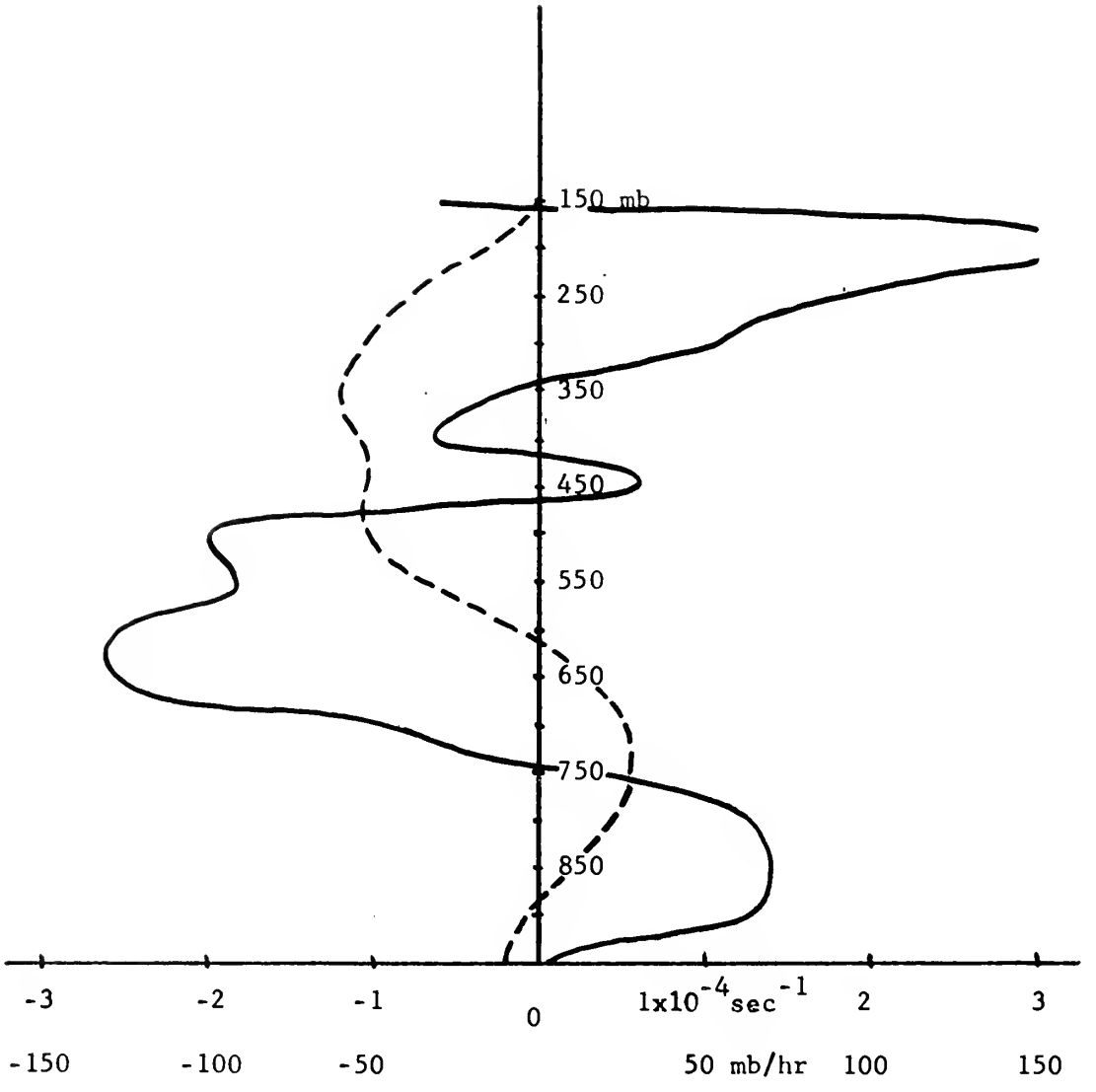

FIG. 4. Vertical profiles of divergence (——) and vertical motion (---), determined by the completely corrected kinematic method, for grid point (5, 5) (Wichita Mountains) at 1700 GMT on 30 May 1967.

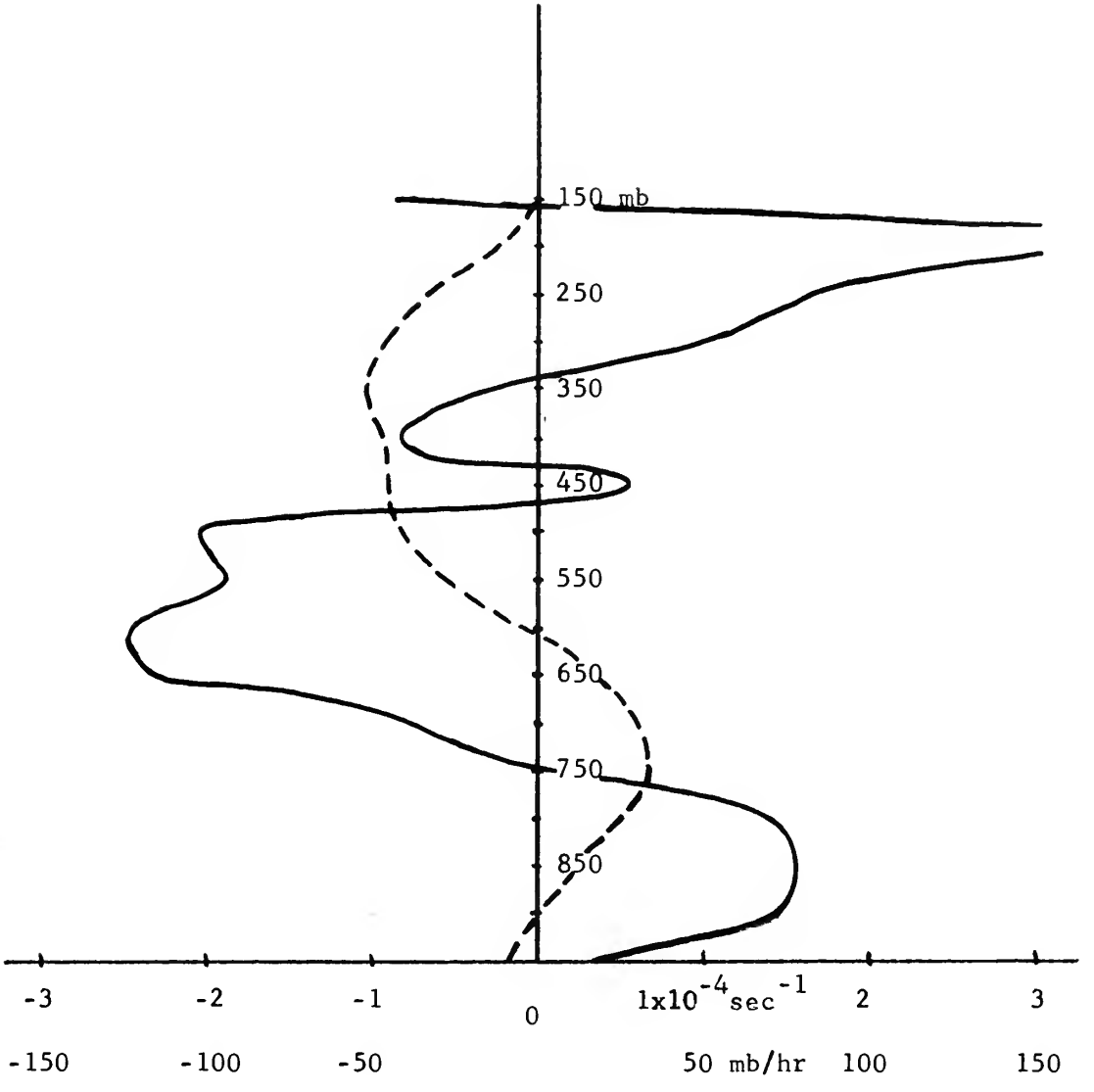

FIG. 5. Vertical profiles of divergence (——) and vertical motion (---), determined by K/9 times the complete correction for the kinematic method, for grid point (5, 5) (Wichita Mountains) at 1700 GMT on 30 May 1967.

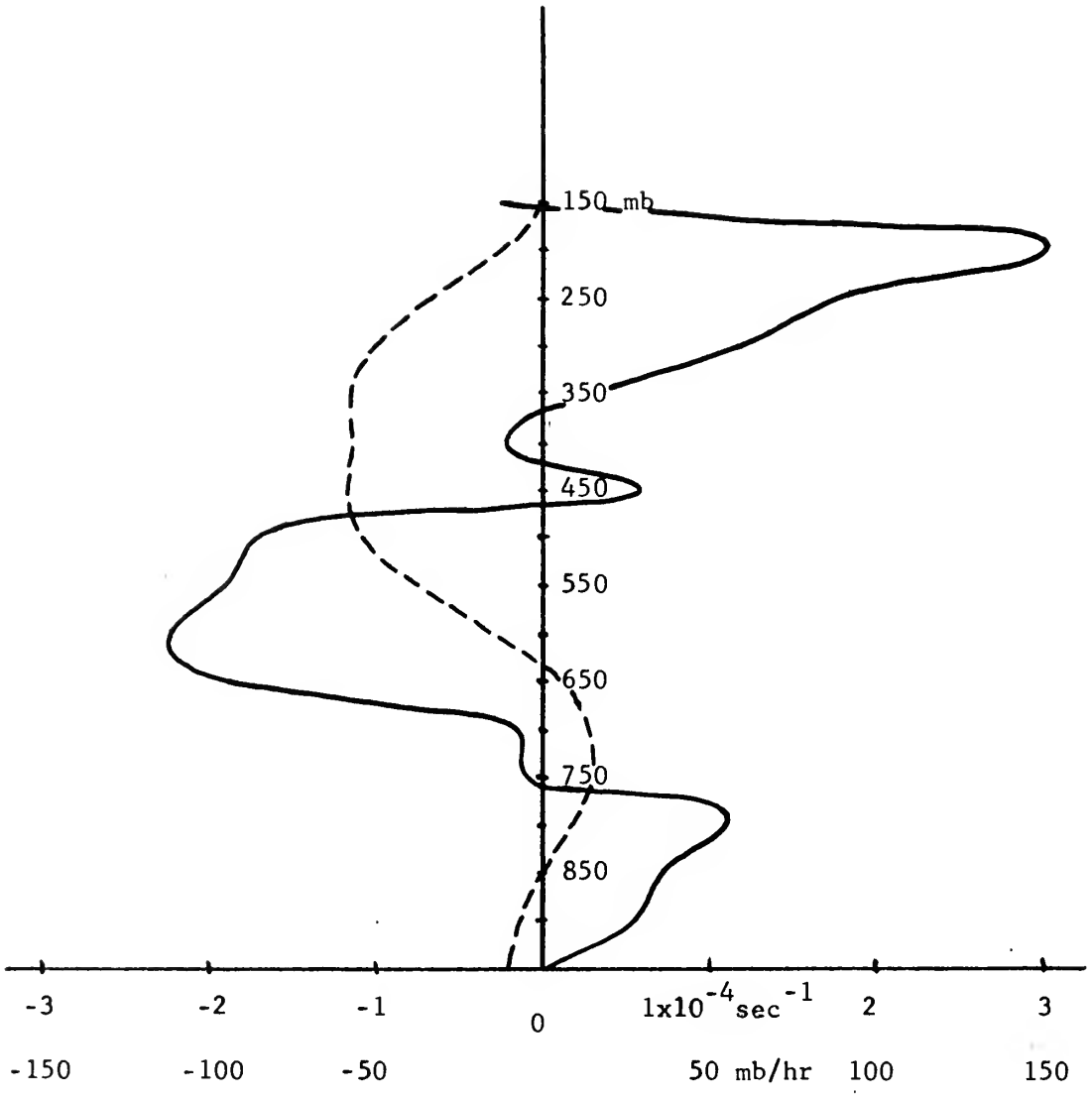

FIG. 6. Vertical profiles of divergence (——) and vertical motion (---), determined by K/9 times the complete correction for the kinematic method with a horizontal divergence smoother, for grid point (5, 5) (Wichita Mountains), at 1700 GMT on 30 May 1967.

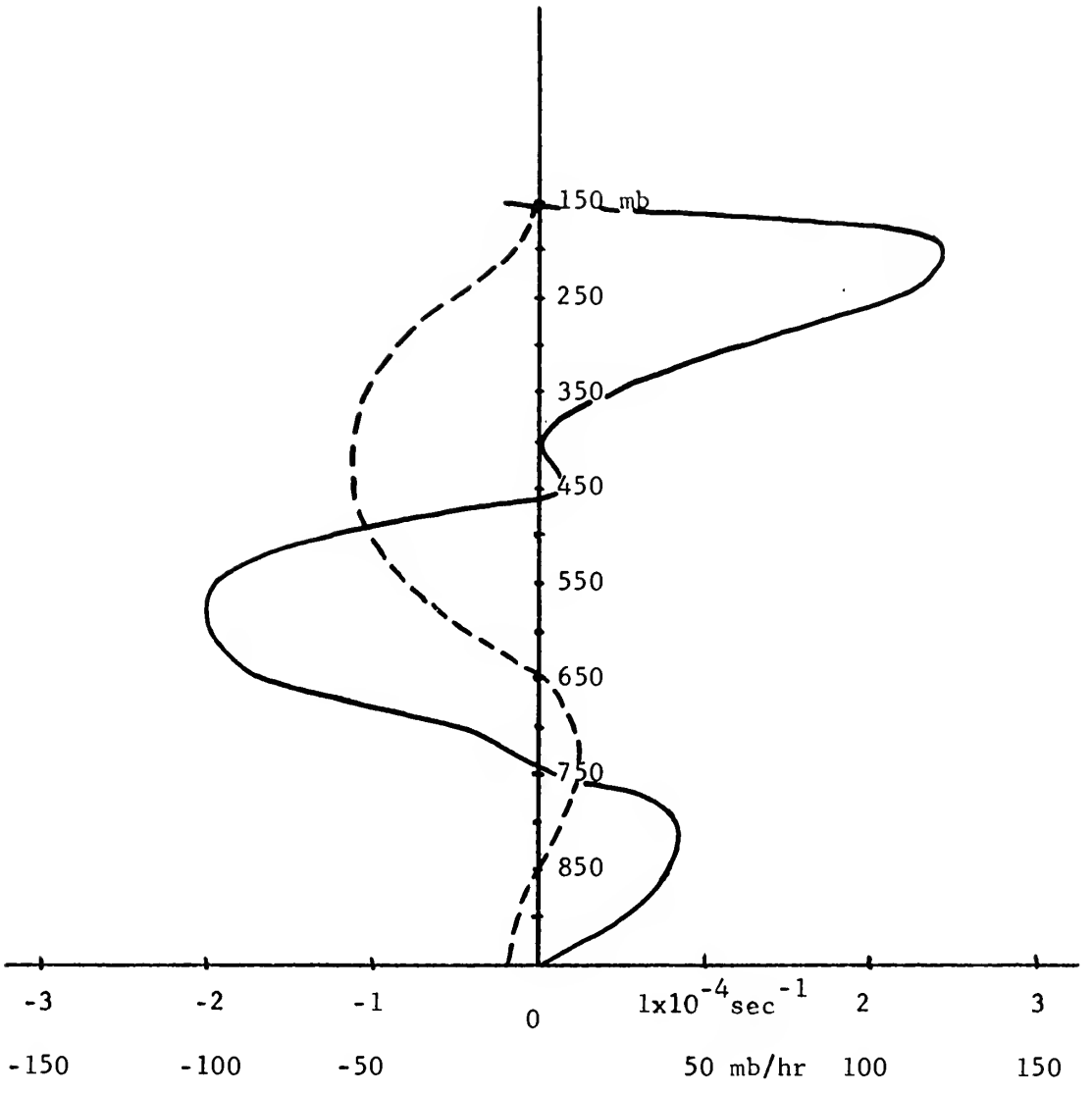

FIG. 7. Vertical profiles of divergence (——) and vertical motion (---), determined by K/9 times the complete correction for the kinematic method with a horizontal and vertical divergence smoother, for grid point (5, 5) (Wichita Mountains) at 1700 GMT on 30 May 1967. This is the adjusted kinematic technique.

200 mb are adjusted to more realistic values, but the general patterns of divergence and vertical motion are unchanged. Therefore, it was concluded that vertical motions determined by step (5) above most closely represent the real atmosphere. All vertical motion fields presented in this study were determined in this manner.

It is interesting to note the area of maximum convergence which appears near the 600 mb level in Figs. 3 - 7, which appears to be a prevalent condition in all the shower areas as noted in a later section.

D. THE COMPLETE VORTICITY METHOD

The vorticity equation in pressure coordinates (neglecting friction) is

$$\frac{d\zeta_a}{dt} + \zeta_a \nabla\cdot\mathbf{V} + \frac{\partial\omega}{\partial x}\frac{\partial v}{\partial p} - \frac{\partial\omega}{\partial y}\frac{\partial u}{\partial p} = 0. \qquad (3)$$

The following derivation gives the basis for the vorticity method chosen. Expansion of (3) gives

$$\frac{\partial\zeta_a}{\partial t} + \mathbf{V}\cdot\nabla\zeta_a + \omega\frac{\partial\zeta_a}{\partial p} + \zeta_a\nabla\cdot\mathbf{V} + \frac{\partial\omega}{\partial x}\frac{\partial v}{\partial p} - \frac{\partial\omega}{\partial y}\frac{\partial u}{\partial p} = 0. \qquad (4)$$

Since $\frac{\partial\zeta_a}{\partial t} = \frac{\partial\zeta_r}{\partial t}$, (4) becomes

$$\frac{\partial\zeta_r}{\partial t} + \mathbf{V}\cdot\nabla\zeta_a + \omega\frac{\partial\zeta_a}{\partial p} + \zeta_a\nabla\cdot\mathbf{V} + \frac{\partial\omega}{\partial x}\frac{\partial v}{\partial p} - \frac{\partial\omega}{\partial y}\frac{\partial u}{\partial p} = 0. \qquad (5)$$

By making the continuity equation substitution of $\nabla\cdot\mathbf{V} = -\frac{\partial\omega}{\partial p}$, (5) becomes

$$\frac{\partial\zeta_r}{\partial t} + \mathbf{V}\cdot\nabla\zeta_a + \left[\omega\frac{\partial\zeta_a}{\partial p} - \zeta_a\frac{\partial\omega}{\partial p}\right] + \frac{\partial\omega}{\partial x}\frac{\partial v}{\partial p} - \frac{\partial\omega}{\partial y}\frac{\partial u}{\partial p} = 0. \qquad (6)$$

Now, combining the bracketed terms in (6) gives

$$\frac{\partial\zeta_r}{\partial t} + \mathbf{V}\cdot\nabla\zeta_a - \zeta_a^2\frac{\partial}{\partial p}\left(\frac{\omega}{\zeta_a}\right) + \frac{\partial\omega}{\partial x}\frac{\partial v}{\partial p} - \frac{\partial\omega}{\partial y}\frac{\partial u}{\partial p} = 0. \qquad (7)$$

By rearranging, one obtains

$$\frac{\partial}{\partial p}\left(\frac{\omega}{\zeta_a}\right) = \frac{\frac{\partial \zeta_r}{\partial t} + W\cdot\nabla\zeta_a}{\zeta_a^2} + \frac{\frac{\partial \omega}{\partial x}\frac{\partial v}{\partial p} - \frac{\partial \omega}{\partial y}\frac{\partial u}{\partial p}}{\zeta_a^2}. \tag{8}$$

Integrating (8) gives

$$\frac{\omega_L}{\zeta_{a_L}} - \frac{\omega_u}{\zeta_{a_u}} = \int_{p_u}^{p_L} \frac{\frac{\partial \zeta_r}{\partial t} + W\cdot\nabla\zeta_a}{\zeta_a^2}\,\delta p + \int_{p_u}^{p_L} \frac{\frac{\partial \omega}{\partial x}\frac{\partial v}{\partial p} - \frac{\partial \omega}{\partial y}\frac{\partial u}{\partial p}}{\zeta_a^2}\,\delta p. \tag{9}$$

Since omega occurs on both sides of the equation, a first approximation must be made and then convergence must occur for the equation to be satisfied.

The method of approach used here is to define

$$\text{FUN1} \equiv \frac{\frac{\partial \zeta_r}{\partial t} + W\cdot\nabla\zeta_a}{\zeta_a^2},$$

$$\text{FUN2} \equiv \frac{\frac{\partial \omega}{\partial x}\frac{\partial v}{\partial p} - \frac{\partial \omega}{\partial y}\frac{\partial u}{\partial p}}{\zeta_a^2}.$$

For the first approximation, the same type scheme is used as was used in the adjusted kinematic method. Using only FUN1, find the average FUN1 for a vertical column. Then determine the average FUN1 which satisfies the integral constraint. This is done by substituting FUN1 and FUN2 into (9) to get

$$\frac{\omega_{sfc}}{\zeta_{a_{sfc}}} - \frac{\omega_{150}}{\zeta_{a_{150}}} = \overline{\text{FUN1}}^{wwww}\,\Delta p + \overline{\text{FUN2}}^{vwww}\,\Delta p, \tag{10}$$

where $\overline{\overline{FUN1}}^{wwww}$ = vertically averaged FUN1,

$\overline{\overline{FUN2}}^{wwww}$ = vertically averaged FUN2, and

$\Delta p = p_{sfc} - 150$ mb.

As in the adjusted kinematic method, if ω_{150} (at 150 mb) is assumed to be zero, (10) can be rewritten as,

$$\frac{\omega_{sfc}}{\zeta_{a_{sfc}}^{\Delta p}} = \overline{\overline{FUN1}}^{wwww} + \overline{\overline{FUN2}}^{wwww}. \qquad (11)$$

The left side of (11) then acts as a constraint on both $\overline{\overline{FUN1}}^{wwww}$ and $\overline{\overline{FUN2}}^{wwww}$, and will hereafter be referred to as the integral constraint. Since (11) contains two unknowns, the following procedure was used in solving it. First, one may determine $\overline{\overline{FUN1}}^{wwww}$ by the integral constraint by assuming $\overline{\overline{FUN2}}^{wwww}$ is zero. Then, vertically average the FUN1 values at all 17 levels through the column by mass-weighting them. The difference between this averaged $\overline{\overline{FUN1}}^{wwww}$ and that determined by the integral constraint is called CORVF1 (see Appendix B). This CORVF1 then is the average correction which must be made to the column so that the integral constraint is satisfied. The same K/9 times CORVF1 correction technique as was used in the adjusted kinematic technique is used to correct the FUN1 values at each level.

Using these corrected FUN1 values, and assuming that all FUN2 terms (the twisting term) are zero (as is done on the synoptic scale), one may use (9) to integrate upward from the surface a level at a time to get a first approximation for the omega field.

The next step is to determine the fields of FUN2. This is done by using the first approximation omega fields just found. In satisfying the integral constraint (11), it was determined that $\overline{\overline{FUN2}}^{wwww}$ must

be zero. The FUN2 values at all 17 levels through the column are vertically averaged using mass-weighting, as was done in FUN1. So, to meet the integral constraint, this vertically averaged $\overline{FUN2}$ must be zero. If it isn't, the average correction, called CORVF2, is used to correct the FUN2 fields in a manner similar to the one used to correct the FUN1 fields. The difference is that neither the top nor bottom FUN2 fields are corrected. The lowest FUN2 field is specifically determined by the terrain effect, and the top FUN2 field (at 150 mb) was determined so that the omega field here was zero. Both of these then must be kept intact (see the Fortran IV computer program - subroutine VOROMG for details).

With the corrected FUN1 and FUN2 fields (9) may be used to determine the omega or vertical motion field. This field must then be compared to the first approximation field obtained from the FUN1 field alone. If any set of omegas in the two omega fields differ by some predetermined epsilon, then the last omega field replaces the first approximation field and one recycles through the $\overline{FUN2}$ correction procedure and determines a new omega field. This field is checked against the old one, and the procedure continues until a satisfactory omega field is found.

The results of this vorticity method are found in Appendix B.

The Fortran IV computer program used to determine all the variables described in this section is found at the end of this text. A determined effort has been made to provide sufficient comment cards to make this program self explanatory. The adjusted kinematic technique is the subroutine KINOMG, and the vorticity method is the subroutine VOROMG. The nomenclature used in the above explanations is that which is used in the computer program.

V. RESULTS

A. POSSIBLE PROBLEMS

Since the storm began near 1530 GMT and was still active as a squall line at 2000 GMT, even though beginning to dissipate, it is considered to be a mature, active squall line throughout the 1700 to 2000 GMT period of study. The severity and intensity of the squall is indicated by the report of hail 20 miles southeast of Altus (LTS) at 1600 GMT. Therefore, a close look at the mesoscale environment in and around the squall line area becomes a necessity. However, because the squall line has reached maturity before the mesonetwork is activated, it has definitely begun to interact with and possibly reshape the mesoscale environment in which it is embedded. The effect the squall line, or any such mesoscale phenomenon, has on its environment is yet a mystery. Data which was possibly under the effect of the squall line was used with this in mind, if used at all. The above should always be kept in mind when evaluating the resultant fields which describe the mesoscale environment.

B. THE MESOSCALE ENVIRONMENT AT 1700 GMT

At 1700 GMT, the active squall line was oriented generally north-south along a line just west of Wichita Falls (SPS) and Fort Sill (FSI). Fig. 8 shows the streamline and isotach fields for representative levels at this time. General cyclonic curvature is found over the squall line in the low levels and anti-cyclonic curvature in the middle and upper troposphere. A wind maximum at 200 mb overlaps a minimum at 500 mb over the squall line indicating large shears.

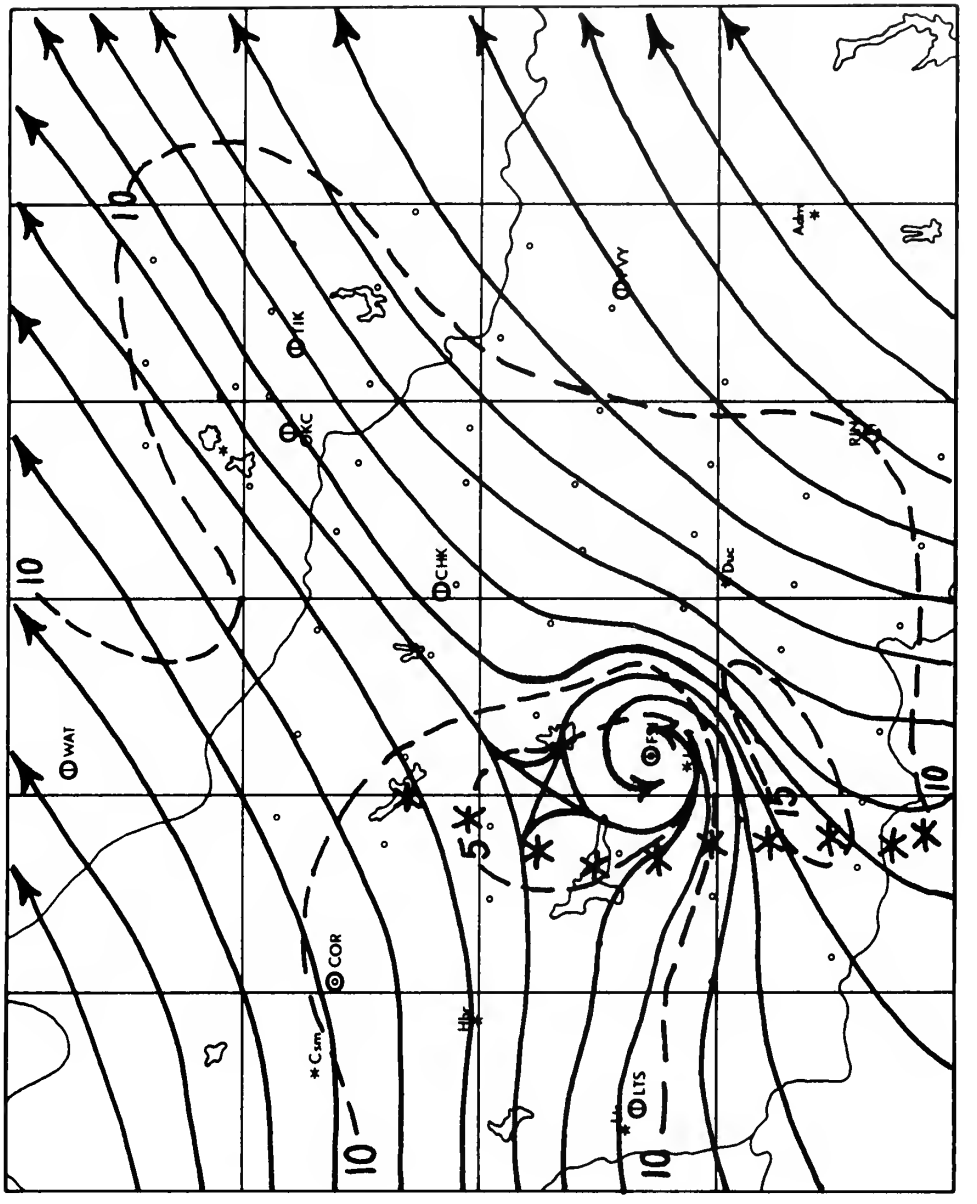

FIG. 8a. Streamlines (⟶), isotachs (---) (m sec^{-1}), and the axis of the squall line (***) for 700 mb at 1700 GMT on 30 May 1967.

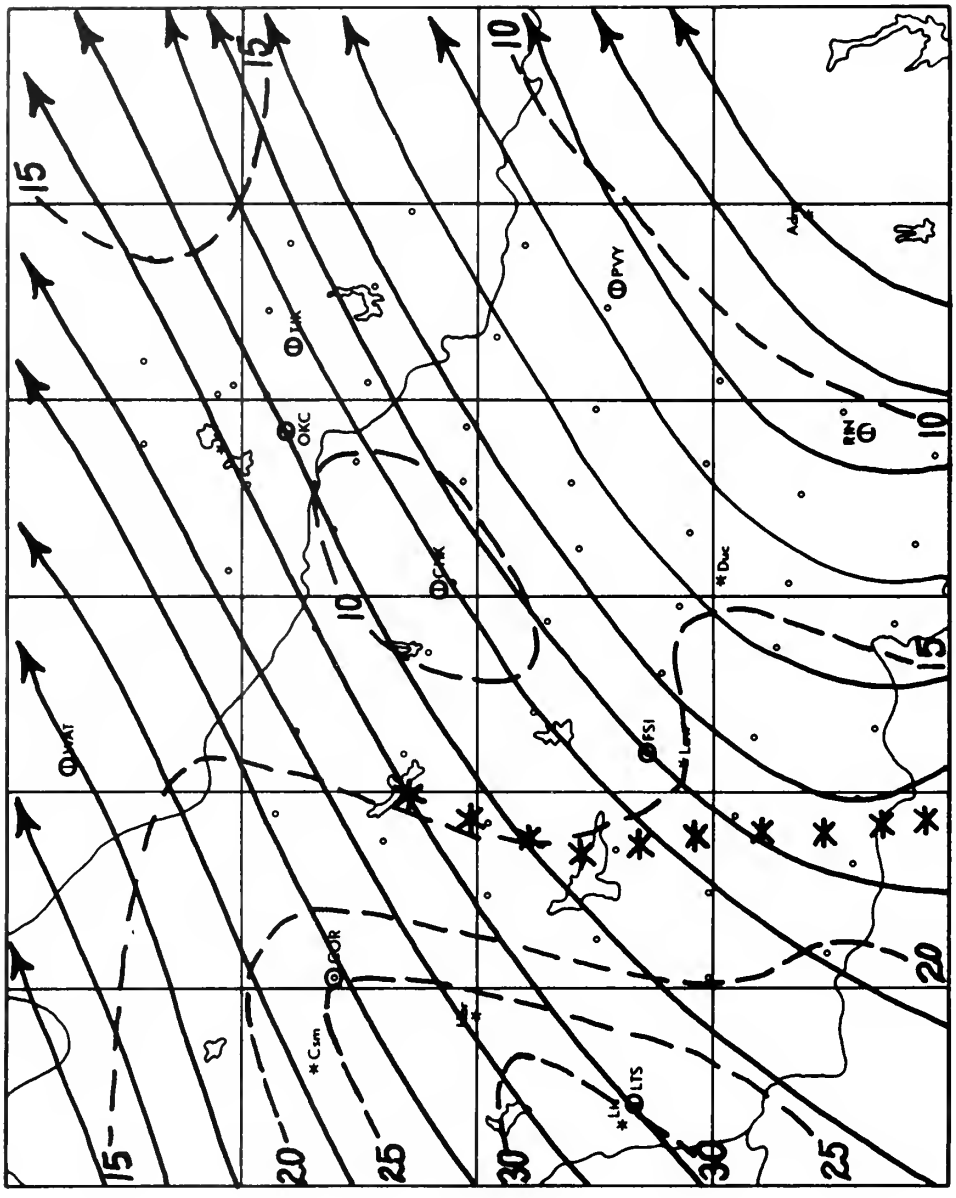

FIG. 8b. Streamlines (—>), isotachs (---) (m sec^{-1}), and the axis of the squall line (***) for 500 mb at 1700 GMT on 30 May 1967.

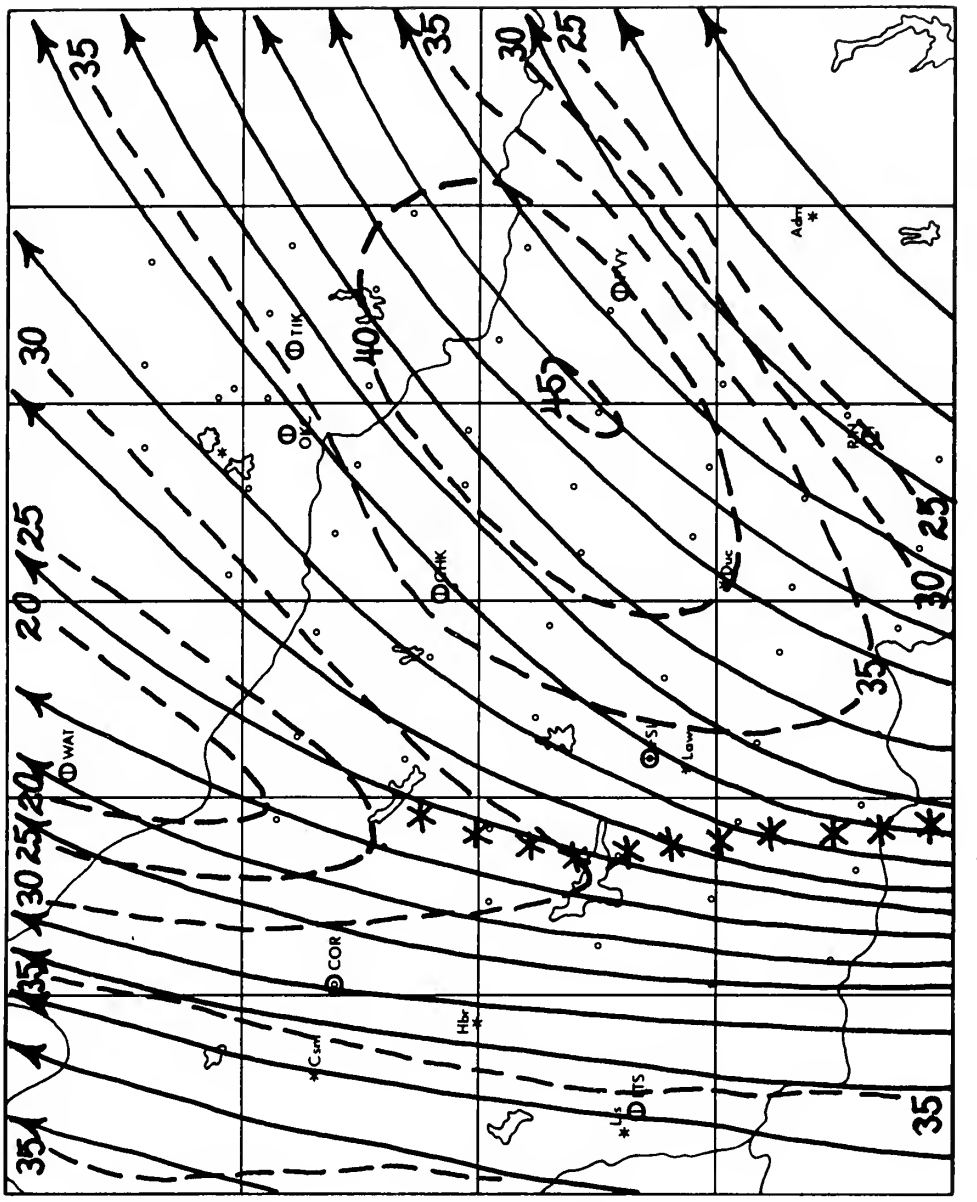

FIG. 8c. Streamlines (—>), isotachs (---) (m sec^{-1}), and the axis of the squall line (***) for 200 mb at 1700 GMT on 30 May 1967.

Fig. 9 shows the squall line and the lower tropospheric fields associated with it. Convergence at 950 mb is indicated over most of the mesonetwork area, with the maximum area of convergence oriented parallel to and just east or downwind of the squall line. Although this area of convergence is similar to that noted by Matsumoto (1967) and Matsumoto et al (1967a, b), it is not so strong (only a small area of magnitude 10^{-4} sec^{-1}) and generally precedes the squall line rather than encompassing it. This seems plausible since the squall line is moving rather rapidly eastward, as is noted later in this section. The vertical motions shown here, as those shown for all times, are those determined by the adjusted kinematic technique (as noted in Fig. 7). The vertical motion field at 800 mb seems rather complicated and difficult to explain. The relative humidity pattern shows that the most moist air (90% or greater) at 850 mb is also oriented parallel to and just east of the squall line. A large gradient of humidity is noted westward of this area, with rather dry air (30% or less) indicated behind the squall line near the western edge of the grid area. Therefore a good energy source in the form of low level, convergent moist air is apparently present to sustain the squall line.

Fig. 10 shows the squall line and the mid-troposphere divergence and omega fields. Also noted is the 1-1/2 hour rainfall record. Of most importance here is the fact that all the convective activity is in the area of upward vertical motion at 450 mb. This level was chosen so that comparisons could be made with Fankhauser (1969). He found that all the convective activity studied in the area two days before was also determined by the vertical motion at 450 mb. He determined an average magnitude of near 75 mb hr^{-1} in the vicinity

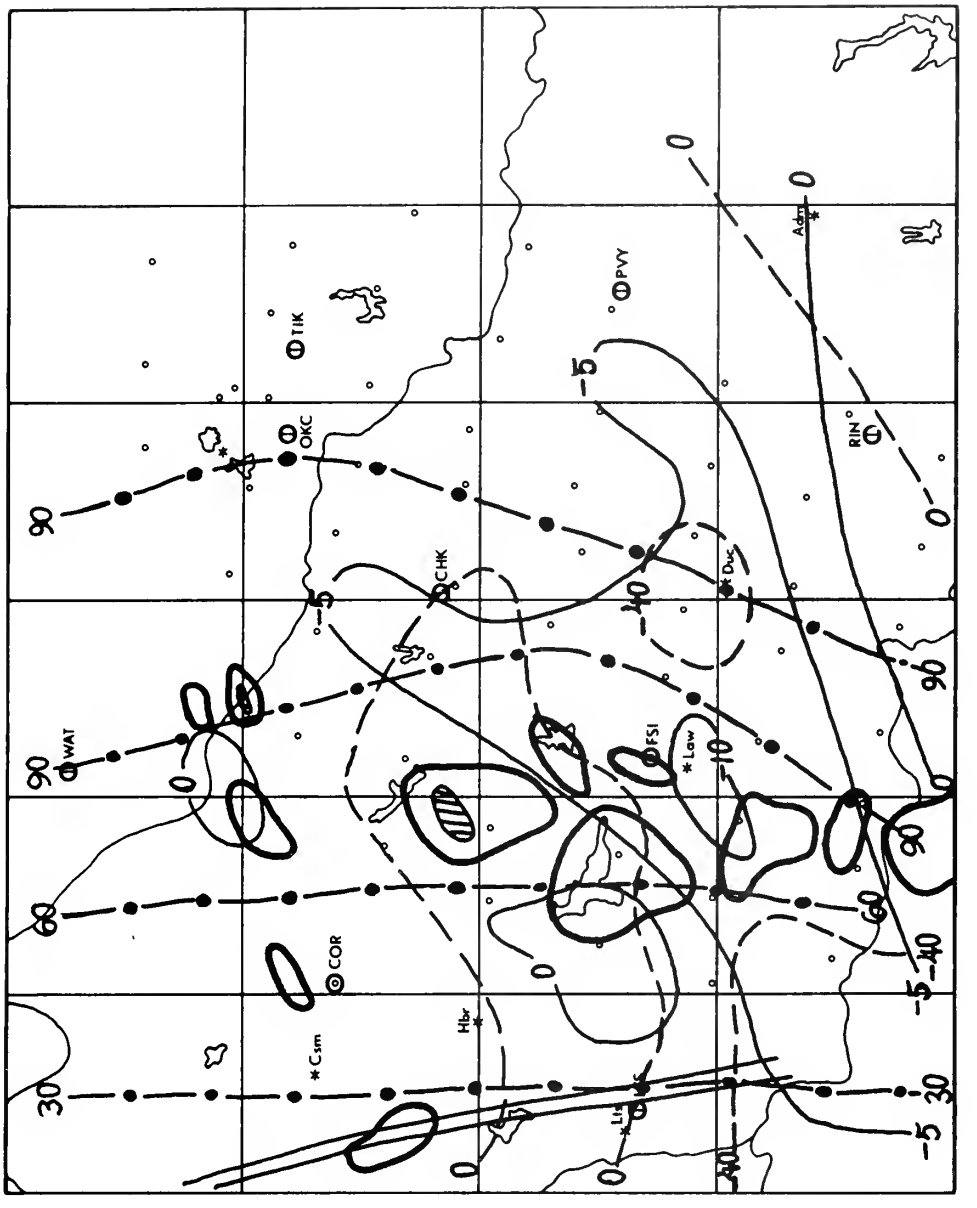

FIG. 9. Squall line and low level fields at 1700 GMT on 30 May 1967.

950 mb divergence (——) 10^{-5} sec^{-1}
800 mb vertical motion (---) mb hr^{-1}
850 mb relative humidity (-·-) %
700 mb trough (═══)
Radar return (▬▬)

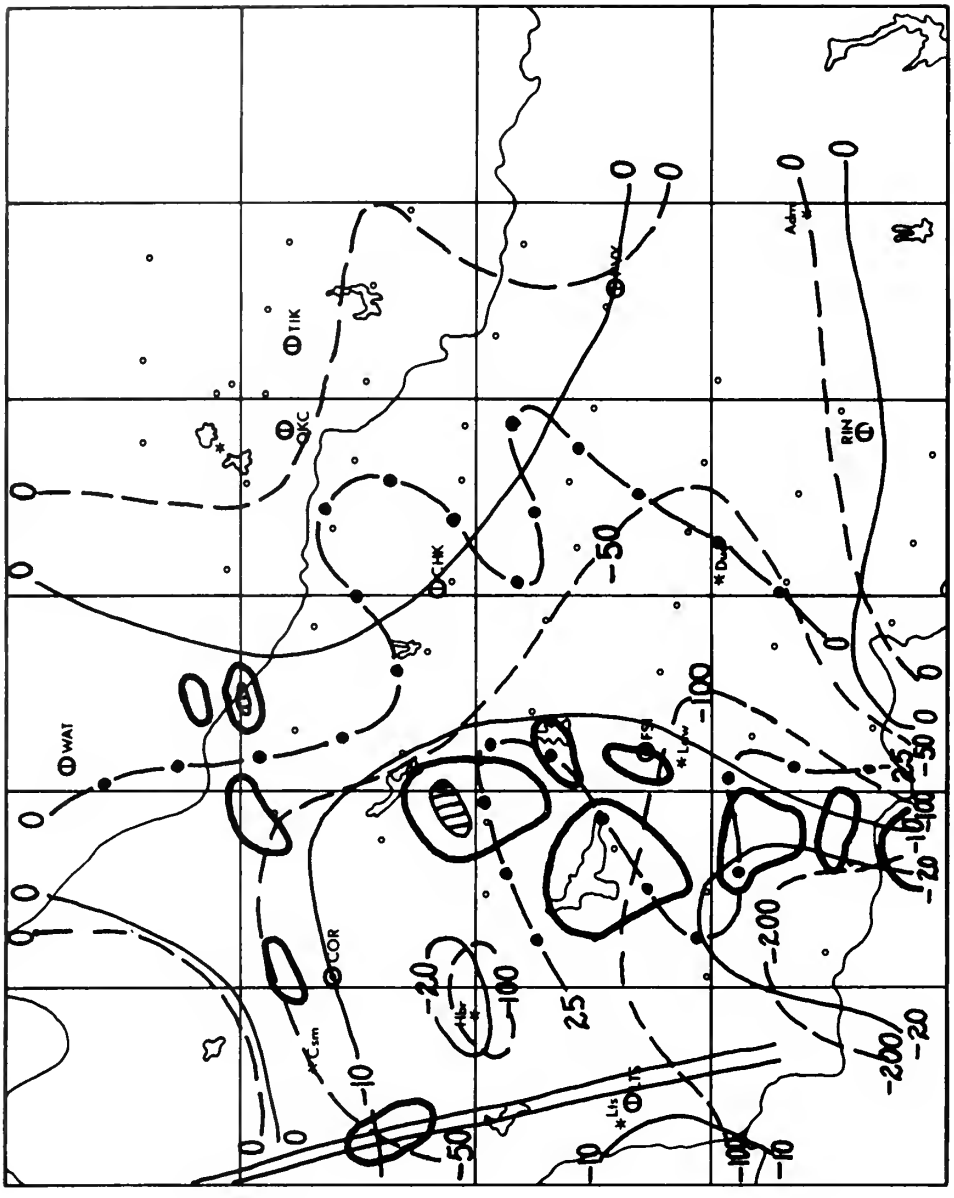

FIG. 10. Squall line and mid-troposphere fields at 1700 GMT on 30 May 1967.

550 mb divergence (——) 10^{-5} sec^{-1}
450 mb vertical motion (---) mb hr^{-1}
3-hour rainfall pattern centered at 1700 GMT (-·-) hundredths of inch
700 mb trough (═══)
Radar return (▬▬)

of the showers. Vertical motions in Fig. 10 appear somewhat greater. The maximum of near 240 mb hr^{-1} west of SPS seems somewhat large, but reanalysis in this area produced no change. The vertical motion maximum axis appears parallel to but slightly behind or upwind of the squall line. This is somewhat surprising, but a possible explanation will be made later. Areas of maximum rainfall are in good agreement with this vertical motion pattern. Strong convergence is found at 550 mb over and to the rear (upwind) of the squall line. Similar findings were noted by Fankhauser (1969) and the NSSP staff (1961), however no attempt has been made in either of these cases to determine the significance, if any, of this strong convergence pattern at this level.

C. THE MESOSCALE ENVIRONMENT AT 1830 GMT

By 1830 GMT, the squall line has remained intact and moved rapidly eastward to the vicinity of Tinker (TIK) and Chickasha (CHK). Fig. 11 shows the streamline and isotach pattern over the area at this time. At 700 mb and to some extent at 500 mb cyclonic curvature is found just west of the squall line and anticyclonic curvature over the squall line. At 200 mb, as at 1700 GMT, anticyclonic curvature is noted in the vicinity of the squall. Also, as at 1700 GMT, an area of maximum winds at 200 mb appears in the vicinity of a wind minimum at 500 mb over the squall line.

Fig. 12 shows the squall line and low level fields at this time. Unfortunately, since the line is over the WSR-57 radar at Norman, the activity within 25 n.m. of Norman is deleted from the return by the STC component in operation. However, the rainfall record in Fig. 13 indicated that there was activity within this area during the period.

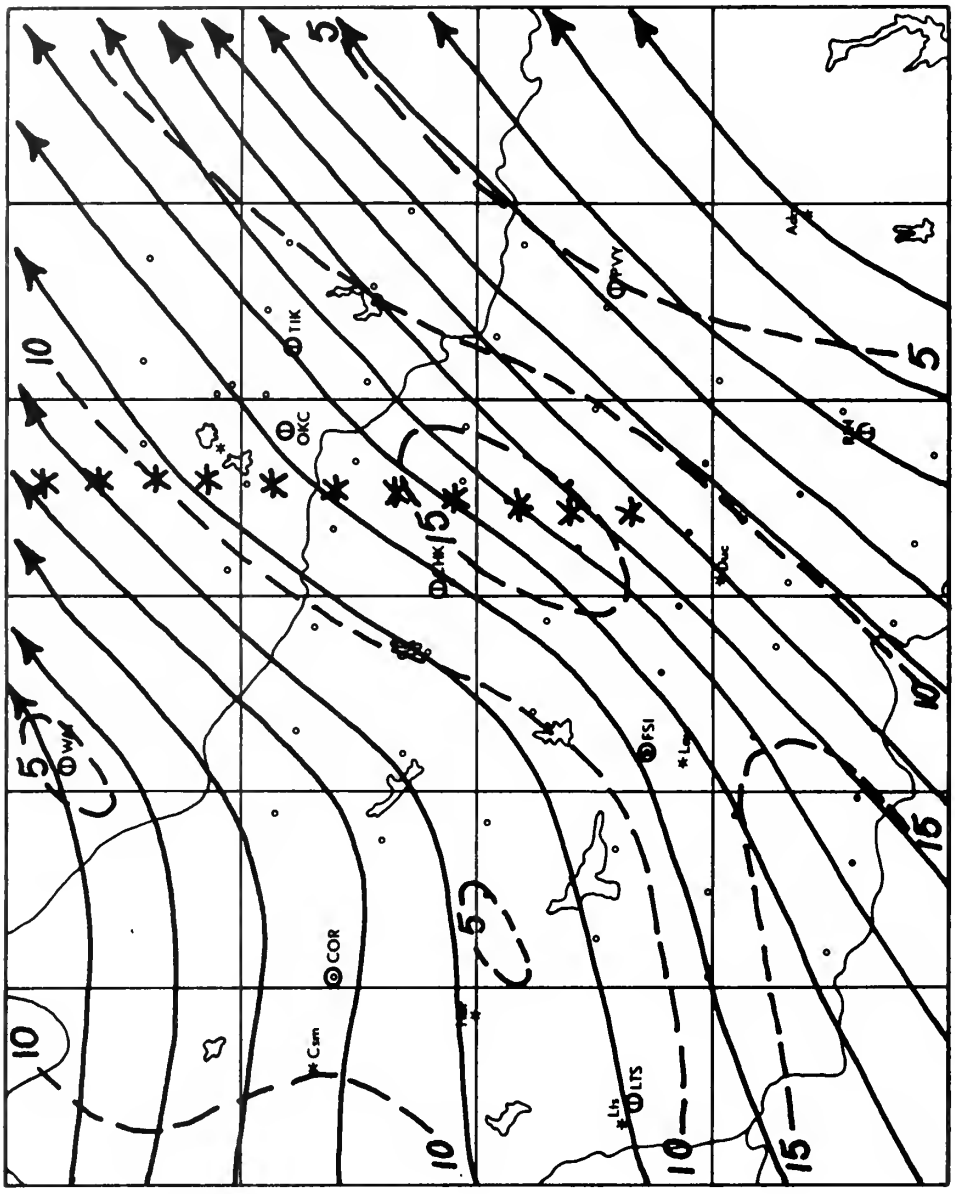

FIG. 11a. Streamlines (—>), isotachs (---) (m sec^{-1}), and the axis of the squall line (***) for 700 mb at 1830 GMT on 30 May 1967.

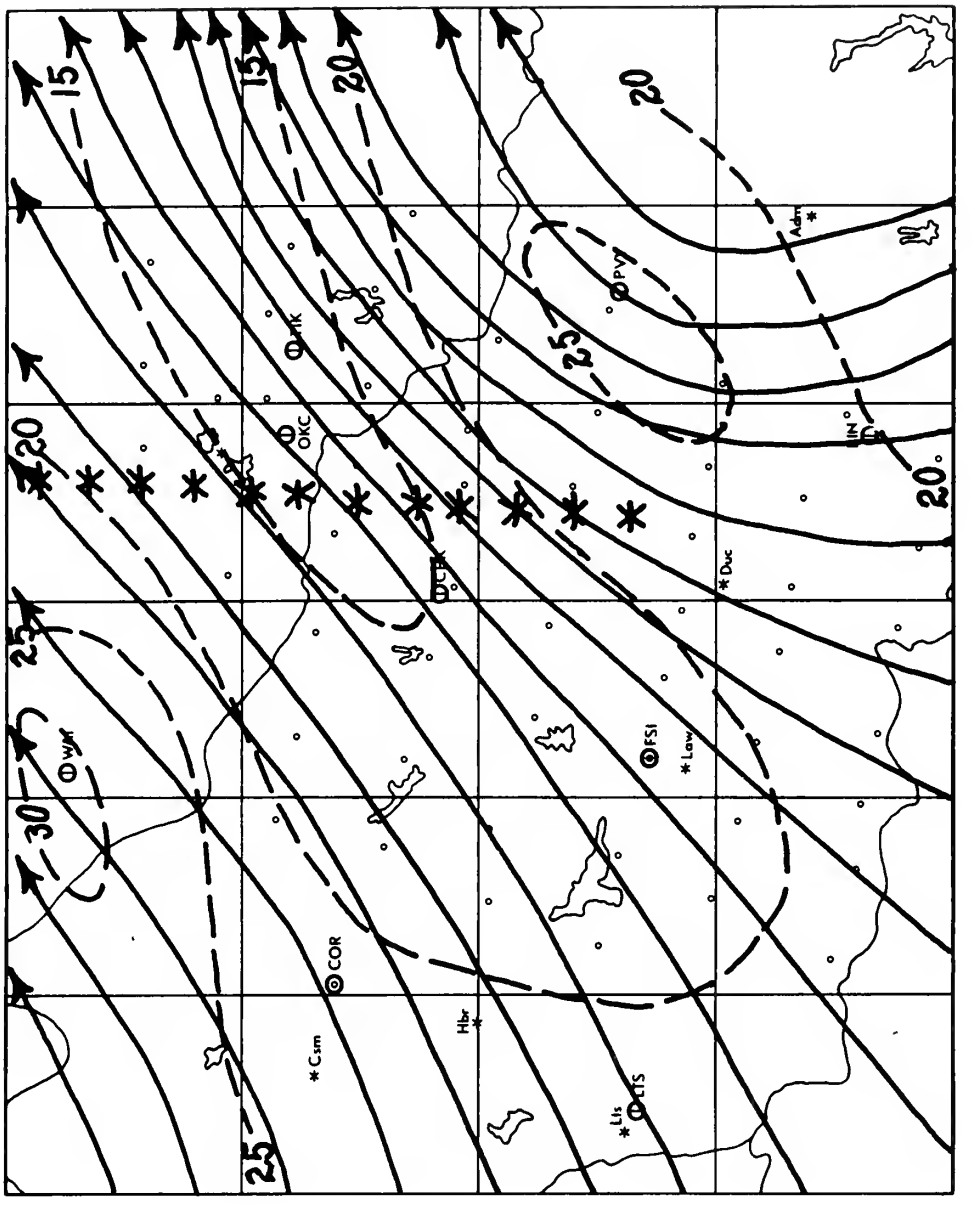

FIG. 11b. Streamlines (—>), isotachs (---) (m sec^{-1}), and the axis of the squall line (***) for 500 mb at 1830 GMT on 30 May 1967.

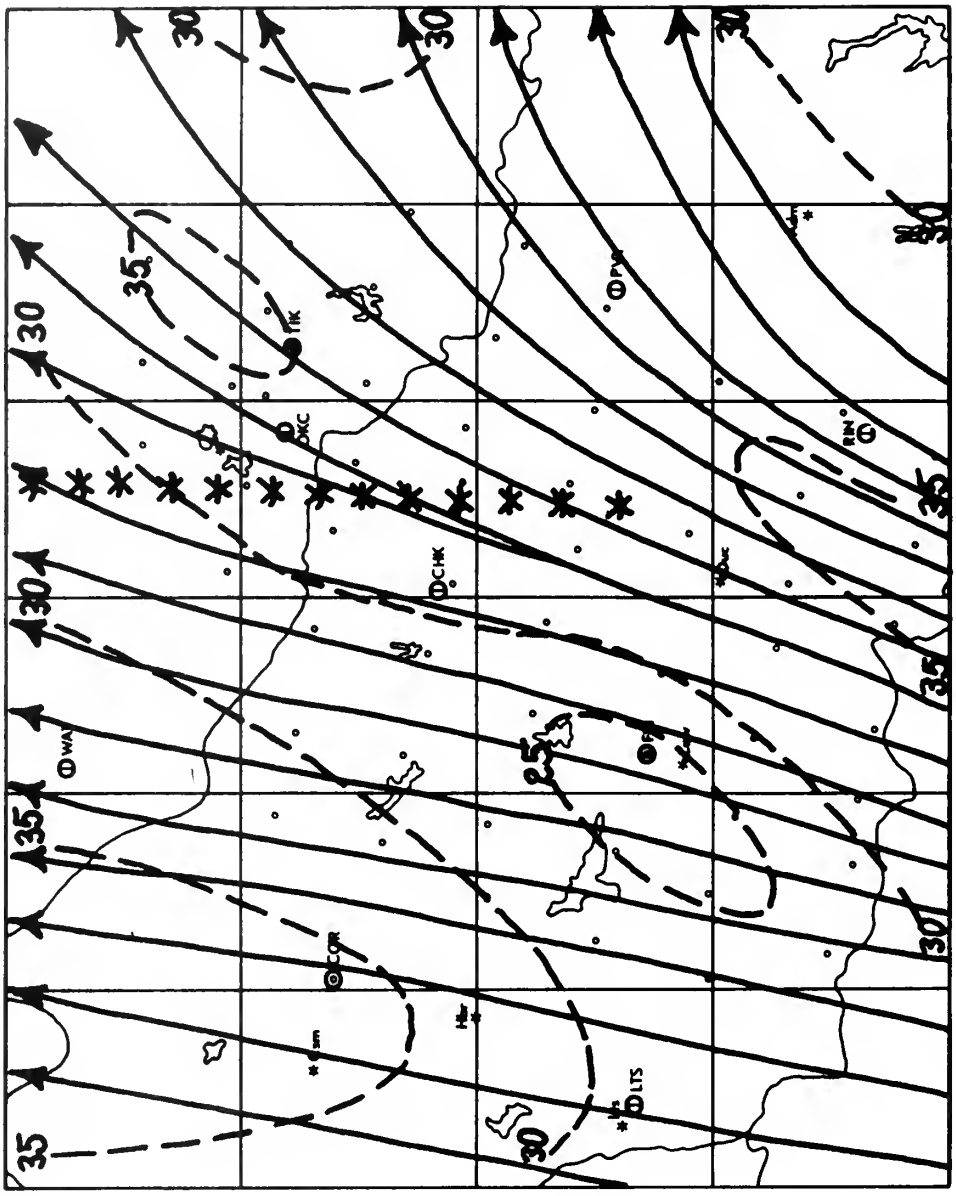

FIG. 11c. Streamlines (—>), isotachs (---) (m sec^{-1}), and the axis of the squall line (***) for 200 mb at 1830 GMT on 30 May 1967.

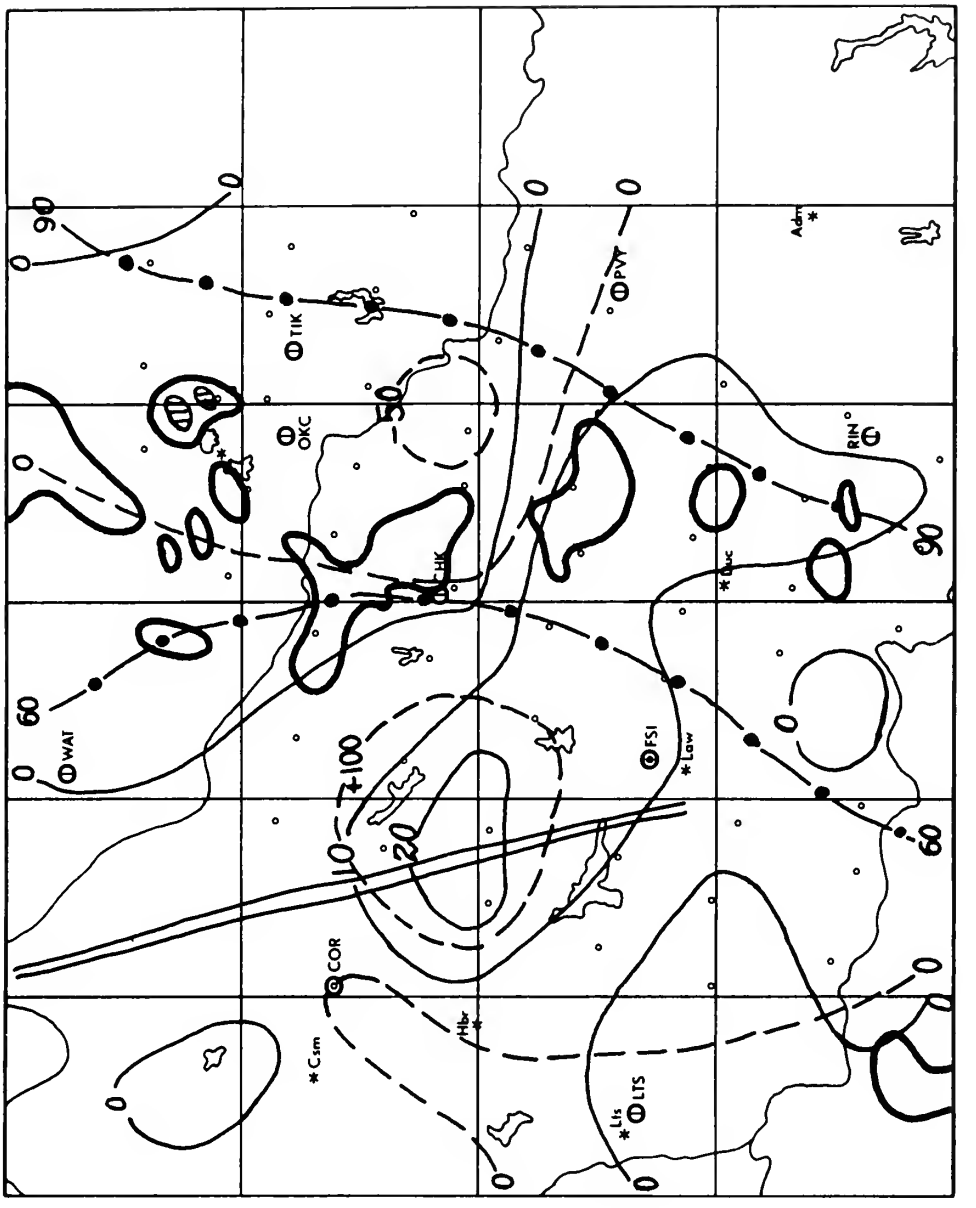

FIG. 12. Squall line and low level fields at 1830 GMT on 30 May 1967. Note: No radar return OKC-TIK area because STC component was in operation.

950 mb divergence (——) 10^{-5} sec^{-1}
800 mb vertical motion (---) mb hr^{-1}
850 mb relative humidity (-·-) %
700 mb trough (═══)
Radar return (▬▬)

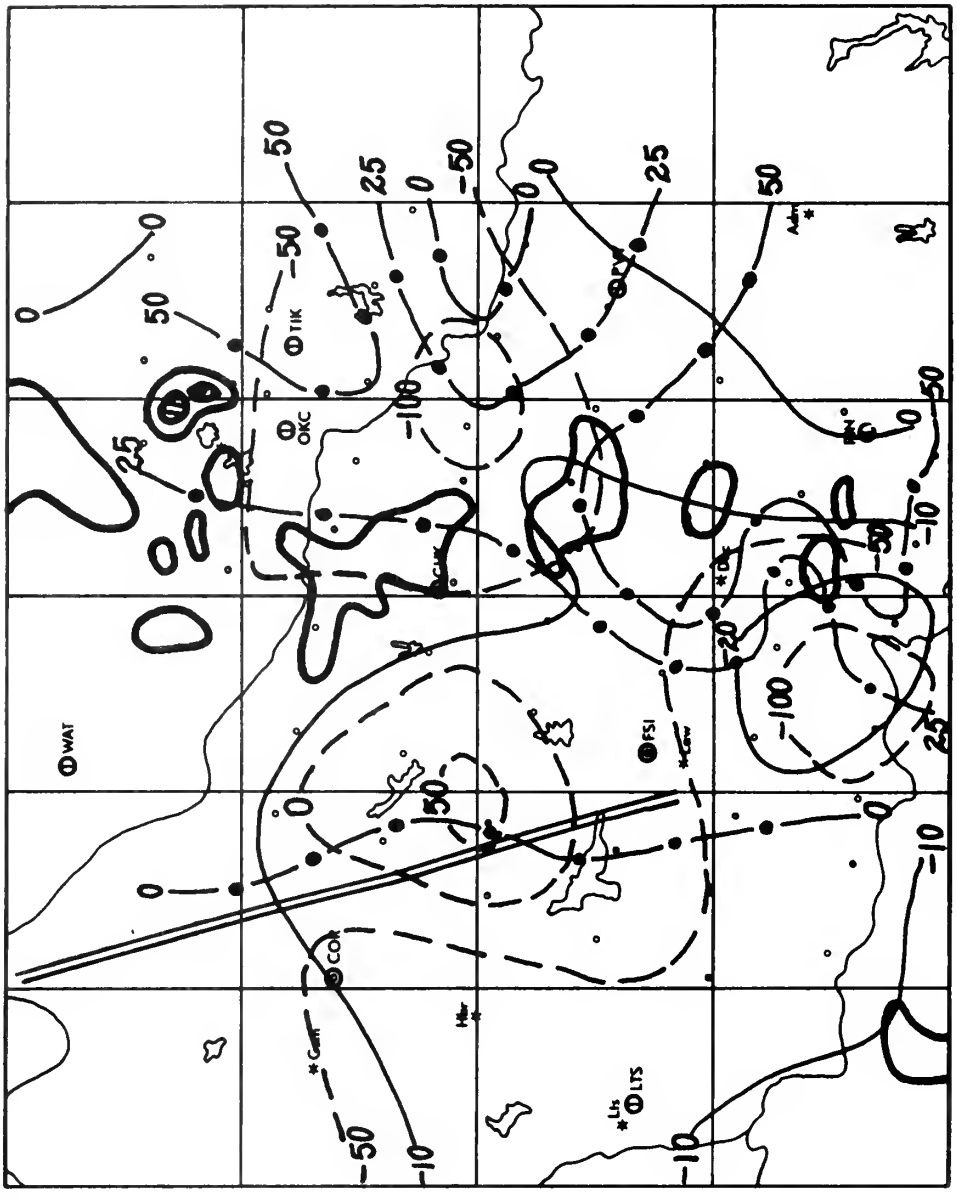

FIG. 13. Squall line and mid-troposphere fields at 1830 GMT on 30 May 1967. Note: No radar return OKC-TIK area because STC component was in operation.

550 mb divergence (——) 10^{-5} sec^{-1}
450 mb vertical motion (---) mb hr^{-1}
3-hour rainfall pattern centered at 1830 GMT (·--) hundredths of inch
700 mb trough (═══)
Radar return (▬▬)

Fig. 12 shows a weak area of convergence in the vicinity of and just preceding the squall line. A strong area of divergence is located north of Fort Sill (FSI). This is directly associated with the strong downward vertical motion in the area, and appears to be well confirmed by the relative humidity, which is a minimum in this area. Again, high relative humidity appears to be associated with the area of convergence, but this is not as clear as was the case at 1700 GMT. The upward vertical motion maximum at 800 mb is in the area of the squall line.

Fig. 13 shows the mid-tropospheric environment and squall line. As at 1700 GMT, all the echoes are within the upward motion area at 450 mb. The field seems very realistic here, with two maximum upward motion areas of 100 mb hr^{-1}. These don't exactly overlay the two maximum rainfall areas, but they are connected by the same axis which connects the rainfall maximum. Since the vertical motions are instantaneous and the rainfall occurs over a 1-1/2-hour interval, this relationship seems very encouraging.

As at 1700 GMT, large convergences appear behind or upwind of the squall line at 550 mb.

D. THE MESOSCALE ENVIRONMENT AT 2000 GMT

By 2000 GMT the squall line is just passing out of the eastern end of the grid area. It is aligned generally north-south from $96^{\circ}30'W$ in the north to $97^{\circ}00'W$ in the south. Fig. 14 shows the streamline and isotach fields for representative levels at this time. The curvature at all three levels is slightly anticyclonic over the squall line at this time. A wind maximum remains at 200 mb over the far northern end of the squall line. At 500 mb a weak tongue of maximum wind is indicated over the northern end of the squall line. At

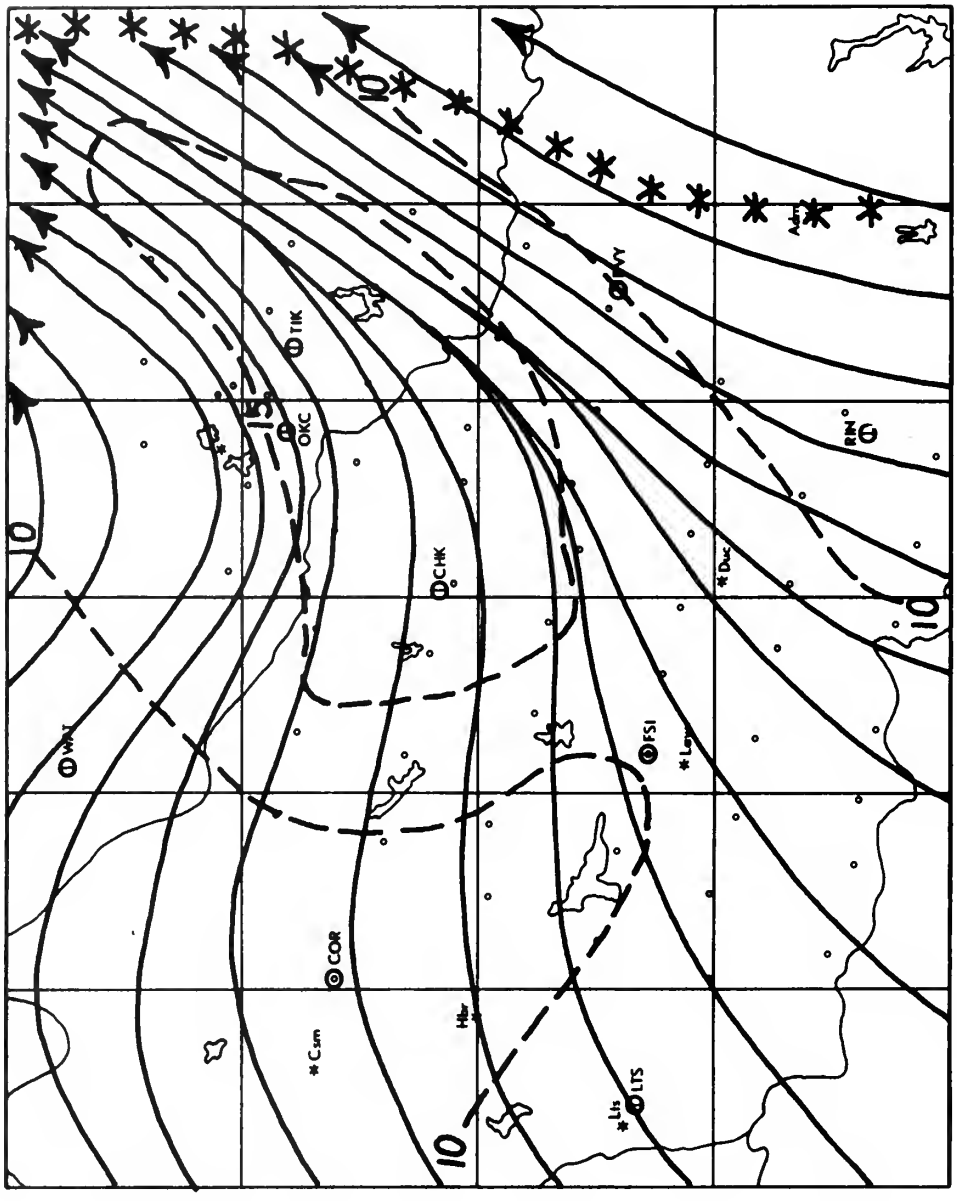

FIG 14a. Streamlines (—>), isotachs (---) (m sec^{-1}), and the axis of the squall line (***) for 700 mb at 2000 GMT on 30 May 1967.

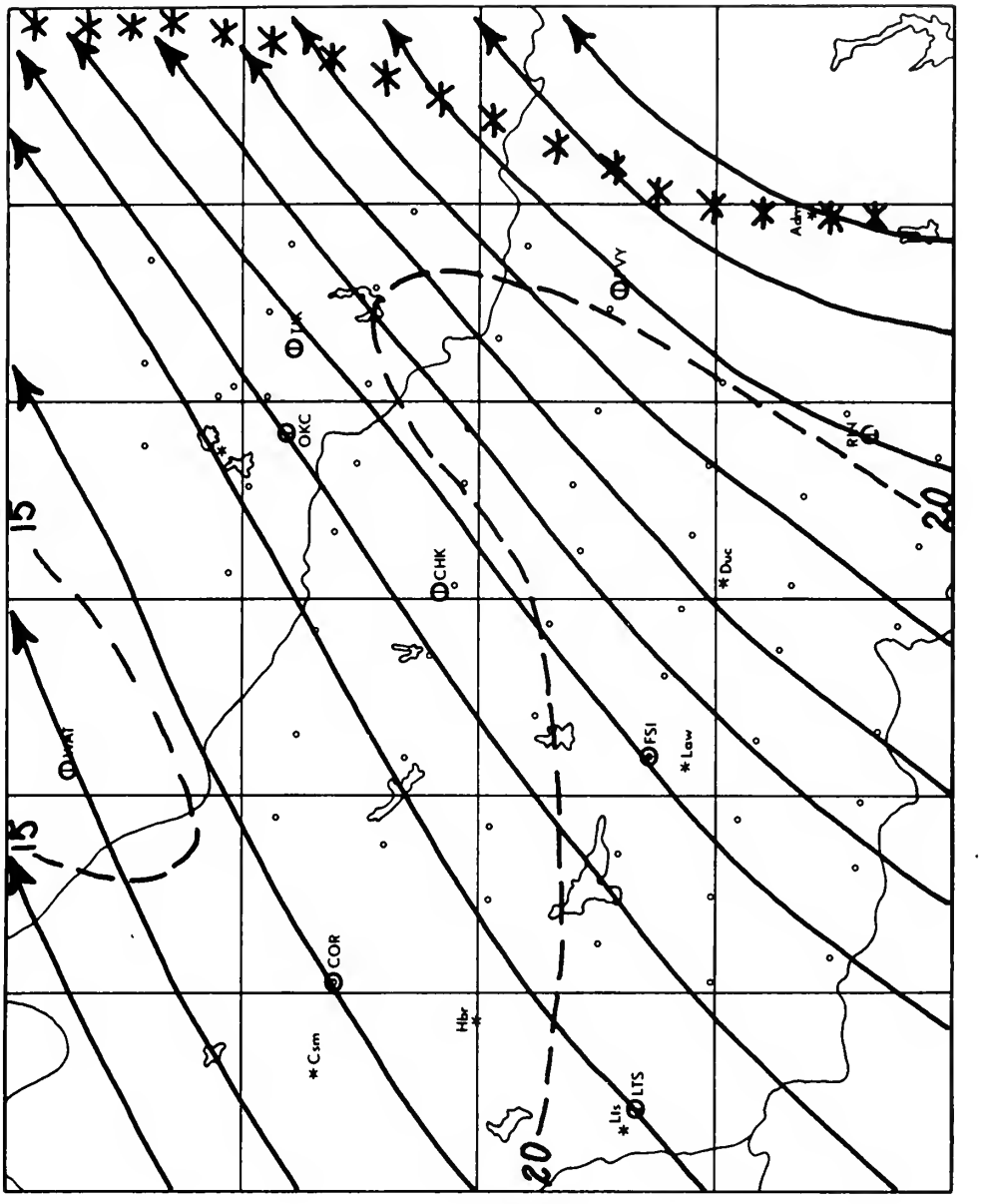

FIG. 14b. Streamlines (—>), isotachs (---) (m sec^{-1}), and the axis of the squall line (***) for 500 mb at 2000 GMT on 30 May 1967.

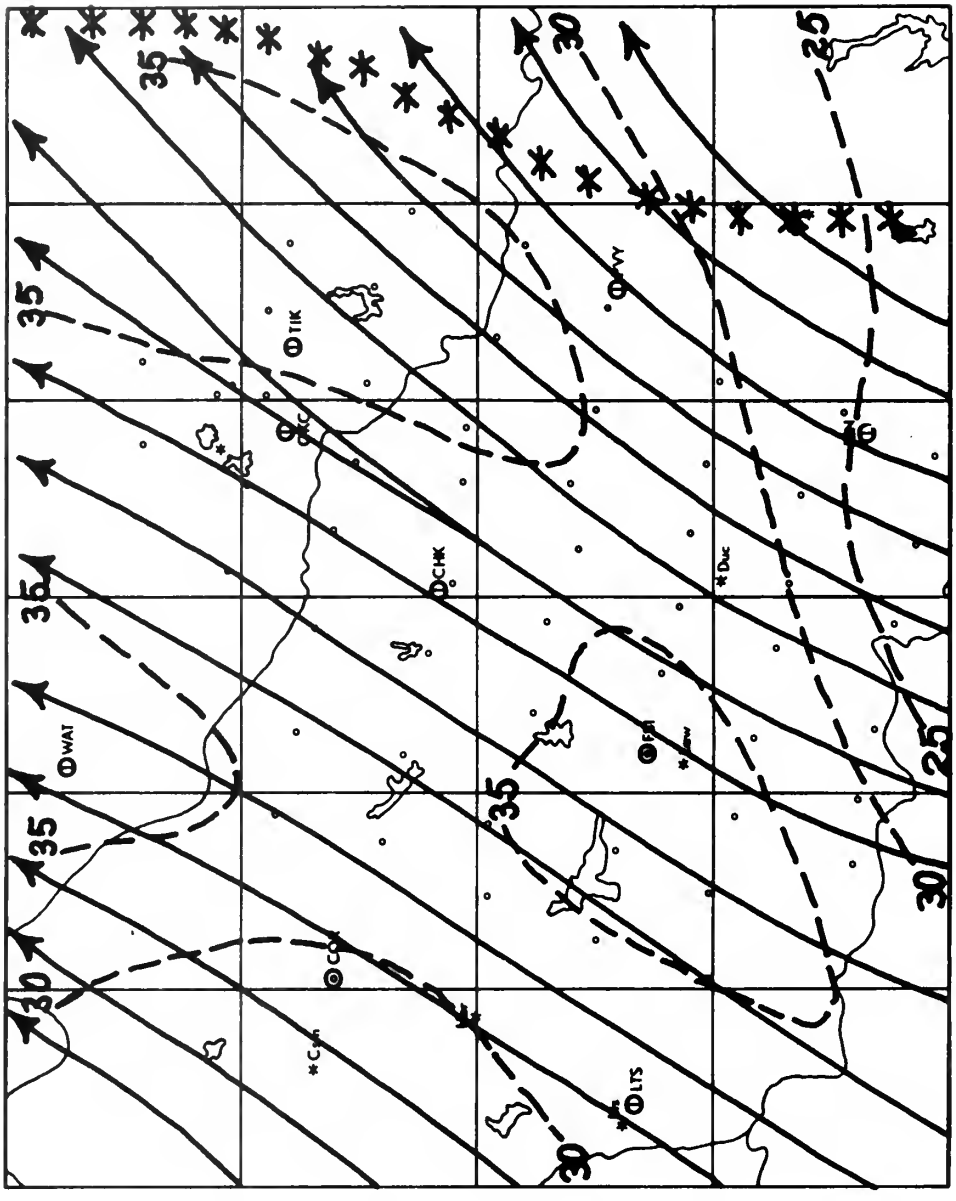

FIG. 14c. Streamlines (—>), isotachs (---) (m sec^{-1}), and the axis of the squall line (***) for 200 mb at 2000 GMT on 30 May 1967.

700 mb strong cyclonic curvature or troughing is located to the west of the squall between CHK and TIK, with a wind maximum of 19 m sec^{-1} noted at CHK.

Fig. 15 shows the radar return and the lower tropospheric fields at 2000 GMT. The squall line at the far eastern edge of the area is notably more diffuse and the individual cells it contains are smaller and weaker than at either of the previous times. However, note the "explosion" of minor, microscale echoes throughout most of the area at this time. No clearcut reason is evident for this random breakout, but it may be due to local heating effects since this is the maximum heating time of the day (1400 CST). Since calculations of vertical motion and divergence end at $97^{o}00'W$, only the southern end of the squall line is covered by these parameters. Fig. 15 shows strong sinking motions and divergence over most of the area in the lower levels. Weak upward motions and weak convergence is indicated in the far northwestern and southwestern parts of the area. Again, relative humidities decrease from values greater than 80% in the far east to a large circular area of 30% or less near the center of the area (FSI and CHK).

Fig. 16 shows the mid-tropospheric environment at 2000 GMT. Most of the area is covered by upward motion at 450 mb. However, an L-shaped area of sinking motion extends generally from the northern edge of the area south along $98^{o}W$ to CHK then eastward. A maximum of 20 mb hr^{-1} sinking is noted just north of CHK. A few cells exist in the northern edge of the area where sinking is very weak, but as a rule the area of sinking motion is practically clear of echo returns, expecially when contrasted to adjacent areas to the south and northeast.

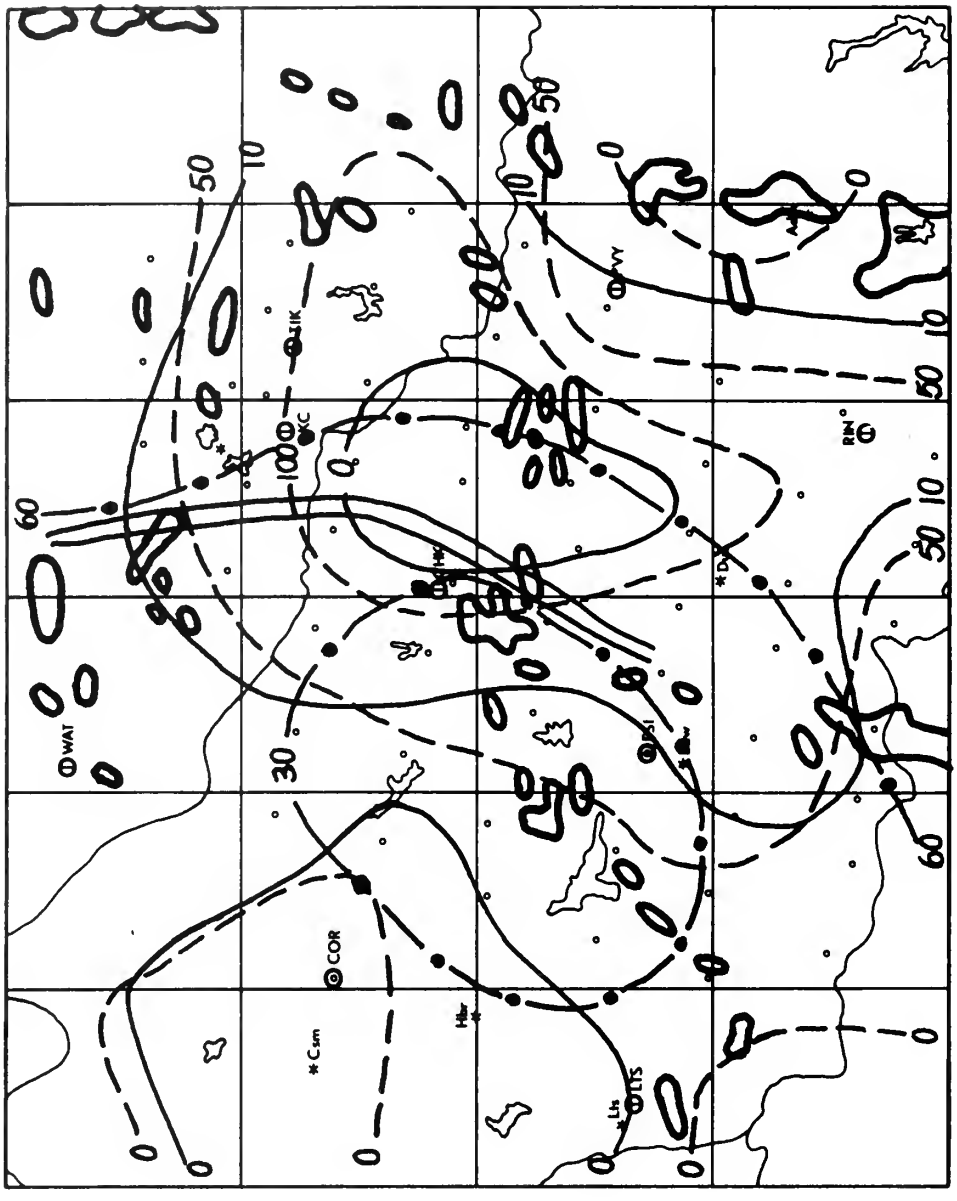

FIG. 15. Squall line and low level fields at 2000 GMT on 30 May 1967.

950 mb divergence (——) 10^{-5} sec^{-1}
800 mb vertical motion (---) mb hr^{-1}
850 mb relative humidity (-·-) %
700 mb trough (═══)
Radar return (▬▬)

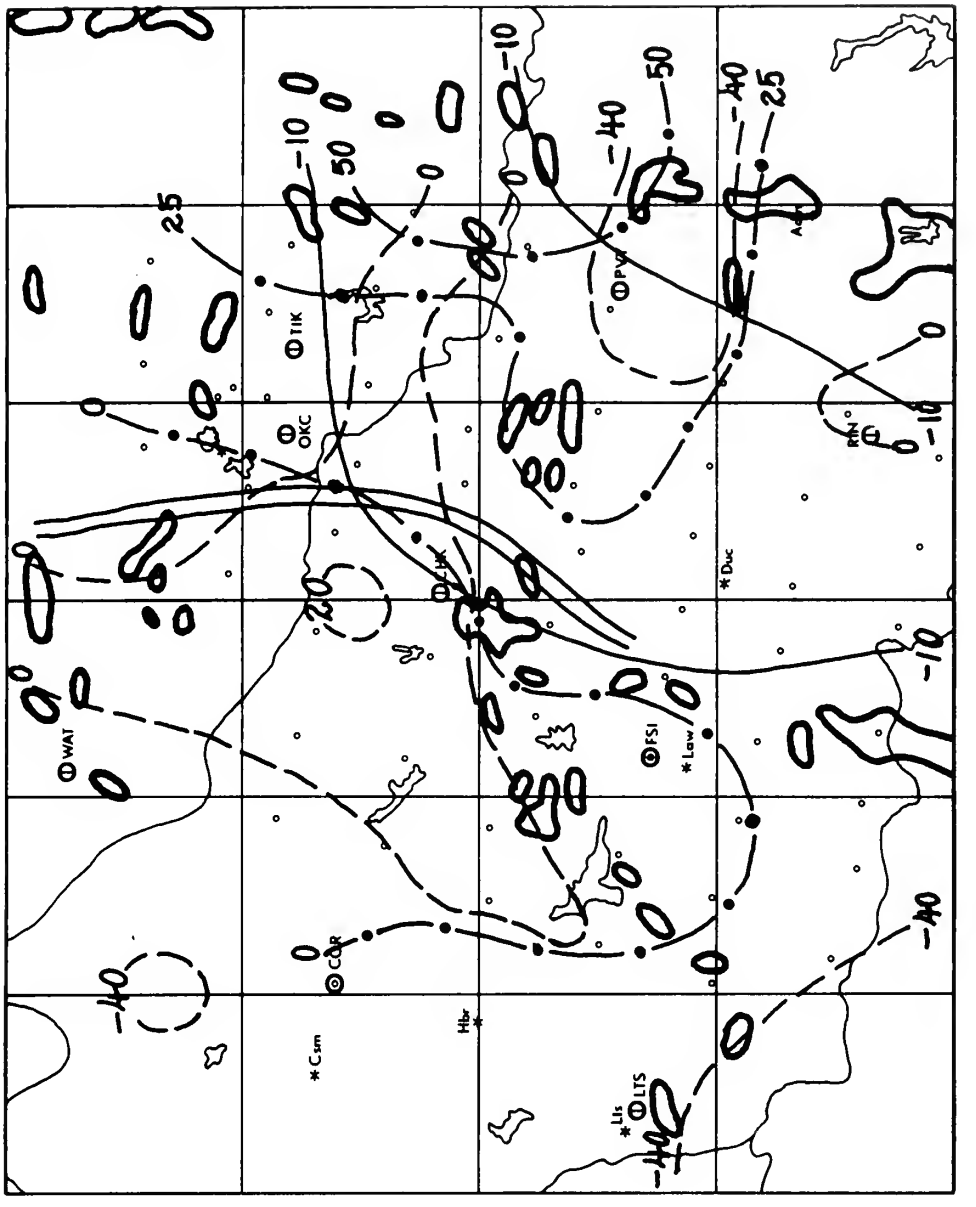

FIG. 16. Squall line and mid-troposphere fields at 2000 GMT on 30 May 1967.

550 mb divergence (——) 10^{-5} sec^{-1}
450 mb vertical motion (---) mb hr^{-1}
3-hour rainfall pattern centered at 2000 GMT (·-·) hundredths of inch
700 mb trough (═══)
Radar return (▬▬)

As has been noted at all three times and also by Fankhauser (1969), in parctically all cases echoes exist only if there is upward motion present in the middle troposphere. However, the echoes present may be very weak and shallow, regardless of the vertical motion at lower levels. Fig. 16 shows convergence over the whole area at 2000 GMT, with values of order 10^{-4} sec^{-1} in the area just behind the squall line. The rainfall for the period 1915 to 2045 GMT noted in Fig. 16 indicates the majority of rainfall during the period was caused by the squall line (maximum of 0.50 in at the eastern edge). Therefore, it is impossible to correlate it with the vertical motion picture at 2000 GMT, except possibly on the southern end of the squall line which is still in the area. Here a maximum area of upward motion of 40 mb hr^{-1} over Pauls Valley (PVY) is in good agreement with a bulge of the 0.25 in isopleth of rainfall.

E. EVIDENCE OF A 700 MB MESOSCALE WAVE

1. As a Possible Cause of the Squall Line

The large areas of convergence found in the middle troposphere and the apparent association of celular activity and the 450 mb upward motion area suggest that a possible mechanism for initiation and maintenance of the squall line system might be found in the middle troposphere.

As mentioned previously, Matsumoto et al (1967a) found strong low level convergence definitely associated with organized convective activity, but they also noted pressure anomoly lines associated with such activity. They noted that these pressure anomoly lines moved in the direction of the 700 mb wind with a speed of about 45 knots. Matsumoto did not make streamline analyses above the surface, and no

attempt to determine the possible presence of a 700 mb mesoscale wave was made.

Investigation of the middle and upper troposphere streamline fields (every 50 mb) showed that a trough existed in the 700 to 600 mb layer at all three times to the rear of the squall line, and is best noted at 700 mb. It can be seen in Figs. 8a, 11a, and 14a. A definite trough was not found at any other levels aloft. The trough moved in the same direction (ENE) as the squall line but slowly lost ground to it. The wavelength of the trough appeared to be approximately 90 n.m. The trough moved at an apparent speed of 20 knots from 1700 GMT to 1830 GMT, and 30 knots from 1830 GMT to 2000 GMT. Since the trough was moving generally from west to east, a comparison of its speed to the u component of the wind was necessary to determine its movement relative to the air parcels at that level. The average u value for 700 mb over the entire grid for 1700 GMT was 11 knots, at 1830 GMT was 13 knots, and at 2000 GMT was 10 knots. Therefore, the trough moved at an average speed of 25 knots from 1700 to 2000 GMT, but the air parcels at 700 mb moved only at an average of 12 knots. The trough then moved at a phase speed over twice as fast as the air parcels. At the same time the squall line moved at 30 knots from 1700 to 1830 GMT and 37 knots from 1830 to 2000 GMT, or an average of 33 knots for the 3-hour period. Therefore, the squall line slowly moved away from the trough during this period. The rapid rate of speed of this squall is hard to correlate with any particular level, but seems to best fit the 450 to 500 mb level where the average eastward component of the wind for the 3-hour period was near 25 knots, a maximum for all layers. Since this is only the eastward component of the wind (500 mb wind direction is generally from

the southwest) and the squall moved slightly ENE, it seems that this level is best correlated with the moving, mature squall line during this period.

The trailing 700 mb trough moving slower than the squall but faster than the wind at 700 mb poses the interesting question of whether it is a possible cause or effect of the squall. A first indication that it is a cause rather than effect is the fact that its movement appears nearly independent of the movement of the squall. Another indication is the observation made earlier that the shower activity appears to correlate well with the vertical motion pattern in the middle troposphere. How does this 700 mb trough appear in other fields? Is it supported or not? That is to say, is it really there?

It has been seen that the 700 mb trough appears in the streamline field. An analysis of the surface pressure tendency was done for 1-1/2-hour periods centered on 1700, 1830, and 2000 GMT. These analyses are seen in Figs. 17a, 17b, and 17c respectively. These analyses showed a definite negative surface pressure tendency line. This line paralleled the 700 mb trough axis determined by the streamlines and was positioned about 10 n.m. in front of it at 1700 and 1830 GMT. At 2000 GMT the pressure tendency line was somewhat more complex and appeared to be misshapen by the random local cells in the area, but as a whole still preceded the 700 mb trough position determined by the streamline field by an average of 10 to 15 n.m. This seems to support the proposed trough at 700 mb, and indicates that at least to this extent it is affecting conditions at the surface.

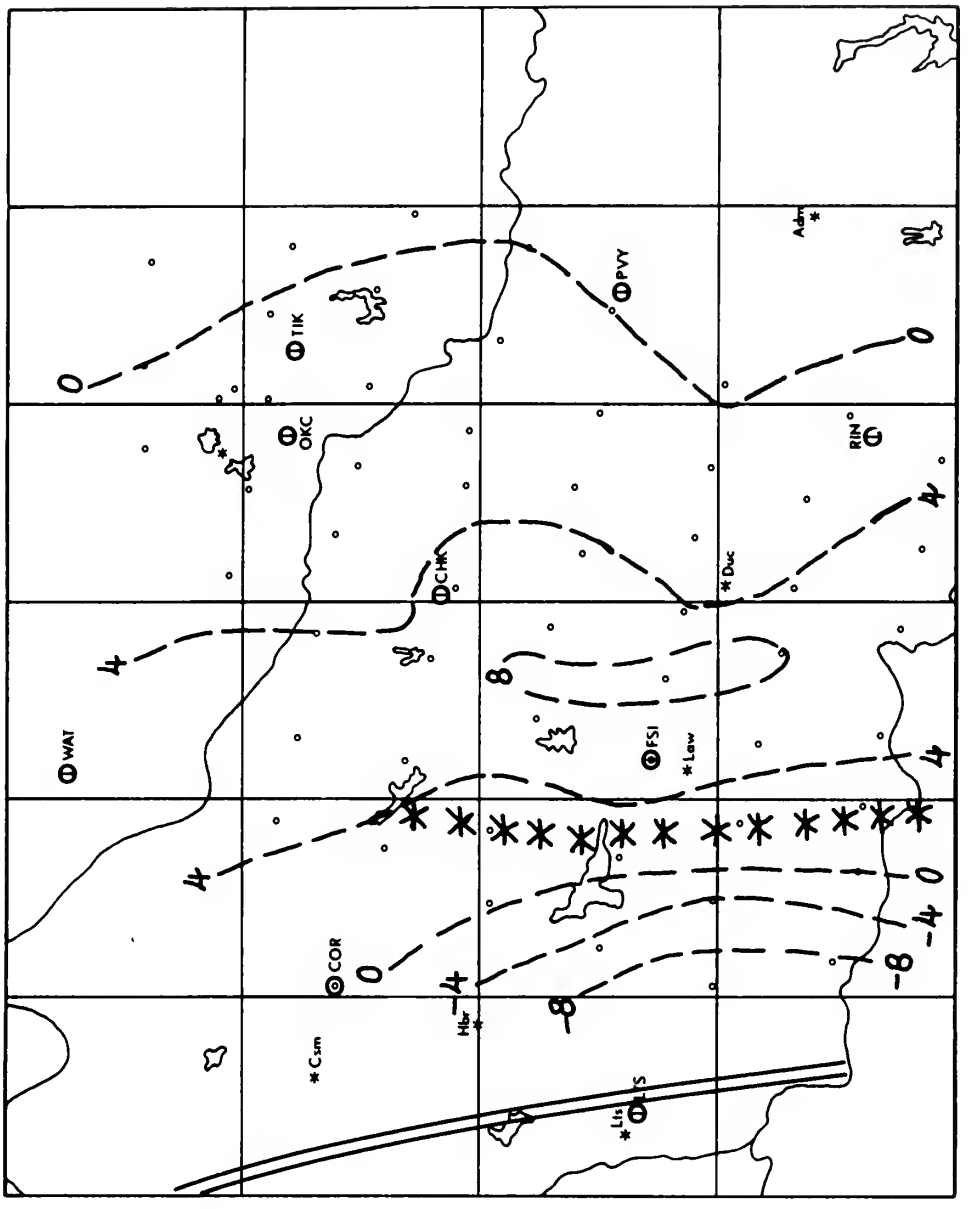

FIG. 17a. The 700 mb trough, squall line axis, and surface pressure tendency at 1700 GMT.

700 mb trough (═══)
Squall line axis (***)
3-hour surface pressure tendency centered at 1700 GMT (---) hundredths of inch of Hg

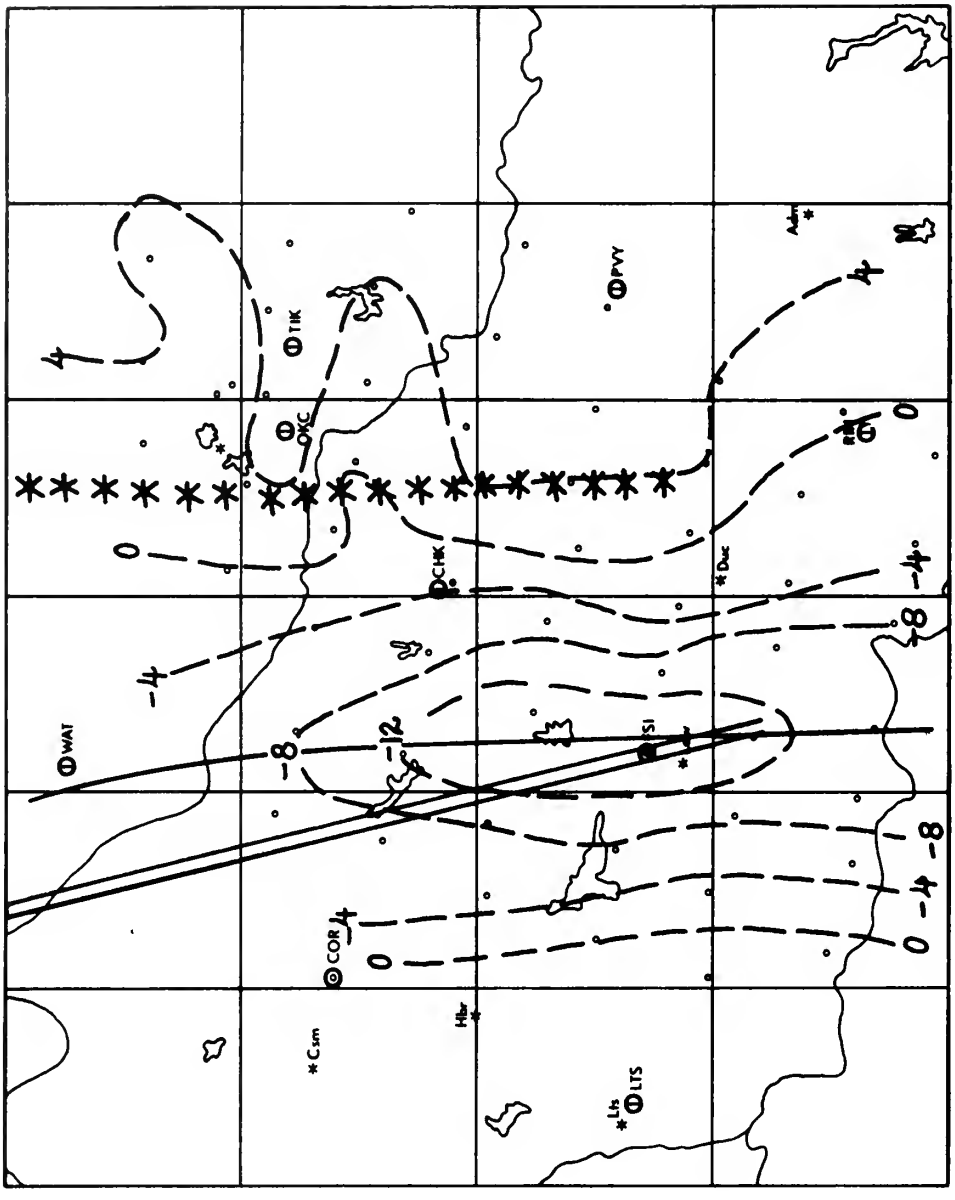

FIG. 17b. The 700 mb trough, squall line axis, and surface pressure tendency at 1830 GMT.

700 mb trough (═══)
Squall line axis (***)
3-hour surface pressure tendency centered at 1830 GMT (---) hundredths of inch of Hg
Negative surface pressure tendency axis (——)

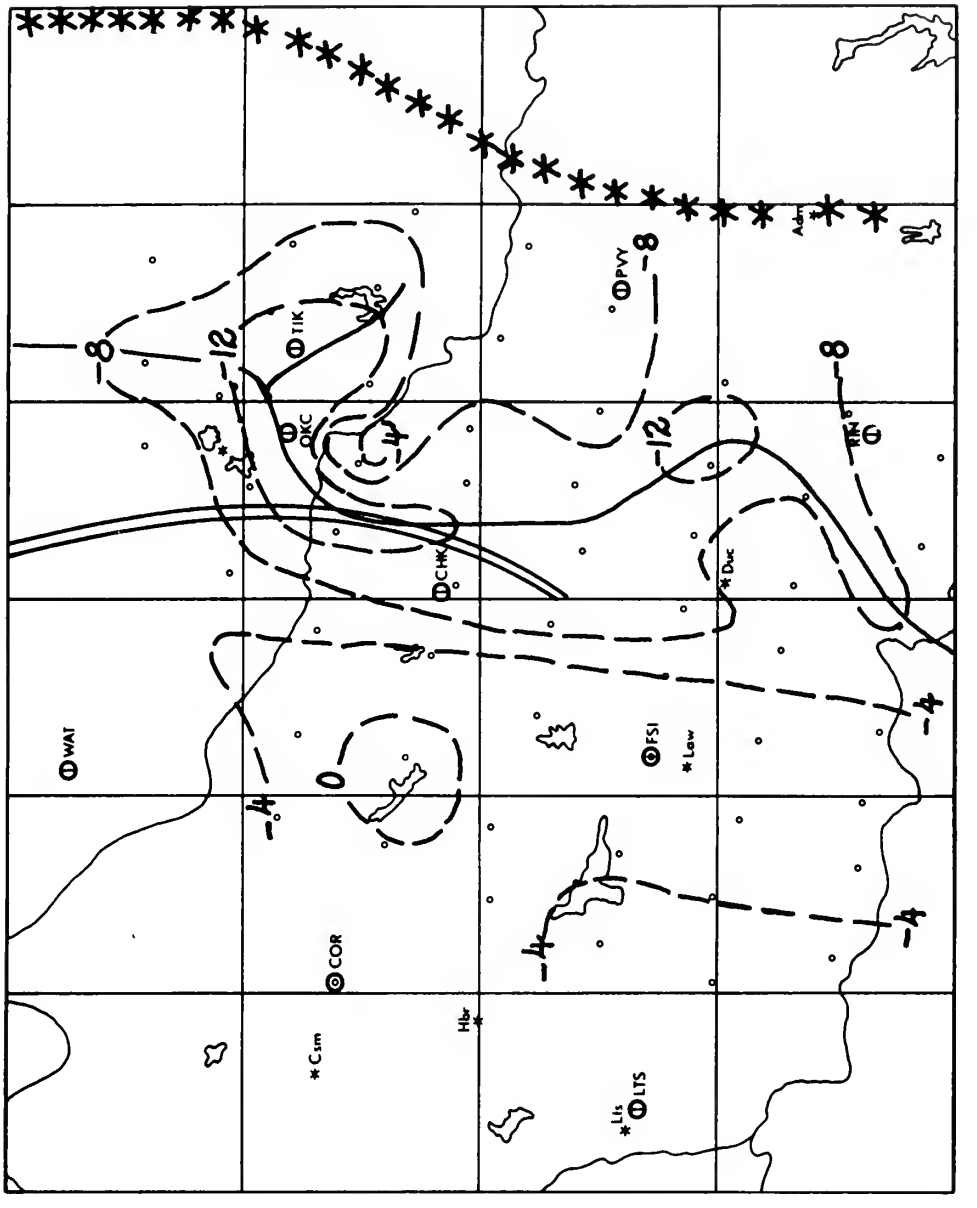

FIG. 17c. The 700 mb trough, squall line axis, and surface pressure tendency at 2000 GMT.

700 mb trough (═══)
Squall line axis (***)
3-hour surface pressure tendency centered at 2000 GMT (---) hundredths of inch of Hg
Negative surface pressure tendency axis (——)

It has been shown that the trough is moving faster than the air parcels at 700 mb. Therefore, with respect to the trough, air parcels are moving toward and through it from the east, and away from it to the west, even though both the trough and air parcels are moving in the same absolute direction. Since the trough is generally not in a shower or echo area, it is reasonable to assume that adiabatic motion takes place, or that air parcels moving into the trough are travelling on an isentropic (θ) surface. It is well known that potential vorticity (P) is conserved on a θ surface, or

$$\frac{dP}{dt} = \frac{d}{dt}\left(-\frac{\partial\theta}{\partial p}\zeta_a\right) = 0.$$

Expansion of the above expression gives

$$\frac{d}{dt}\left(-\frac{\partial\theta}{\partial p}\zeta_a\right) = \zeta_a \frac{d}{dt}\left(-\frac{\partial\theta}{\partial p}\right) + \left(-\frac{\partial\theta}{\partial p}\right)\frac{d}{dt}\zeta_a$$

$$= \zeta_a \frac{d}{dt}\left(-\frac{\partial\theta}{\partial p}\right) + \left(-\frac{\partial\theta}{\partial p}\right)\frac{d}{dt}\left(V_s K_s - \frac{\partial V_s}{\partial n}\right) = 0,$$

where $\zeta_r = V_s K_s - \frac{\partial V_s}{\partial n}$, in natural coordinates.

Inspection of Figs. 8a, 11a, and 14a shows that in the last term, as a parcel moves into the trough, the curvature part of the term is much greater than the shear part $\left(V_s K_s >> \frac{\partial V_s}{\partial n}\right)$. As a parcel moves into the trough the curvature term increases ($V_s K_s$), or relative vorticity (ζ_r) increases. As it moves westward out of the trough, the curvature term, which is a maximum in the trough, decreases, or ζ_r decreases. Consequently, ζ_r should be a maximum in the trough.

For potential vorticity to be conserved, the above expansion shows that an increase in relative vorticity must be accompanied by a decrease in stability $\left(-\frac{\partial\theta}{\partial p}\right)$. An analysis of $(\gamma_d - \gamma)$, which is a form of static stability proportional to $\left(-\frac{\partial\theta}{\partial p}\right)$, was made for all three

times. If a relative vorticity maximum does occur along the proposed trough, then it should be accompanied by a stability minimum.

Therefore, if the trough exists it should contain a minimum of stability in association with the maximum of relative vorticity along its axis. Figs. 18, 19, and 20 show the relative vorticity field, the static stability field, and the trough axis at 700 mb at 1700, 1830, and 2000 GMT respectively. At 1700 GMT the trough is near the edge of the grid area and is not too clearly defined, but at 1830 and 2000 GMT it is unmistakably there. Therefore, the static stability minimum and vorticity maximum are in the trough to the rear of the squall line at all three times.

Following the logic above, it is seen that if relative vorticity increases in front of the trough, the vorticity equation on a constant pressure surface (neglecting friction and assuming the twisting term is negligible)

$$\frac{d}{dt}\zeta_a + \zeta_a \nabla\cdot\mathbb{V} = 0$$

shows that there must be an increase in convergence. This convergence would be most pronounced near the inflection point in front of the trough. This convergence would normally cause a downward motion at the inflection point and below it, and an upward motion above 700 mb. The reverse would be true behind the trough. At all three times the divergence fields at 700 mb show a weak area of convergence in front of the trough in the area of the inflection point. From 750 mb to the surface there is generally divergence, but this is not so clear near the lower levels because of the terrain effect. However, the area of convergence is stronger above 700 mb with a maximum near 550

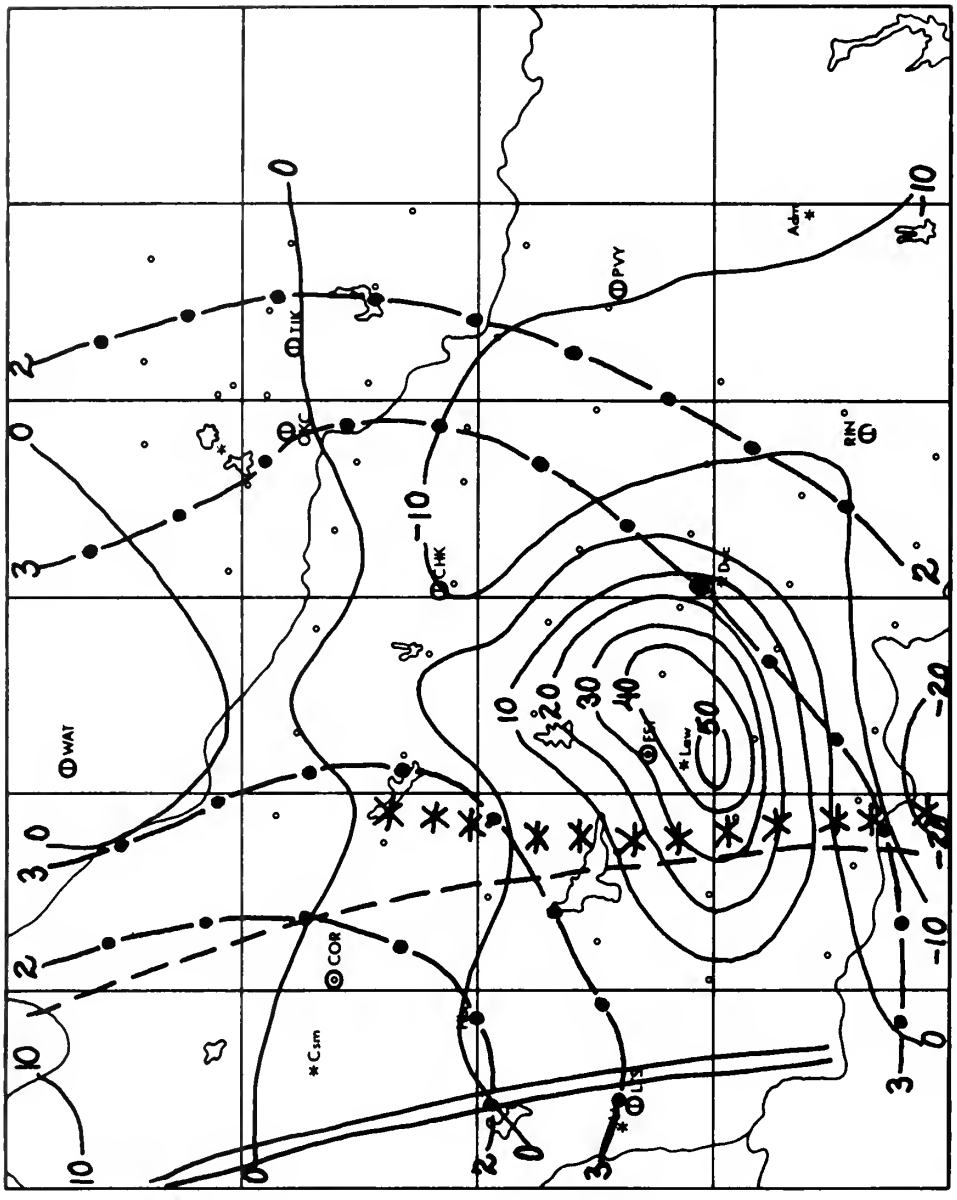

FIG. 18. 700 mb trough, vorticity, and static stability at 1700 GMT on 30 May 1967.

700 mb trough (═══)
Isobaric relative vorticity (——) 10^{-5} sec^{-1}
Static stability (γ_d-γ) (-·-)
Inflection axis 1/4 wavelength in front of 700 mb trough (---)
Axis of squall line (***)

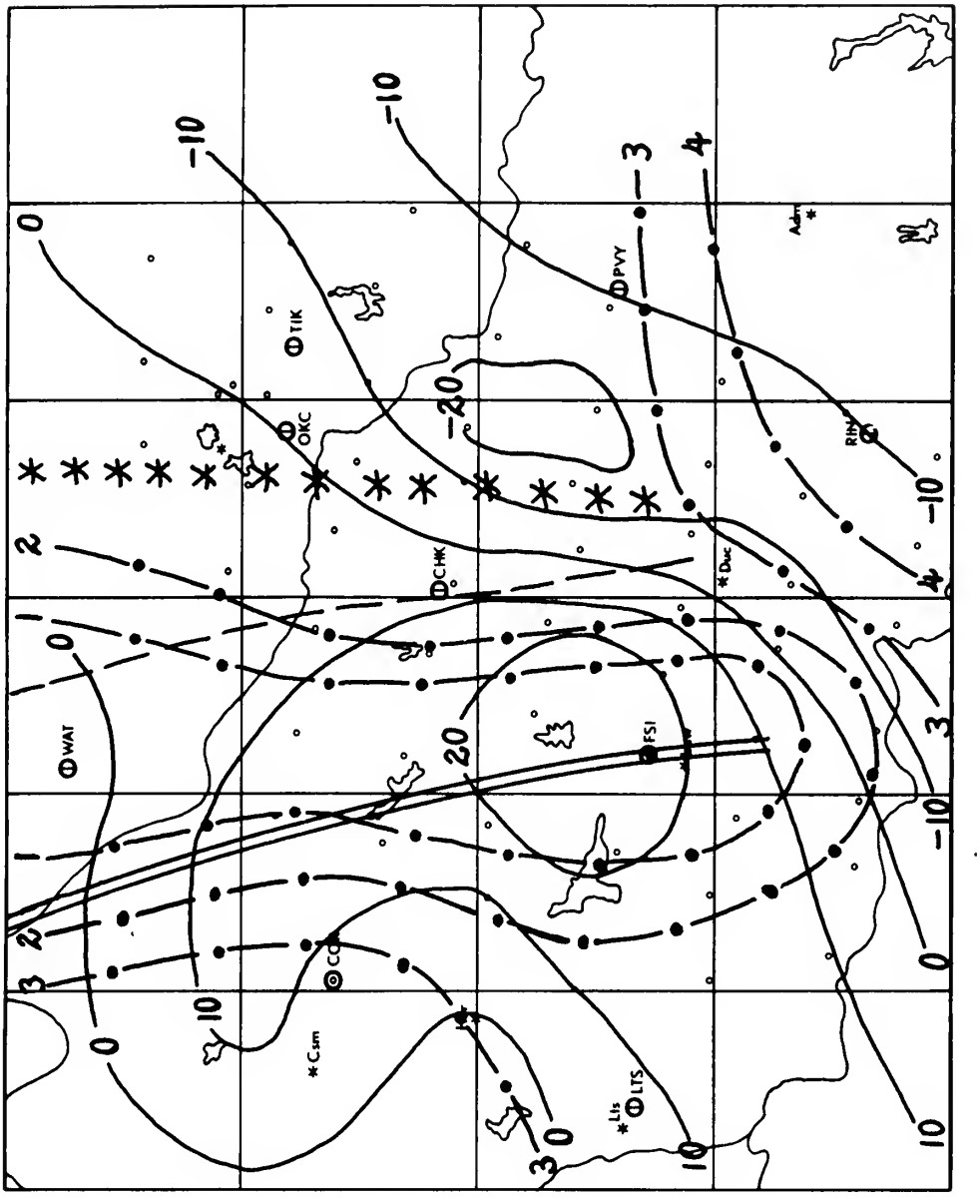

FIG. 19. 700 mb trough, vorticity, and static stability at 1830 GMT on 30 May 1967.

700 mb trough (═══)
Isobaric relative vorticity (——) 10^{-5} sec^{-1}
Static stability (γ_d-γ) (·-·)
Inflection axis 1/4 wavelength in front of 700 mb trough (---)
Axis of squall line (***)

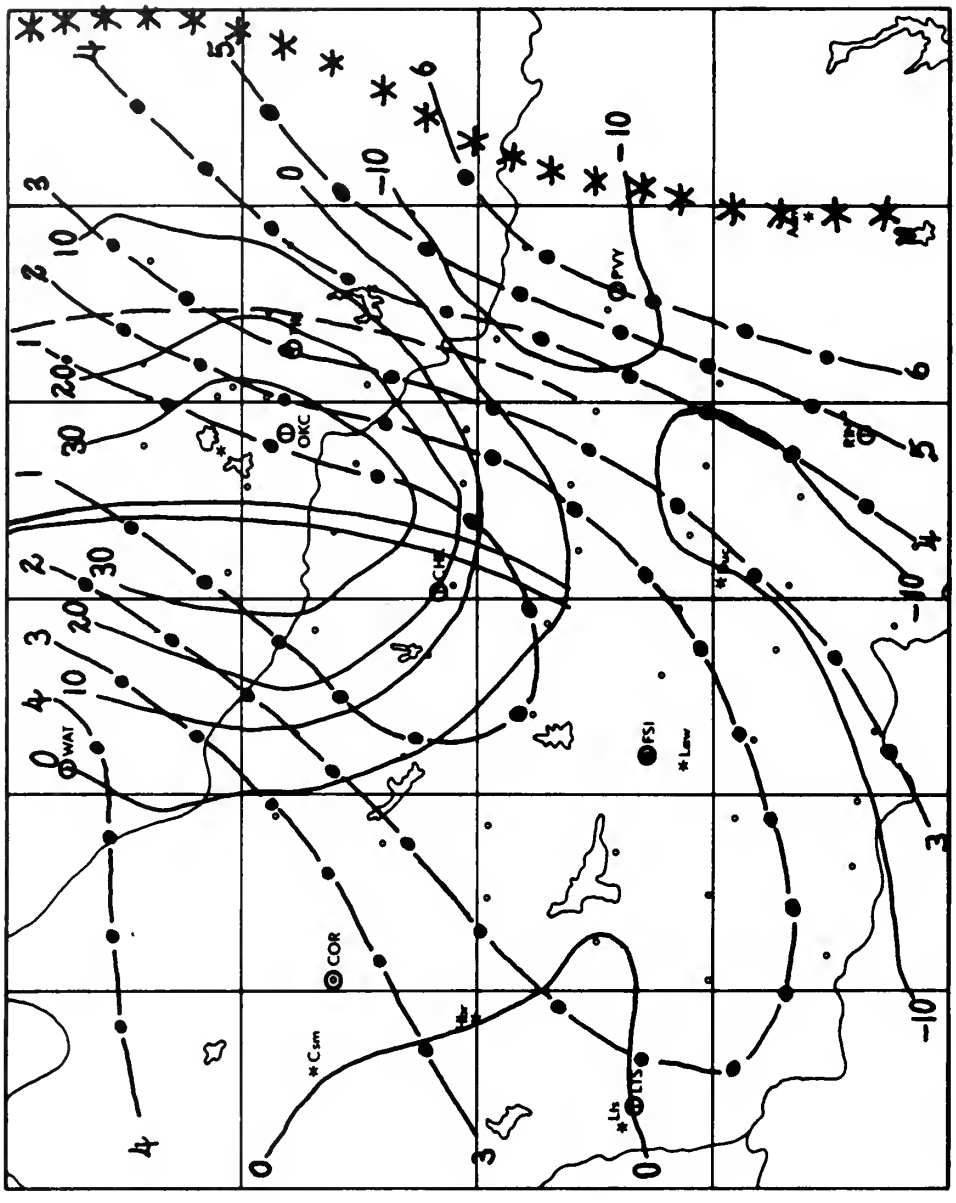

FIG. 20. 700 mb trough, vorticity, and static stability at 2000 GMT on 30 May 1967.

700 mb trough (═══)
Isobaric relative vorticity (——) 10^{-5} sec^{-1}
Static stability (γ_d-γ) (-·-)

Inflection axis 1/4 wavelength in front of 700 mb trough (---)
Axis of squall line (***)

mb. This is more true at 1830 GMT than at the other two times. This would naturally cause a larger depth of sinking air than a maximum convergence at 700 mb would.

The existence of this trough before the development of the squall line would cause sinking and divergence at 700 mb and below and rising and convergence above 700 mb in front of the trough. Unfortunately, since the mesonetwork was not activated until 1700 GMT and the initial echo was recorded at 1530 GMT, whether or not such a state existed in the mesoscale environment is impossible to determine for this case. If the 700 mb trough is moved back in time at its average propogation from 1700 to 2000 GMT to where it would have been at 1530 GMT, how would it compare to the position of the initial echo? Fig. 21 shows this estimated position and the initial echo at 1530 GMT. It shows that the initial echo is almost exactly under the inflection point in front of the 700 mb trough. This is the area of upward motion above 700 mb with increasing vorticity and decreasing stability. This then strongly indicates that the storm was initiated aloft and worked down through the lower levels.

Van Sickle (1969), in a study of the storms in the same area on 28 May 1967, also came to the similar conclusion that the storms were initiated aloft. However, he found evidence of a mesoscale wave above 200 mb, therefore his initiation position was below and behind the wave. His wave was very similar in all aspects to the one found here, except that it was evident much higher in the atmosphere.

2. As a Possible Terminator of the Squall Line

If the storm were initiated by upward motion above 700 mb, it would initially produce an echo with a relatively high base. As

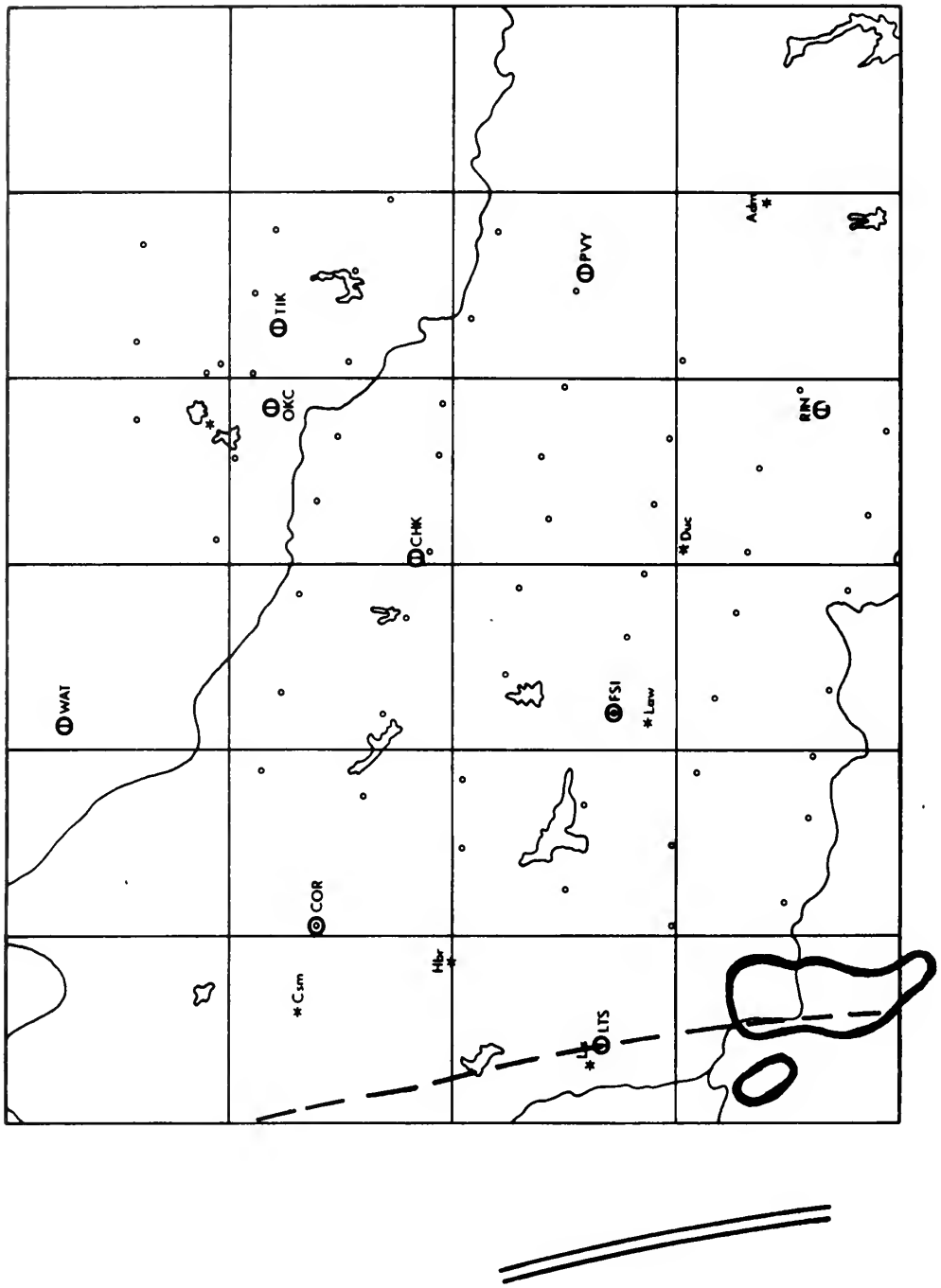

FIG. 21. Estimated position of the 700 mb trough at 1530 GMT and the initial echo.

700 mb trough (═══)
Inflection axis 1/4 wavelength in front of trough (---)
Radar return (▬▬)

the cloud grew it would definitely begin to interact with and reshape the mesoscale environment. As indicated by Takedo (1965), the building echo aloft would cause mass convergence upwind of it because of wind shear in the vertical. This then would cause an increase in the downward motion behind the cloud, and cause the base of the downward motion to rise above 700 mb. This in turn would cause an increased divergence below the inflection point near the surface. It has been shown that the squall line is moving faster than the 700 mb trough. As the echoes build, they not only cause convergence behind them aloft, but also are in turn controlled in movement by some average wind aloft, suggested in this case to be that near 500 mb. This was also the level of control found by Van Sickle (1969). As the cloud works up and down in the atmosphere and slowly moves away from its 700 mb "mother" (the inflection axis in front of the trough), it becomes the dominant feature in the area, its own motions slowly tending to dampen those caused by the environmental 700 mb trough. It soon becomes completely dominant, setting up the large convergences near the surface where the necessary moisture to sustain it is located. During this stage the maximum rainfall is recorded. However, as the squall moves further away from the 700 mb trough, it soon moves into the area of the inflection axis immediately preceding the mesoscale ridge (about 70 n.m. in front of the trough). Here, although definitely weakened by the squall itself, a weak divergence field remains. As the squall moves into it, the area of divergence acts as a destructive mechanism. Since the strongest convergence is near the surface in front of and near 550 mb behind the squall line, the 700 mb level of the squall seems the most susceptible to a divergence mechanism in the mesoscale

environment. Even a slight amount of forced divergence at 700 mb would cause a radical change in the squall. It would provide an outlet for the moist air from below, and cause the vertical motion pattern to decrease and actually reverse aloft. This would in return increase the divergence at 700 mb. The squall would in turn begin to "die" from aloft. Shortly the mesoscale trough-ridge system would once again be the dominant system in the area.

The above proposed life cycle of the squall line as determined by the 700 mb mesoscale wave system admittedly is debatable and difficult to substantiate because of the lack of data at the initiation stage and the movement of the squall outside the computational region as it begins to die at 2000 GMT. Also, knowledge of the amount and timing of the interaction of a squall line and its mesoscale environment and their effects on one another is almost completely lacking. However, some evidence that the 700 mb mesoscale wave is the controlling mechanism can be found in the data.

One indication that the squall was initiated aloft is the report of hail at 1600 GMT 20 n.m. southeast of LTS (directly in line of motion of the initial echo). This would indicate large vertical motions at and above the freezing level. The freezing level reported by LTS at 1700 GMT is between 600 and 650 mb. Yet comparison of the composite rainfall between 1615 and 1745 GMT (Fig. 10) to that between 1745 and 1915 GMT (Fig. 13) shows considerably more rainfall in the latter period. This would indicate that an upward vertical motion was present above 700 mb at 1600 GMT but not necessarily below it, where the vast majority of precipitable water exists.

Referring once again to the general fields calculated at all three times, do they support the life cycle scheme presented? At

1700 GMT, the upper levels (Fig. 10) indicate the maximum vertical motion is oriented parallel to but slightly behind the squall line, almost directly over the inflection point at 700 mb. At the lower levels (Fig. 9) some divergence and sinking is still indicated below the center (youngest part) of the squall line near the inflection axis, yet reasonably large (5 to 10 x 10^{-5} sec^{-1}) convergences are noted in front of the squall. So, this would appear to be a growth stage of the squall, with the squall line and mesoscale environment having approximately the same magnitude of effect on the resultant calculations.

By 1830 GMT, it appears the squall line is the dominant factor controlling the environment in the area. Fig. 13 indicates the maximum rainfall for all three periods considered is during this time. The upper level shows (Fig. 13) strong upward motions over the squall, but now moderate to strong (maximum of 60 mb hr^{-1}) sinking exists between the trailing 700 mb trough and inflection axis. This supports the higher level of strongest convergence mentioned previously which was proposed to be the result of the blocking action of the great heights of the squall cells. (Another factor in favor of the largest cells at this time is the previously mentioned fact that the squall moved faster from 1830 to 2000 GMT than previously.) The lower levels (Fig. 12) show intensified divergence and sinking near the trough, and convergence and upward motion in the squall area, all indicating the squall line is in full swing.

By 2000 GMT the squall line is past the 700 mb mesoscale ridge (Fig. 16) and definitely is weakened. The upper level sinking behind it has weakened sharply (maximum of 20 mb hr^{-1}) and is now centered

behind the 700 mb trough. Except for a weak strip (5 mb hr^{-1}) of sinking across the center of the inflection axis preceding the trough, upward motion appears over the inflection axis. The convergence has decreased in both magnitude and area. The lower levels (Fig. 15) still show divergence and sinking under the trough and inflection axis. Yet, as mentioned previously, numerous cells are now developing throughout the area, and the rainfall isopleths appear to extend backwards into the area (Fig. 16).

The above would seem to support the case that the mesoscale trough system is once more dominant and setting up similar fields to those supposed existing before the initial squall formed at 1530 GMT.

No data was studied after 2000 GMT. However, radar pictures (not presented) indicated some organization of cells in a north-south line coming out of the area under the inflection axis at 2000 GMT. This organization was very weak however, and random cells remained throughout the area.

VI. CONCLUSIONS AND COMMENTS

Analysis of the data for three times covering a 3-hour period of a squall line in central Oklahoma has shown that a mesoscale wave exists at 700 mb with a wavelength of 90 to 100 n.m. in the area at all three times behind the squall line. The wave is moving at nearly twice the speed of the 700 mb wind, but continually loses ground to the squall line, which is apparently being moved at about the speed of the 500 mb wind.

The mesoscale wave causes convergence in front of it, with sinking motion at 700 mb and below, and rising motion above. Its extrapolated position at 1530 GMT (the time of the initial echo) indicates it is causing upward motion above 700 mb with increasing vorticity and decreasing stability over the area where the initial cell developed. This is proposed to be the cause of the squall line.

As the squall line moves to a position approximately one-half of the 700 mb wavelength in front of its birthplace with respect to the 700 mb wave it begins to die. Since the opposite conditions (sinking aloft and rising below 700 mb) exist here than those where the storm was initiated, it is felt the 700 mb pattern causes the death of the squall line.

In between there appears to be a delicate interaction of the squall line and the mesoscale wave, a complete description of which is beyond the scope of this paper, and the science at this date. In general, the mesoscale wave appears to be the controlling factor at the initial and decay stages, and the mature squall line dominates the atmospheric fluctuations in between.

The squall line itself, at least during the time it dominates the tropospheric motions in its vicinity (mature stage), has a structure in general agreement with the classical picture of low level convergence and upper level divergence. The strong convergences (10^{-4} sec^{-1}) in the lowest levels, where sufficient moisture to maintain the squall exists, are found in the vicinity of and preceding the squall. Upward vertical motion maxima are found in and near the strongest cells near 450 mb. Divergence occurs above the jet stream, generally from 200 to 150 mb. The strong convergences noted from 650 to about 400 mb seem to indicate that considerable entrainment may be taking place, although this aspect was not investigated. These large convergences aloft, generally behind the squall, cause strong sinking and associated low relative humidities in the areas immediately proceeding the squall line. They may indeed support the "blocking action" of well organized convection as postulated by Newton (1966) and Alberty (1969). These large convergences aloft, also noted by Fankhauser (1969) and Van Sickle (1969) for the case of 28 May 1967, merit more intensive study.

Because the sounding network is always initiated at 1700 GMT, much of the possible valuable information that could be learned from the data gathered by it is lost, as on many occasions (including the one presented here) considerable activity has already developed by this time. Since a representative picture of the environment before the initial activity cannot be obtained, verification of the initial cause (in this case the 700 mb mesoscale wave) cannot be made satisfactorily. It seems that such an expensive and otherwise highly efficient network is wasting a valuable opportunity by not beginning observations prior to the initiation of convective activity.

APPENDIX A

THE PROBLEMS OF ASCENSION RATE, RELEASE TIME, TIME LAG, AND BALLOON DISPLACEMENT

As mentioned in Section III, the drift of a balloon from its launch position, the time it takes a balloon to reach a pressure level as compared to its launch time, varying launch times, and varying ascension rates of balloons (due to varying amounts of helium) are generally not considered problems on the synoptic scale because of the relatively small magnitude of these variations when compared to synoptic-scale values. However, on the mesoscale, because of the relatively short distances between stations (in this case 40-50 n.m.) and relatively short times between soundings (in this case 1-1/2 hours), these same variations are, relative to the mesoscale values, much larger and could possibly cause a misleading presentation of the atmosphere if not corrected for properly. Fankhauser (1969) has noted all these possible problems on the 28 May 1967 case and attempted to correct them whenever necessary by various means.

In the case examined here, the problems of differing ascent rates and differing times of release of the balloons would appear negligible, considering the extreme care taken to meet the standard requirements set forth to be followed by this network, also noted by Fankhauser (1969). In order to determine whether or not these two possible problems were significant for this case, the release times and ascension rates of the soundings (25 for this 3-hour period) were carefully examined. Table I shows that the maximum variation from the predetermined release time was 15 minutes at TIK at 1700 GMT.

Table II shows that the average ascension rate to 150 mb for all releases was about 49 minutes, with a maximum variation for all 25 soundings of $\pm$ 9 minutes. It is felt that these facts show that varying times of release and ascension rates are generally negligible for this case.

Now consider the possible problems of balloon displacement and time lag. Matsumoto and Ninomiya (1963) have noted that failure to take into account balloon displacement on the mesoscale can lead to errors of as much as 70% in the computation of divergence in the upper levels. However, their argument is not considered too applicable here as they considered a three station Gaussian method of computing divergence, considerably different from the standard method used here and explained in Section IV. Nor did they mention the problem of time lag at the pressure levels.

In order to determine if balloon displacement and time lag were problems in this case which could not be ignored, the following procedure was followed. To construct a vertically consistent sounding at 1830 GMT, nine levels at 1700 GMT and 1830 GMT above 600 mb (550 to 150 mb) were replotted, taking into account balloon displacement (i.e., plotting winds exactly where they were measured with respect to the reporting station). In general, rather light winds and/or winds that shift considerably with height occur at 600 mb and below. Tables II and III show that the errors associated with balloon displacement and time lag below 600 mb (average ascent time of 15 minutes to 600 mb and horizontal displacement of less than 7 km) are within the analysis limitations for a network of this density. These charts (550 to 150 mb) were analyzed and data taken using the 13 x 11 grid previously mentioned in Section I.

STATION	1700 GMT	1830 GMT	2000 GMT
SPS	1651	1828	1952
RIN	1650	1822	MSG
LTS	1656	1821	1951
FSI	1653	1837	2009
PVY	1654	1830	1956
COR	1700	1830	2000
CHK	1651	1819	1950
TIK	1715	MSG	2000
WAT	1700	1830	2000
STANDARD DEVIATION	TIK -15	CHK +11	CHK +10

TABLE I. Release times and maximum deviations from predetermined launch times for the rawinsonde mesonetwork in central Oklahoma on 30 May 1967.

LEVEL (mb)	900	750	600	450	300	150
Average time to (min)	2.21	8.19	15.1	23.47	34.68	48.92
Maximum time to (min)	4.15	10.66	21.11	30.12	42.29	58.44
Minimum time to (min)	1.32	5.81	10.95	14.98	27.85	40.21

TABLE II. Ascent times to various pressure levels of rawinsondes launched between 1700 and 2000 GMT on 30 May 1967 by the mesonetwork in central Oklahoma.

LEVEL (mb)	900	750	600	450	300	150
Average Displacement (km)	1.35	3.77	6.88	15.67	28.93	50.76
Maximum Displacement (km)	2.8	9.4	16.1	27.8	42.5	68.8
Minimum Displacement (km)	0.4	0.6	2.2	8.1	19.4	39.7

TABLE III. Balloon displacement from launch site at various pressure levels of rawinsondes launched between 1700 and 2000 GMT on 30 May 1967 by the mesonetwork in central Oklahoma.

Having balloon displacement solved, the time lag problem must also be solved, at least to the first approximation. Since the balloon displacement has been taken into account previously, it is more correct now to linearly interpolate for time correction (rather than vice-versa). Again, Tables II and III show the time correction to be considerably more linear than balloon displacement. So, using the reported times that the several balloons reached each specific pressure level, an average time for each pressure level (for each of the two general sounding times) was computed. At 1830 GMT, it was determined that all the soundings were representative of the environment and usable. At 1700 GMT, because of the tardiness of the launch at Tinker (TIK) and an early release at Wichita Falls (SPS), these two times were deleted when determining the average times because of their large deviation from the average of the rest of the soundings. The rest of the soundings at both times at each individual level were within a maximum of 14% of the average time of the level, and most cases were within $\pm$ 9 minutes of the average, or 10%. It was decided that the 14% variations were within tolerance, generally in an attempt to maintain as much of the limited data as possible. The 1700 GMT TIK data was used as an approximation, since it appeared to fit the environment. However, little if any use could be made of the SPS sounding, since it was near or in, especially in the upper levels, the leading edge of the squall line.

The general computer program, developed with advice from Dr. J. D. Mahlman, adjusted the u and v components of the wind field at 1830 GMT for time lag before being used for computations. This was done by using the average times computed and stored for each level at both

1700 GMT and 1830 GMT as indicated below:

$$B(1830) = B(t_1) + \left[B(t_2) - B(t_1)\right] \frac{(1830-t_1)}{(t_2-t_1)},$$

where B = any measured or derived variable,

t_1 = computed average time of level for 1700 GMT soundings,

and t_2 = computed average time of level for 1830 GMT soundings.

The above adjustment is made in subroutine COMSND in the computer program.

So, the u and v components of the atmospheric wind field at 1830 GMT on 30 May 1967 in the grid area should be closely represented.

Comparisons of the output fields using these adjusted u and v components and the unadjusted ones at 1830 GMT were made to determine whether or not the data could be used in the general manner without adjustments for balloon displacement and time lag. Figs. 22 - 25 show vertical profiles of adjusted divergence and vertical motion (omega) both uncorrected and corrected at four points in the grid area. For clarity, it is once more emphasized that all vertical motions presented in any figure in Appendix A are those determined by the adjusted kinematic technique (final step) as explained in Section IV-C. For these points, selected because they are in grid areas where significant values of vertical motion ($\pm$) are occurring, the uncorrected fields of u and v give a very close approximation to the profile as determined after corrections for balloon displacement and time lag. It is noted that magnitudes of both divergence and vertical motion vary somewhat, but the variability is small and in the same direction as the corrected profile, therefore causing no drastic change in the overall profile shape, certainly no more than

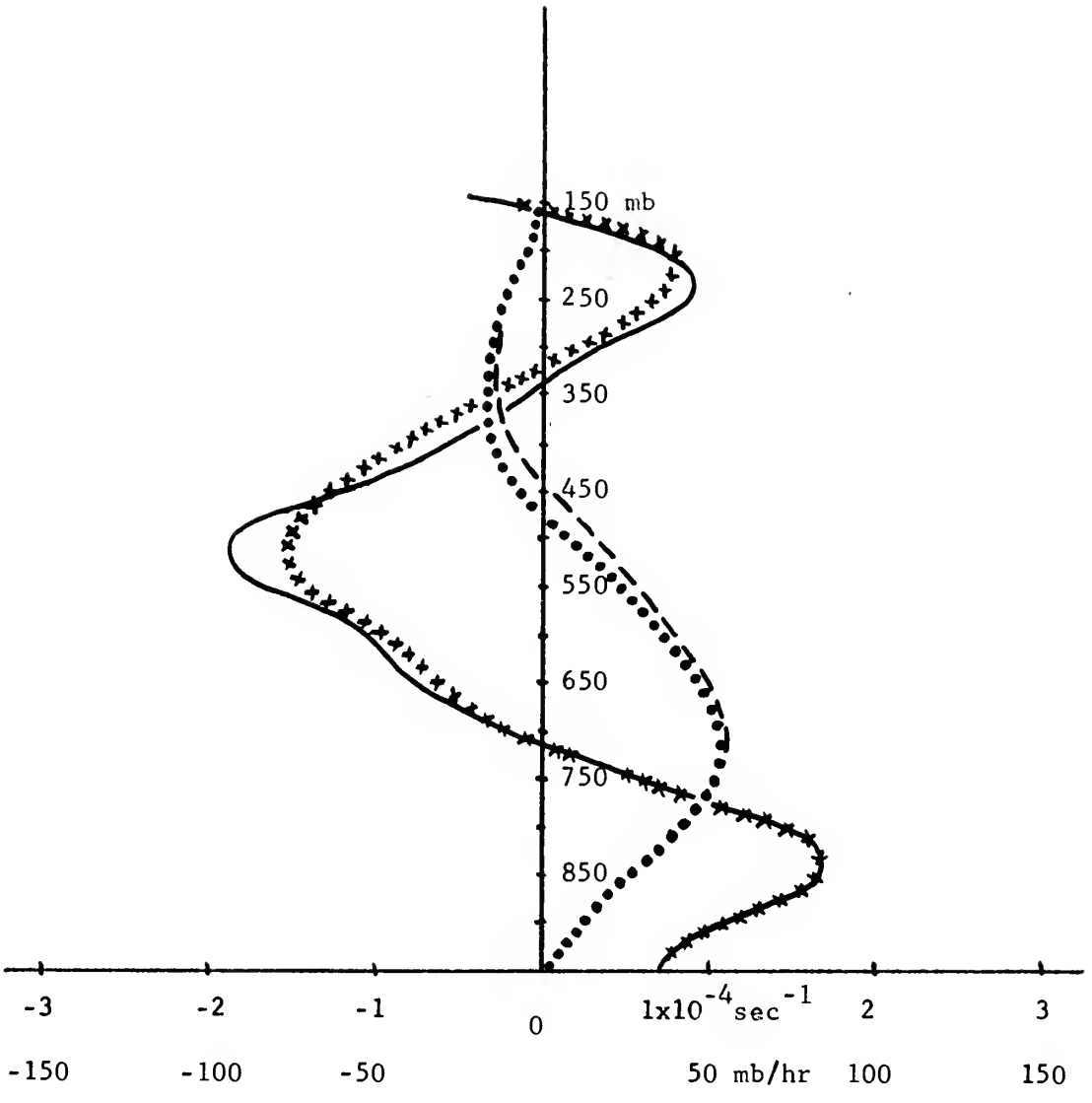

FIG. 22. Uncorrected divergence (xxx) and vertical motion (...) versus divergence (——) and vertical motion (---) corrected for balloon displacement and time lag at 1830 GMT on 30 May 1967 for grid point (5, 5) located in the Oklahoma rawinsonde mesonetwork. (Note: For location of grid points see Fig. 1).

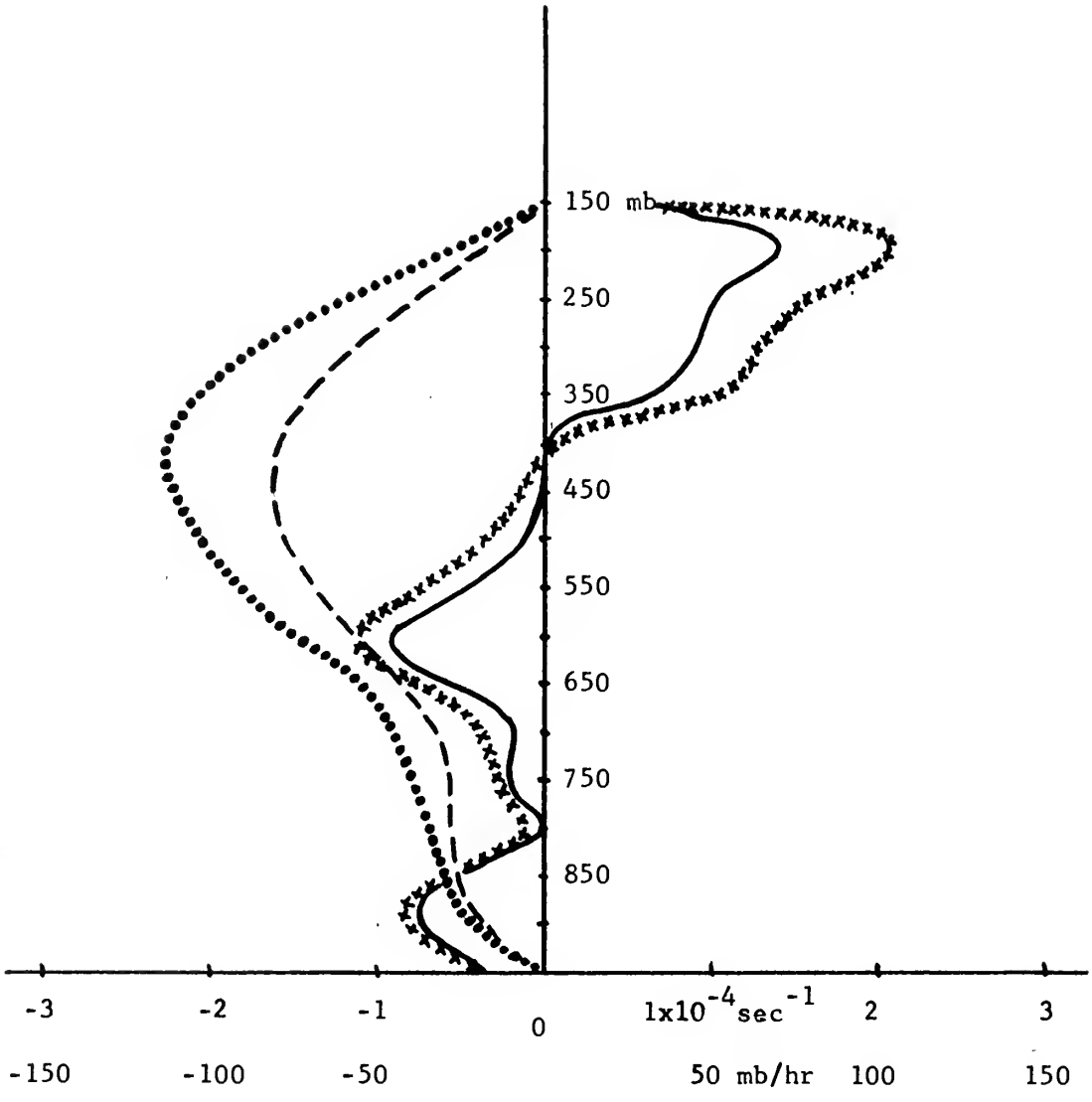

FIG. 23. Uncorrected divergence (xxx) and vertical motion (...) versus divergence (——) and vertical motion (---) corrected for balloon displacement and time lag at 1830 GMT on 30 May 1967 for grid point (9, 7) located in the Oklahoma rawinsonde mesonetowrk. (Note: For location of grid points see Fig. 1).

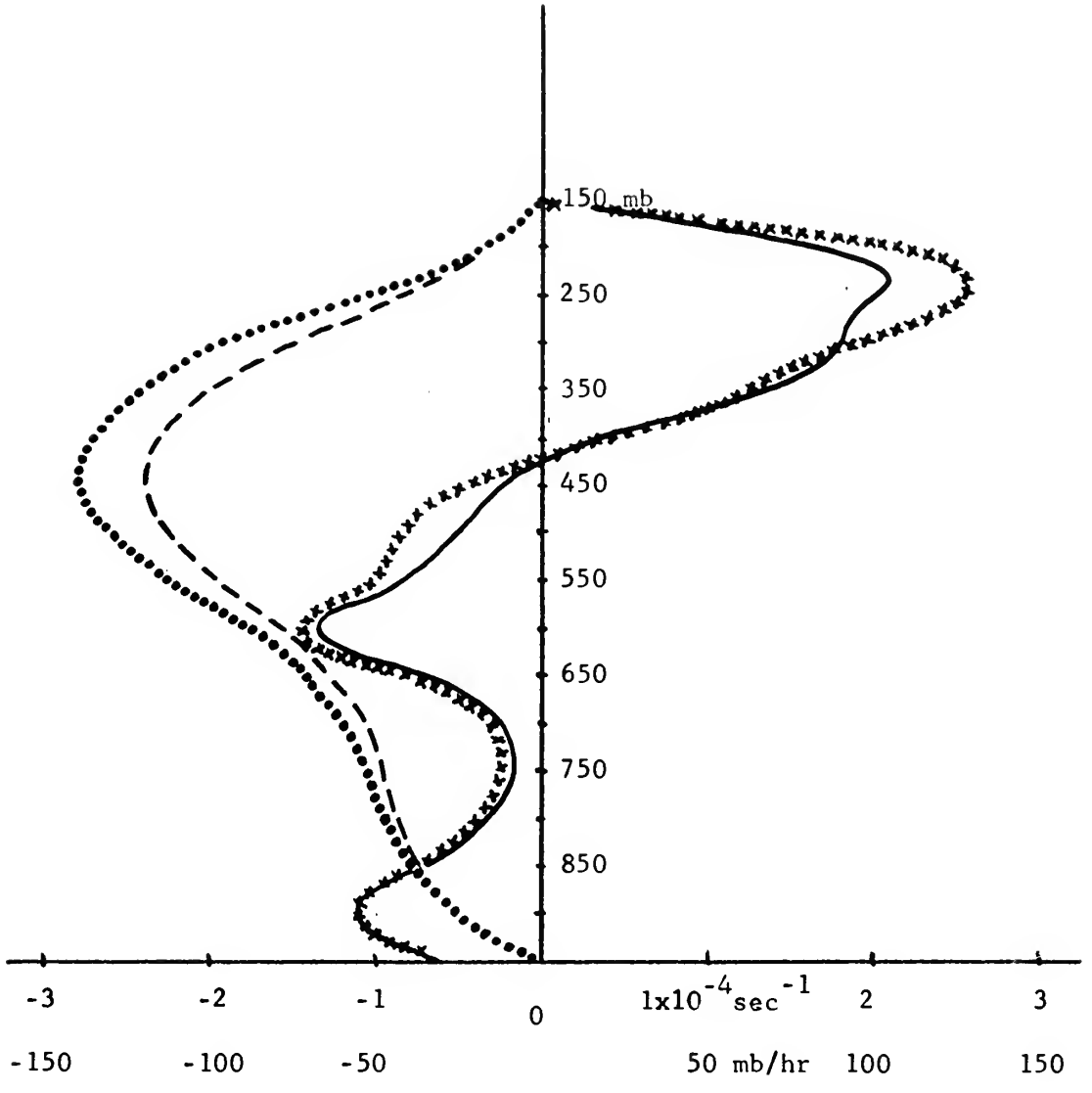

FIG. 24. Uncorrected divergence (xxx) and vertical motion (...) versus divergence (——) and vertical motion (---) corrected for balloon displacement and time lag at 1830 GMT on 30 May 1967 for grid point (10, 6) located in the Oklahoma rawinsonde mesonetwork. (Note: For location of grid points see Fig. 1).

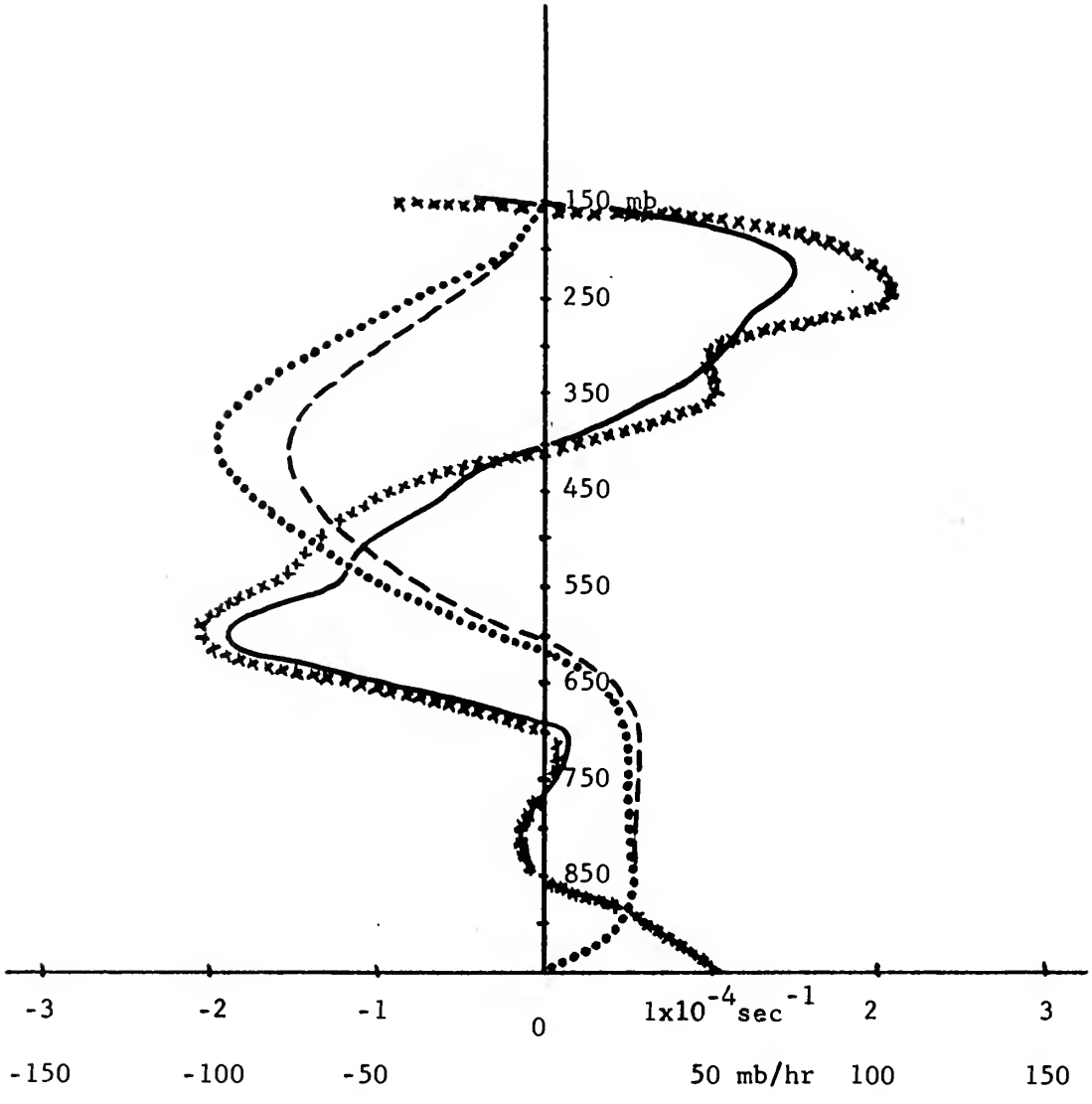

FIG. 25. Uncorrected divergence (xxx) and vertical motion (...) versus divergence (——) and vertical motion (---) corrected for balloon displacement and time lag at 1830 GMT on 30 May 1967 for grid point (9, 5) located in the Oklahoma rawinsonde mesonetwork. (Note: For location of grid points see Fig. 1).

the smoothing process does. It appears that had Matsumoto and Ninomiya (1963) also taken into account the time lag of the balloon from observation time along with balloon displacement, instead of only displacement, considerably less error would possibly have been noted in the upper levels. Of the four profiles noted here, two (Figs. 22 and 25) show a change in sign of the vertical motion with height. It is interesting to note that the corrections caused practically no change in the level at which the change in sign occurred. Also, noting the divergence patterns, the same applies to all four profiles where there is a change in the sign of the divergence. The above seems to indicate that corrections for displacement and time lag are not necessary for this case.

Leaving the vertical for a moment, examine the horizontal fields before and after correction. Figs. 26 and 27 show at 350 mb uncorrected and corrected omega fields at 1830 GMT respectively. A general look appears to indicate very similar patterns, except possibly in the southeast corner. Looking closely at grid points indicates that all maximum positive and negative omegas, although again varying slightly in magnitude, occur at the same grid points, except in two areas. These are the maximum negative center in the east central area and the maximum positive area in the southeast. The negative center has the same orientation on both figures and approximately the same magnitude. However, the maximum value is displaced one grid point. Since the actual maximum value could occur anywhere between the two grid points, one grid point variation is a definite limit of the system. Thus, the only problem area is the relatively large positive center in the southeast in Fig. 26 versus a smaller positive center

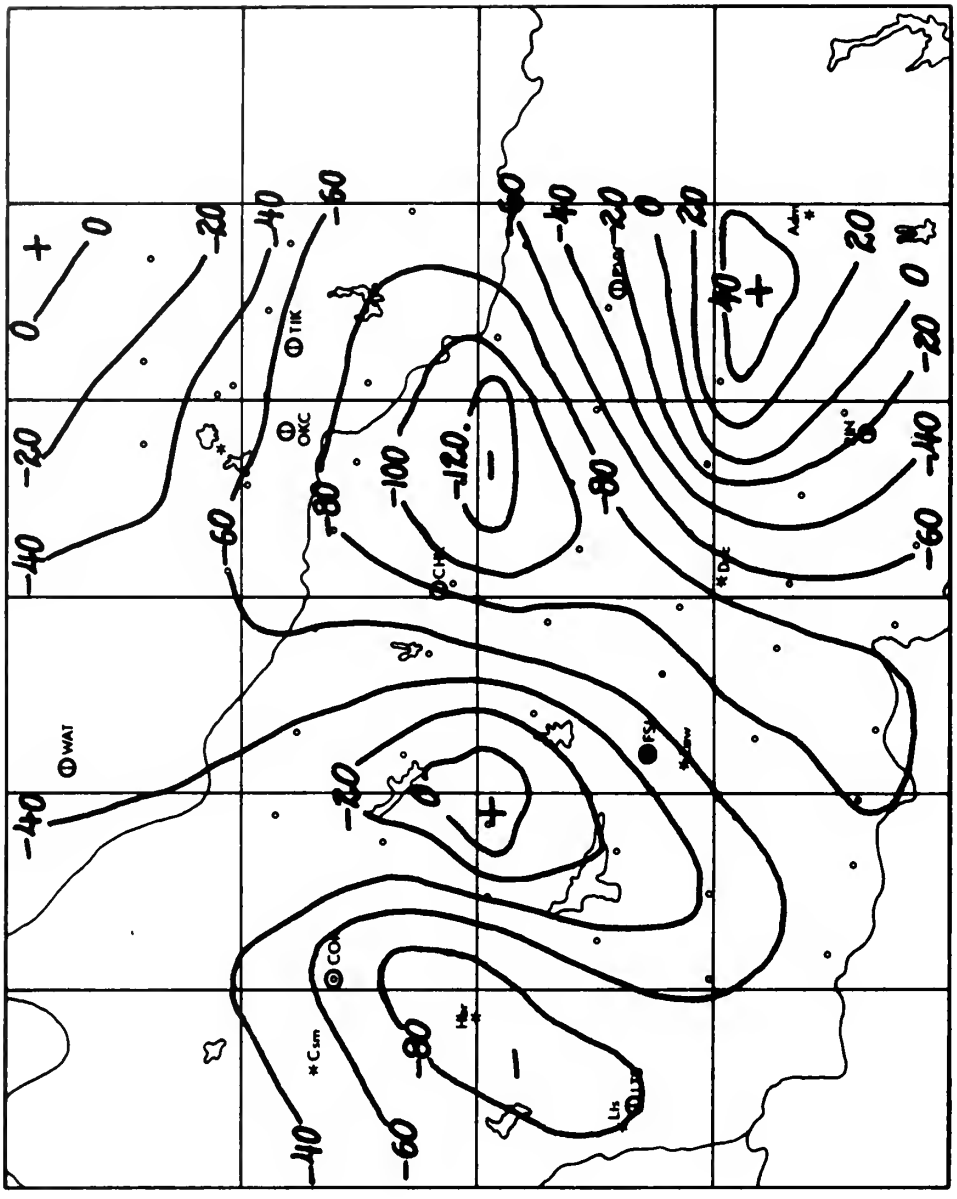

FIG. 26. The 350 mb omega field (mb hr^{-1}) calculated from the wind field which has not been corrected for balloon displacement and time lag at 1830 GMT on 30 May 1967.

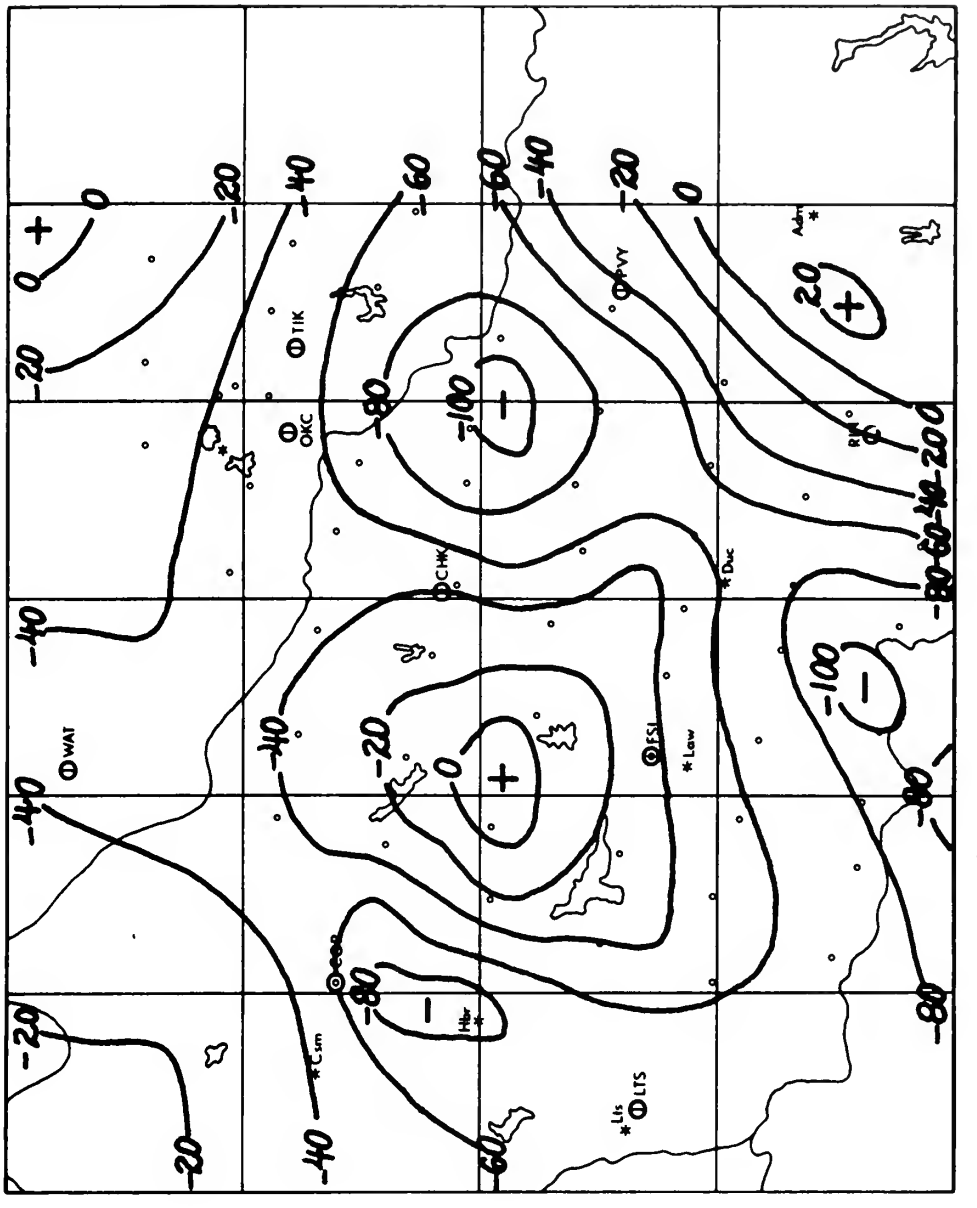

FIG. 27. The 350 mb omega field (mb hr^{-1}) calculated from the wind field which has been corrected for balloon displacement and time lag at 1830 GMT on 30 May 1967.

further to the southeast in Fig. 27. The error here can be represented by comparing the values from both figures at grid point (11, 4) which is just north of the positive center in Fig. 26 (see Fig. 1 for exact position of any grid point). In Fig. 26 it is +35, versus -10 in Fig. 27. Therefore, there is a definite need to correct for balloon displacement and time lag here. Why?

Pose the question of where one would expect the time lag not to cancel out the balloon displacement. It would seem that since the time lag varies almost linearly with height it would fail to approximately balance the balloon displacement when the balloon displacement increased rapidly and non-linearly over the same height. Where would an excessive balloon displacement occur? It would occur when there was a large vertical shear or a considerable change in wind direction with height. The former would cause a non-linear increase in displacement, and the latter a change in displacement direction which would make the fields measured downstream not compatible with that which occurred at the earlier time at the position of interest. Do such conditions occur at time 1830 GMT? If they do, is there any connection with the problematic southeast area noted earlier?

An examination of the isotach and streamline fields at 1830 GMT above 600 mb shows several positions where considerable change in speed or direction with height occurs. Since errors are additive with height and the scheme used for determining omega (Section IV-C) causes more correction with height because of radiosonde errors, concentrate on the first few levels above 600 mb where changes occur.

Figs. 28 and 29 show the streamline and isotach fields at 1830 GMT for 500 and 400 mb respectively. Comparison of the two shows several

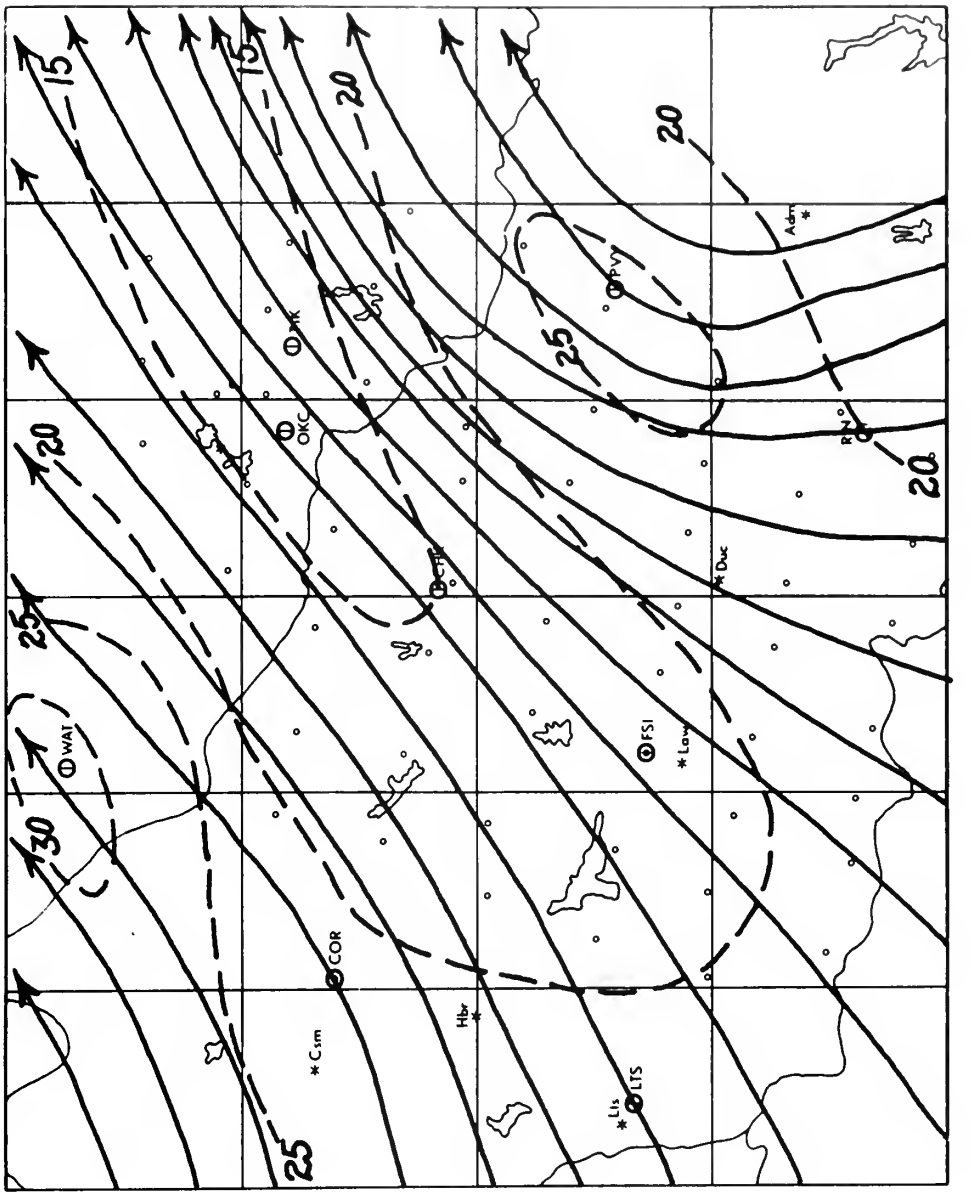

FIG. 28. Streamlines (—>) and isotachs (---) (m sec^{-1}) for 500 mb at 1830 GMT on 30 May 1967.

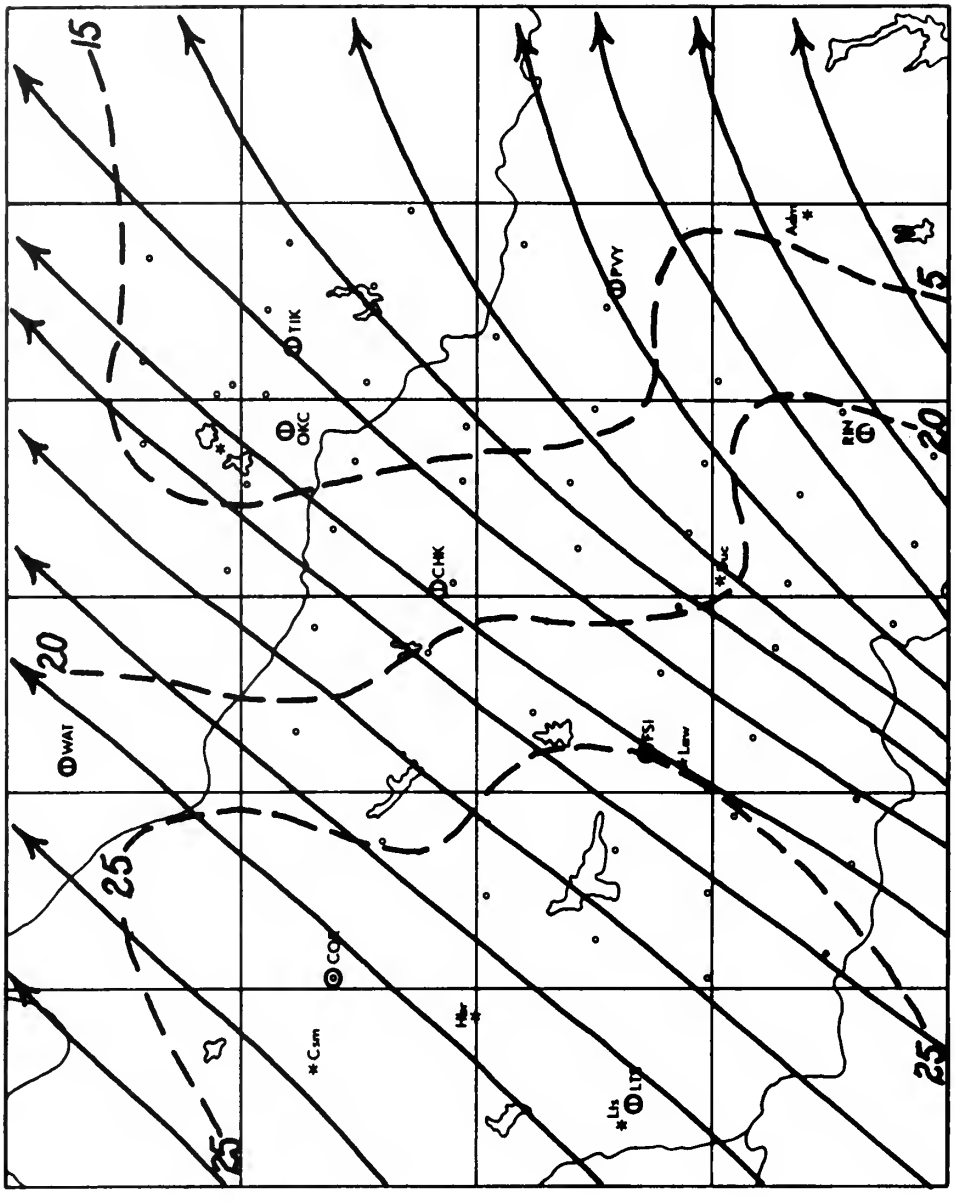

FIG. 29. Streamlines (—>) and isotachs (---) (m sec^{-1}) for 400 mb at 1830 GMT on 30 May 1967.

changes between the two levels. In particular, the wind backs in the northwest, decreases in the east central area, and veers and decreases in the southeastern area with height. It was noted previously that the southeast area was the problem area, as noted by Figs. 26 and 27. The northwest and east central area were considered acceptable. Glancing again at Figs. 26 and 27, pick three points ((2, 8), (11, 5), (11, 4)) which correspond with the northwest, east central, and southeast areas noted above. Figs. 26 and 27 show a general agreement in omega for (2, 8) and (11, 5), but strong disagreement as noted previously at (11, 4). Table IV gives wind directions and speeds for these three grid points at 500 and 400 mb. Table IV and Figs. 26 and 27 then indicate that a change of 45^{o} and 7 m sec^{-1} at (11, 4) per 100 mb is significant, but changes of 15^{o} and 12 m sec^{-1} at (11, 5) and 30^{o} and 1 m sec^{-1} at (2, 8) per 100 mb are not. Vertical plots of these three grid points above 600 mb are shown in Figs. 30 (2, 8), 31 (11, 5), and 32 (11, 4). Comparisons of vertical motions and divergence before and after corrections for displacement and time lag in these figures indicate a generally good agreement in Figs. 30 and 31, but Fig. 32 indicates that corrections must be made to get a representative picture of the environment. Therefore, Table IV, Figs. 26 and 27, and Figs. 30, 31, and 32 are all in agreement.

The above indicates that changes in speed of less than 15 m sec^{-1} or direction of 30^{o} or less per 100 mb by themselves do not necessitate making corrections for balloon displacement and time lag. Seldom, at altitudes above 600 mb will changes greater than these occur, except possibly near the tropopause where necessary corrections are so great because of radiosonde error that results are not particularly dependable anyway.

GRID POINT	500 mb		400 mb	
	Speed (m sec^{-1})	Direction (degrees)	Speed (m sec^{-1})	Direction (degrees)
(2, 8)	26	250	25	220
(11, 5)	26	225	14	240
(11, 4)	23	200	16	245

TABLE IV. Wind speeds and directions for three grid points at 400 and 500 mb at 1830 GMT on 30 May 1967 in the Oklahoma mesonetwork.

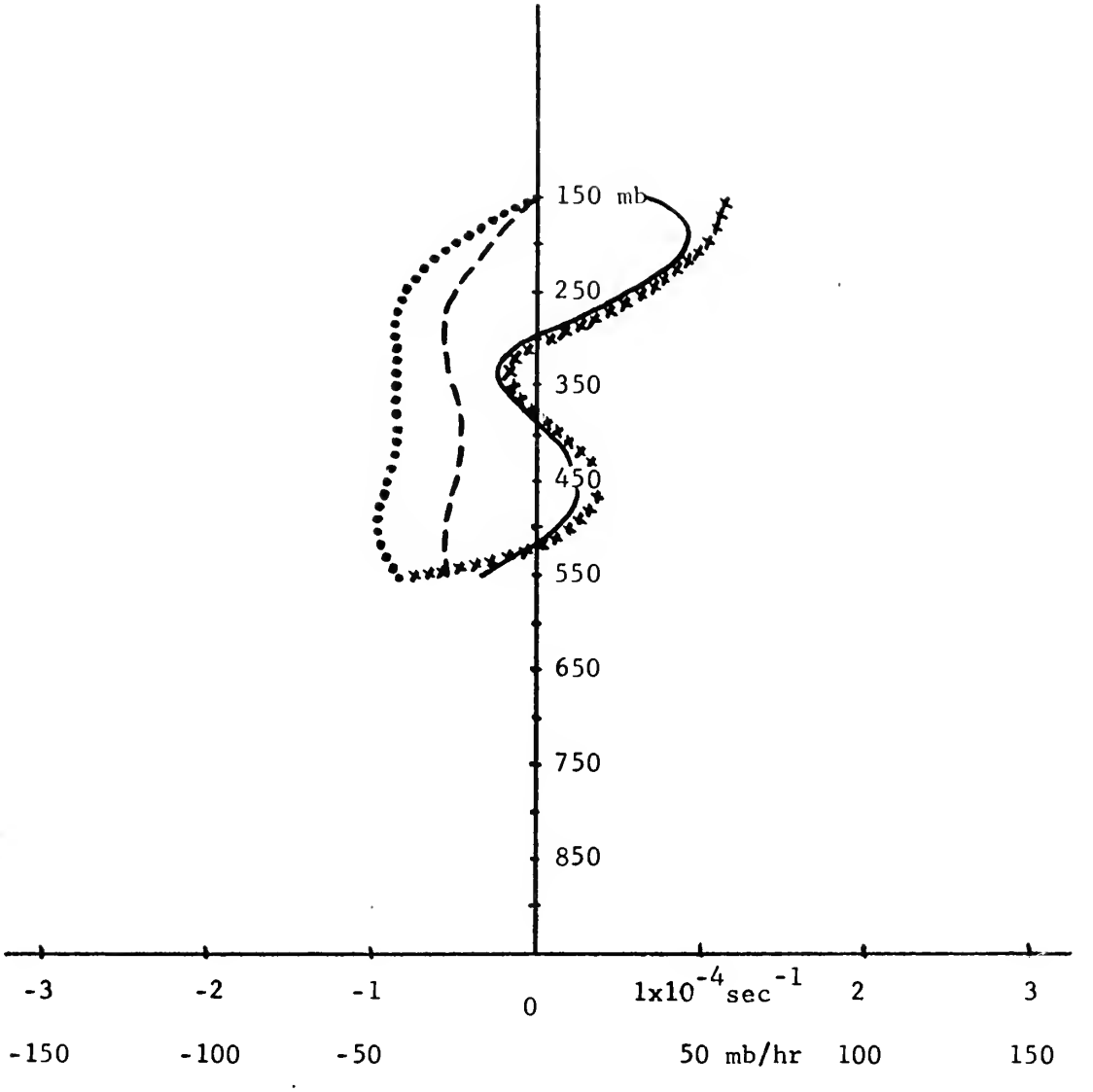

FIG. 30. Uncorrected divergence (xxx) and vertical motion (...) versus divergence (——) and vertical motion (---) corrected for balloon displacement and time lag above 600 mb at 1830 GMT on 30 May 1967 for grid point (2, 8) located in the Oklahoma rawinsonde mesonetwork. (Note: For location of grid points see Fig. 1).

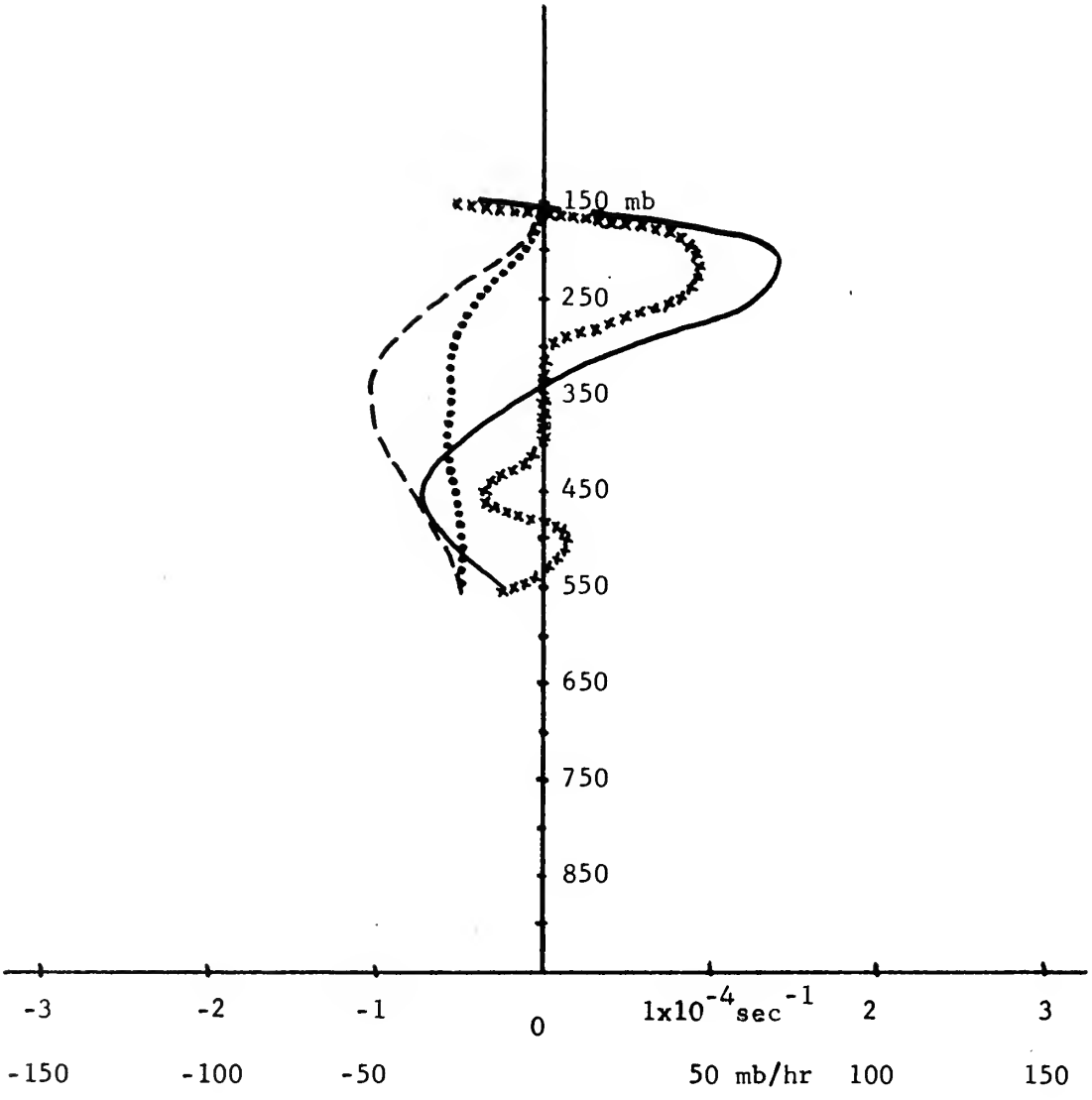

FIG. 31. Uncorrected divergence (xxx) and vertical motion (...) versus divergence (——) and vertical motion (---) corrected for balloon displacement and time lag above 600 mb at 1830 GMT on 30 May 1967 for grid point (11, 5) located in the Oklahoma rawinsonde mesonetwork. (Note: For location of grid points see Fig. 1).

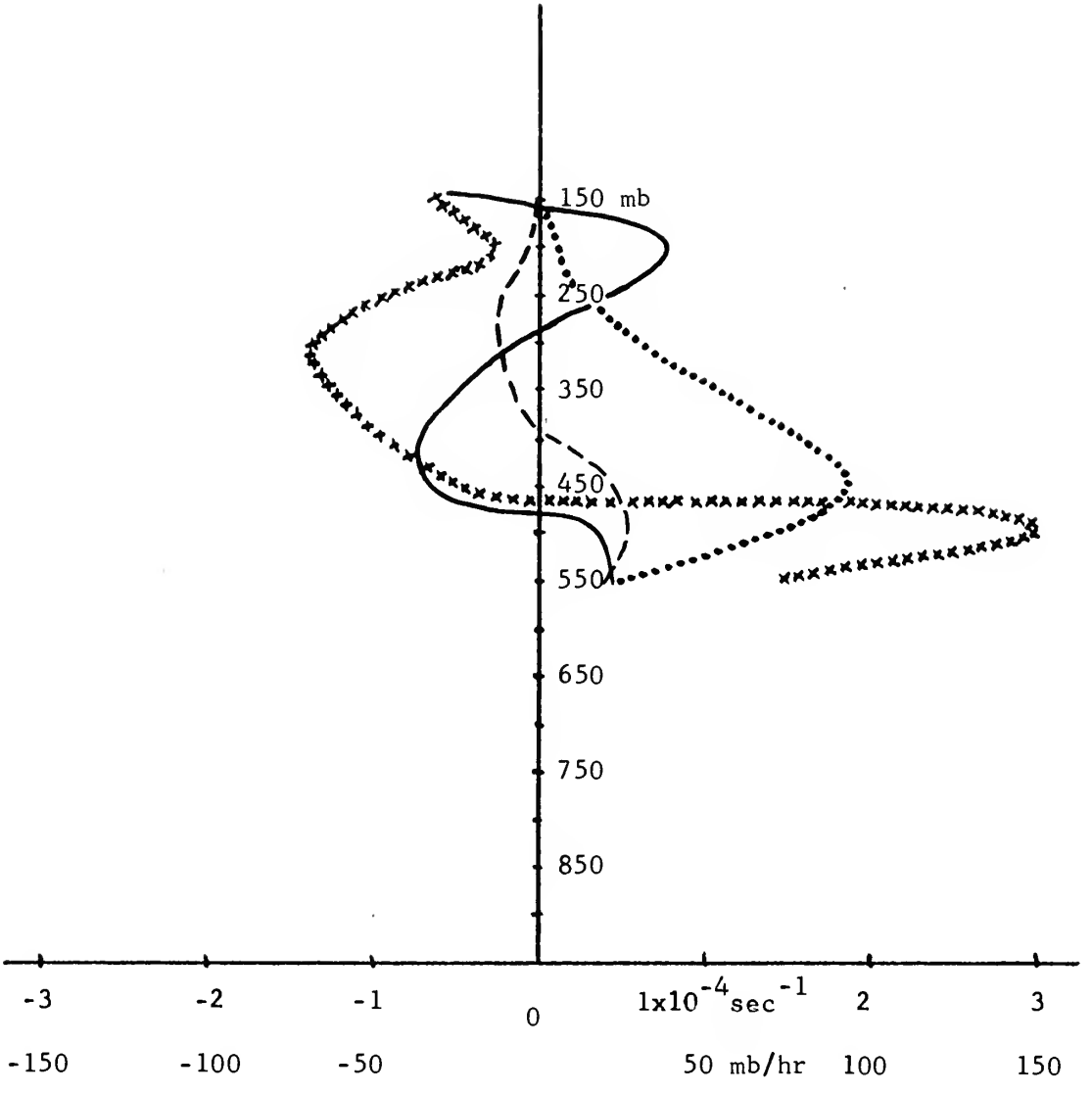

FIG. 32. Uncorrected divergence (xxx) and vertical motion (...) versus divergence (——) and vertical motion (---) corrected for balloon displacement and time lag above 600 mb at 1830 GMT on 30 May 1967 for grid point (11, 4) located in the Oklahoma rawinsonde mesonetwork. (Note: For location of grid points see Fig. 1).

A final check of the 1830 GMT data was made to get a comparison of the u and v components of the uncorrected data versus that corrected for balloon displacement and time lag. This check was a Root Mean Square (RMS) error analysis for several levels carried out by computer. Table V shows the results of this check, showing the RMSu and RMSv errors for several levels and the average u and v components for the uncorrected analyses at a few levels. The RMS values are all relatively small. The worst case shown is the RMSu at 300 mb as compared to the average u value, and that is about 30%, but the RMSv at 300 mb as compared to the average v value is of the order of 15%. As a rule, the RMS values are less than 20% of their average component values at all levels. Considering the density of data (9 stations) and the possible 10 to 20% source of error in analysis techniques alone, the results from Table V would indicate that no gross errors are made by not correcting for balloon displacement and time lag at 1830 GMT.

Therefore, all of the above checks indicate that only a combination of direction and speed changes of greater than approximately 35^{o} and 10 m sec^{-1} per 100 mb, or individual changes of greater than 15 to 20 m sec^{-1} in speed or 40 to 45^{o} in direction per 100 mb necessitate a correction for balloon displacement and time lag. These are rather severe changes, and may be unusual, as is the case of the mesoscale data used here.

The possible erroneous calculations have been noted at 1830 GMT, and the corrected values have been used in this study. The streamline and isotach fields at 1700 and 2000 GMT were checked for possible problem areas using the above stated criteria. Except for a few possible problem areas near 200 mb (the jet stream maximum problem

LEVEL (mb)	RMSu (knots)	RMSv (knots)	Average u (knots)	Average v (knots)
550	2.95	2.86	--	--
500	3.65	9.03	--	--
450	2.41	3.24	26.97	30.60
400	4.77	5.98	--	--
350	8.25	7.29	--	--
300	5.54	5.30	18.09	35.04
250	7.52	6.85	--	--
200	7.05	5.76	--	--
150	3.73	5.78	21.81	29.46

TABLE V. The root mean square (RMS) error of the uncorrected u and v components of the wind versus the u and v components corrected for balloon displacement and time lag, and the average u and v components at specific pressure levels at 1830 GMT on 30 May 1967 in the Oklahoma mesonetwork.

already noted), both 1700 and 2000 GMT data appear to meet the criteria limitations above. Therefore, no correction for balloon displacement and time lag was deemed necessary.

If the criteria stated here can be considered a first approximation for a general rule, then hopefully, since this case appears to be one of reasonably large wind speeds aloft, a more general case might fit the criteria even better, and show even less error in computations when no corrections for balloon displacement and time lag are made. The advantages of being able to use data without corrections are easily seen. Some of these are:

(1) considerable savings in time;

(2) ability to use all data periods reported (correction scheme causes loss of at least one time period due to interpolation requirements);

(3) and one is not dependent on the assumption of linear changes between soundings to construct a new sounding.

Because of our limited ability to measure mesoscale phenomena or to separate mesoscale and microscale motions and their possible interactions, it seems hardly worthwhile and possibly misleading to use detailed techniques to correct admittedly crude data, if the data meets certain general criteria and therefore can be used as is.

APPENDIX B

RESULTS OF THE COMPLETE VORTICITY METHOD (VOROMG)

The complete vorticity method, labelled VOROMG in the computer program, was used in an attempt to determine vertical motion fields at 1830 GMT (one time was all that was possible because of the $\frac{\partial \zeta_r}{\partial t}$ term - found in FUN1).

The same program, with minor alterations, was used by Dr. J. D. Mahlman to determine omega fields on the synoptic scale. He obtained total convergence in less than five cycles. The fields of omega obtained from this method (VOROMG) compared favorably with fields obtained by a separate omega equation method and those determined by the adjusted kinematic method (KINOMG). However, the VOROMG omegas were somewhat larger on the average than those determined by KINOMG. Mahlman also found that the twisting term (FUN2), which is shown to be negligible on the synoptic scale by scale analysis, is in reality quite often a significant contribution to the final answer. This is in good agreement with the previously noted results of Yanai and Nitta (1967).

The success of the vorticity method on the synoptic scale was encouraging. However, all attempts to obtain convergence on the mesoscale failed. The method always diverged on the mesoscale, even though a first approximation using only FUN1 (equation without the twisting term) showed that the requirement that omega be zero at the top of the atmosphere (150 mb) had been met. This same first approximation indicated enormous (500 to 1000 mb hr^{-1}) vertical motions in

the middle troposphere, with a few cases of adjacent values being near this size and of opposite sign! The problem apparently was caused by the advection of vorticity in FUN1. Printouts of vorticity, especially in the lower and middle troposphere, showed much more complex fields than was the case for divergence. Apparently, cases of adjacent large values of vorticity of opposite sign, when acted upon by the vorticity advection term, caused fatally large values. These extremely large and sometimes random values of omega shown by the first approximation frustrated any possible attempt towards convergence. Attempts to smooth the vorticity field and to control the size of absolute vorticity (ζ_a - found in the denominator of both FUN1 and FUN2) were not successful.

Even though the method failed on the mesoscale, its use on the synoptic scale may prove useful and very informative, especially in regard to the size of the formerly disregarded twisting term.

```
C
C     DETERMINATION OF VORTICITY, DIVERGENCE, AND VERTICAL MOTION BY THE
C     ADJUSTED KINEMATIC AND COMPLETE VORTICITY METHODS.
C
C     THIS PROGRAM WAS ESPECIALLY DEVELOPED BY R. J. COLEMAN WITH ADVICE
C     FROM DR. J. D. MAHLMAN AT THE U. S. NAVAL POSTGRADUATE SCHOOL
C     FOR USE ON A MESOSCALE RAWINSONDE DATA NETWORK IN CENTRAL
C     OKLAHOMA.  IT WAS USED FOR COMPUTATIONS IN THE AUTHORS MASTERS
C     THESIS TITLED ' A DIAGNOSTIC ANALYSIS OF THE 30 MAY 1967 SQUALL
C     LINE IN CENTRAL OKLAHOMA '. THIS STUDY WAS CONDUCTED IN THE
C     SPRING AND SUMMER OF 1969 AT THE U. S. NAVAL POSTGRADUATE
C     SCHOOL .  THE THESIS ADVISOR WAS DR. J. D. MAHLMAN.
C
C     THE PURPOSE OF THE MAIN PROGRAM IS TO CALL SUBROUTINES .
C
      COMMON NI, NJ, NK, NL, BL, BLI, PIE,
     1DX(11),U(13,11,17,3),V(13,11,17,3),DY2,CF(11),VOR(13,11,17,3),
     2MJ,MI,DIV(13,11,17,3),ABSVOR(13,11,17,3),OMEGK(13,11,17,3),
     3NKM1,NKM2,DP,DX2(11),PSFC(13,11),P(17),DP1,DT,NIM2,NIM3,NJM2,
     4NJM3,FUN1(13,11,17,1),FUN2(13,11,17,1),WN(13,11,17,1),
     5WNPLS1(13,11,17,1),EPS,T(9,2)
C
      DIMENSION DD(13,11,17,3), FF(13,11,17,3)
      EQUIVALENCE (U,DD), (V,FF)
C
      CALL RREAD
      CALL CONST
      CALL COMSND
      CALL VORTY
      CALL DIVERG
      CALL KINOMG
      CALL VOROMG
      CALL PRINT1
      STOP
      END
```

```
      SUBROUTINE RREAD
C
C     THE PURPOSE OF THIS SUBROUTINE IS TO READ THE DATA:
C     DD= WIND DIRECTION IN DEGREES
C     FF= WIND FORCE IN METERS PER SECOND
C     BL= BASE LATITUDE OF GRID IN DEGREES MINUS BLI
C     BLI=LATITUDE INCREMENT OF GRID POINTS
C     DP =LAYER DEPTH IN MB THRU WHICH EACH INTEGRATION OCCURS
C     NI =NUMBER OF X DATA POINTS
C     NJ =NUMBER OF Y DATA POINTS
C     NK =NUMBER OF Z LEVELS
C     NL =NUMBER OF TIME INCREMENTS
C     PSFC=THE SURFACE PRESSURE IN MBS DETERMINED FROM THE STANDARD
C     ATMOSPHERE FOR EACH ELEVATION.
C     DT =TIME INCREMENT IN SECONDS
C
C     AND TO CONVERT FF INTO KNOTS.
C
C     GRID SIZE = NI BY NJ
C
      COMMON NI, NJ, NK, NL, BL, BLI, PIE,
     1DX(11),U(13,11,17,3),V(13,11,17,3),DY2,CF(11),VOR(13,11,17,3),
     2MJ,MI,DIV(13,11,17,3),ABSVOR(13,11,17,3),OMEGK(13,11,17,3),
     3NKM1,NKM2,DP,DX2(11),PSFC(13,11),P(17),DP1,DT,NIM2,NIM3,NJM2,
     4NJM3,FUN1(13,11,17,1),FUN2(13,11,17,1),WN(13,11,17,1),
     5WNPLS1(13,11,17,1),EPS,T(9,2)
C
      DIMENSION DD(13,11,17,3), FF(13,11,17,3)
      EQUIVALENCE (U,DD), (V,FF)
C
      READ(5,5) NI, NJ, NK, NL, BL, BLI, DP, DT
    5 FORMAT(4I2,4F5.0)
      READ(5,9)  ((((DD(I,J,K,L),I=1,NI),J=1,NJ),K=1,NK),L=1,NL)
      READ(5,10) ((((FF(I,J,K,L),I=1,NI),J=1,NJ),K=1,NK),L=1,NL)
      READ(5,9)  ((PSFC(I,J),I=1,NI),J=1,NJ)
    9 FORMAT(13(F3.0,2X))
   10 FORMAT(13F5.0)
      READ(5,11) ((T(K,L),K=1,9),L=1,2)
   11 FORMAT(9F5.0)
C
C     CONVERT FF FROM METERS PER SECOND TO KNOTS
      DO20L=1,NL
      DO20K=1,NK
      DO20J=1,NJ
      DO20I=1,NI
      FF(I,J,K,L)=FF(I,J,K,L)*1.9424
   20 CONTINUE
      RETURN
```

```
      END



      SUBROUTINE CONST
C
C     THE PURPOSE OF THIS SUBROUTINE IS TO DETERMINE THE U AND V
C     COMPONENTS OF THE WIND. ALSO , DETERMINE THE LATITUDE INTERVALS
C     DX IN TERMS OF RADIANS. DY2 = TWICE THE LATITUDE INTERVAL IN
C     NAUTICAL MILES FOR USE IN PARTIAL DIFFERENTIATION.
C     DX2(J) = TWICE THE LONGITUDE INTERVAL IN NAUTICAL MILES.
C
      COMMON NI, NJ, NK, NL, BL, BLI, PIE,
     1DX(11),U(13,11,17,3),V(13,11,17,3),DY2,CF(11),VOR(13,11,17,3),
     2MJ,MI,DIV(13,11,17,3),ABSVOR(13,11,17,3),OMEGK(13,11,17,3),
     3NKM1,NKM2,DP,DX2(11),PSFC(13,11),P(17),DP1,DT,NIM2,NIM3,NJM2,
     4NJM3,FUN1(13,11,17,1),FUN2(13,11,17,1),WN(13,11,17,1),
     5WNPLS1(13,11,17,1),EPS,T(9,2)
C
      DIMENSION DD(13,11,17,3), FF(13,11,17,3)
      EQUIVALENCE (U,DD), (V,FF)
C
      PIE=3.141593
      DO10L=1,NL
      DO10K=1,NK
      DO10J=1,NJ
      DO10I=1,NI
C     CONVERT DEGREES TO RADIANS
      RAD=DD(I,J,K,L)*PIE/180.0
C     DETERMINE U AND V IN NAUTICAL MILES PER SECOND
      U(I,J,K,L)=-FF(I,J,K,L)*SIN(RAD)/3600.0
      V(I,J,K,L)=-FF(I,J,K,L)*COS(RAD)/3600.0
   10 CONTINUE
C
C     COMPUTE 2 DY
      DY2=BLI*2.0*60.0
C     COMPUTE DX
      DO20J=1,NJ
      DX(J)=(BL+BLI*J)*PIE/180.0
      DX2(J)=DY2*COS(DX(J))
   20 CONTINUE
C
C     COMPUTE CORIOLIS FORCE
      DO30J=1,NJ
      CF(J)=2.0*0.72921E-04*SIN(DX(J))
   30 CONTINUE
C
```

```
C       COMPUTE NUMEROUS LIMITS TO BE USED IN PROGRAM
        NI=NI-1
        NIM2=NI-2
        NIM3=NI-3
        NJ=NJ-1
        NJM2=NJ-2
        NJM3=NJ-3
        NKM1=NK-1
        NKM2=NK-2
C
C       SET EPSILON FOR USE IN VOROMG
C       EPS USED HERE IS ABOUT 1.5 MB/HR
        EPS=0.5E-03
C
        GO TO 50
C     THIS IS TO BE USED FOR PRINTING OLD U AND V
C     CONVERT U AND V TO KNOTS
CC
     35 DO40K=1,NK
        DO40J=1,NJ
        DO40I=1,NI
        U(I,J,K,2)=U(I,J,K,2)*3600.
        V(I,J,K,2)=V(I,J,K,2)*3600.
     40 CONTINUE
        DO45K=1,NK
        DO45J=1,NJ
     45 WRITE(7,46) (U(I,J,K,2),I=1,NI), J, K
     46 FORMAT(13F5.1,5X,2I2)
        DO47K=1,NK
        DO47J=1,NJ
     47 WRITE(7,46) (V(I,J,K,2),I=1,NI), J, K
     50 RETURN
        END



        SUBROUTINE COMSND
C
C       THE PURPOSE OF THIS SUBROUTINE IS TO TAKE DATA ABOVE 600 MB AT
C       TIMES 1 AND 2 AND CONSTRUCT A VERTICAL SOUNDING AT TIME 2. IT
C       IS FOUND THAT FOR THE CASE BEING STUDIED THE BALLOONS REACH THE
C       600 MB LEVEL IN AN AVERAGE TIME OF 15 MINUTES, AND HAVE AN AVERAGE
C       HORIZONTAL DISPLACEMENT OF 6.88 KM. BOTH OF THESE ARE CONSIDERED
C       ACCEPTABLE DEVIATIONS CONSIDERING THE ABILITY TO ANALYZE A FIELD
C       OF DATA FROM STATIONS AN AVERAGE OF 70 KM APART AND SOUNDINGS AT
C       90 MINUTE INTERVALS.
C
```

```
      COMMON NI, NJ, NK, NL, BL, BLI, PIE,
     1DX(11),U(13,11,17,3),V(13,11,17,3),DY2,CF(11),VOR(13,11,17,3),
     2MJ,MI,DIV(13,11,17,3),ABSVOR(13,11,17,3),OMEGK(13,11,17,3),
     3NKM1,NKM2,DP,DX2(11),PSFC(13,11),P(17),DP1,DT,NIM2,NIM3,NJM2,
     4NJM3,FUN1(13,11,17,1),FUN2(13,11,17,1),WN(13,11,17,1),
     5WNPLS1(13,11,17,1),EPS,T(9,2)
C
C      REFIGURE SOUNDING AT TIME 2 ABOVE 600 MB TAKING INTO ACCOUNT
C      TIME AND SPACE ( BALLOON DISPLACEMENT ) VARIATIONS.
C
C    THIS SUBROUTINE, STARTING WITH TOT, ALSO FIGURES THE AVERAGE
C    UBAR AND VBAR IN KNOTS AT ALL TIMES AND AT LEVELS 900, 750,
C    600, 450, 300, AND 150
C
C      IT ALSO FIGURES THE ROOT MEAN SQUARE ERROR (RMSU,RMSV) OF THE
C      CORRECTED U AND V VERSUS THE UNCORRECTED U AND V AT 1830Z.
C
C
      DO10I=1,NI
      DO10J=1,NJ
      DO10K=1,9
      U(I,J,K+8,2)= U(I,J,K+8,1)+(U(I,J,K+8,2)-U(I,J,K+8,1))*
     1(1830.-T(K,1))/(T(K,2)-T(K,1))
      V(I,J,K+8,2)=V(I,J,K+8,1)+ (V(I,J,K+8,2)-V(I,J,K+8,1))*
     1(1830.-T(K,1))/(T(K,2)-T(K,1))
   10 CONTINUE
C
  200 DO15K=1,NK
      RMSU = 0.0
      RMSV = 0.0
      DO11I=1,NI
      DO11J=1,NJ
      RMSU=RMSU+(WN(I,J,K,1)-U(I,J,K,2)*3600.)**2
      RMSV=RMSV+(WNPLS1(I,J,K,1)-V(I,J,K,2)*3600.)**2
   11 CONTINUE
C
      RMSV=RMSV/(NI*NJ)
      RMSU=RMSU/(NI*NJ)
C
      RMSV=RMSV**.5
      RMSU=RMSU**.5
C
      KLEV=1000.-K*50
      WRITE(6,25)  KLEV, RMSU, RMSV
   25 FORMAT(/' AT LEVEL ',I4,' THE RMSU IS ',F6.2,' AND THE '
     *' RMSV IS ',F6.2,' KNOTS'/)
   15 CONTINUE
C
```

```
      GO TO 40
C    TAKE OUT IF UBAR AND VBAR NOT WANTED
C
  100 TOT=NI*NJ
      DO20L=1,NL
      DO18K=2,NK,3
      SUMU=0.0
      SUMV=0.0
      DO16I=1,NI
      DO16J=1,NJ
      SUMU=SUMU+U(I,J,K,L)
      SUMV=SUMV+V(I,J,K,L)
   16 CONTINUE
      SUMU=SUMU*3600./TOT
      SUMV=SUMV*3600./TOT
      KLEV=1000.-K*50
      WRITE(6,30) L, KLEV, SUMU, SUMV
   30 FORMAT(/' AT TIME ',I2,' AND LEVEL ',I4,' THE UBAR IS ',F6.2,' '
     1'AND VBAR IS ',F6.2,' KNOTS'/)
   18 CONTINUE
   20 CONTINUE
   40 RETURN
      END
```



```
      SUBROUTINE VORTY
C
C     THE PURPOSE OF THIS SUBROUTINE IS TO COMPUTE THE RELATIVE
C     VORTICITY (VOR) PER SECOND AT ALL THE GRID POINTS FOR
C     ALL THE LEVELS AND ALL THE TIMES REQUIRED. ALSO TO DETERMINE
C     ABSOLUTE VORTICITY (ABSVOR) AT THESE SAME POINTS.
C     DY2=TWICE THE LATITUDE INTERVAL IN NAUTICAL MILES.
C     DX2(J) = TWICE THE LONGITUDE INTERVAL IN NAUTICAL MILES.
C
      COMMON NI, NJ, NK, NL, BL, BLI, PIE,
     1DX(11),U(13,11,17,3),V(13,11,17,3),DY2,CF(11),VOR(13,11,17,3),
     2MJ,MI,DIV(13,11,17,3),ABSVOR(13,11,17,3),OMEGK(13,11,17,3),
     3NKM1,NKM2,DP,DX2(11),PSFC(13,11),P(17),DP1,DT,NIM2,NIM3,NJM2,
     4NJM3,FUN1(13,11,17,1),FUN2(13,11,17,1),WN(13,11,17,1),
     5WNPLS1(13,11,17,1),EPS,T(9,2)
C
C     DETERMINE RELATIVE VORTICITY AT THE INTERIOR GRID POINTS
C     USING CENTRAL DIFFERENCING SCHEME.
C
      DO10L=1,NL
      DO10K=1,NK
```

```
      DO10J=2,MJ
      DO10I=2,MI
      VOR(I,J,K,L)=((V(I+1,J,K,L)-V(I-1,J,K,L))/DX2(J)
     1-(U(I,J+1,K,L)-U(I,J-1,K,L))/DY2)
   10 CONTINUE
C
C     DETERMINE RELATIVE VORTICITY AT THE BOUNDARIES USING
C     NON-CENTERED DIFFERENCING SCHEMES.
      DO15L=1,NL
      DO15K=1,NK
C
C     FOR ALL J=1 AND J=NJ AND I=2,MI
      DO11I=2,MI
      VOR(I,1,K,L)=(V(I+1,1,K,L)-V(I-1,1,K,L))/DX2(1)-
     1(U(I,2,K,L)-U(I,1,K,L))/(0.5*DY2)
      VOR(I,NJ,K,L)=(V(I+1,NJ,K,L)-V(I-1,NJ,K,L))/DX2(NJ)
     1-(U(I,NJ,K,L)-U(I,MJ,K,L))/(0.5*DY2)
   11 CONTINUE
C
C     FOR ALL I=1 AND I=NI AND J=2,MJ
      DO12J=2,MJ
      VOR(1,J,K,L)=(V(2,J,K,L)-V(1,J,K,L))/(0.5*DX2(J))
     1-(U(1,J+1,K,L)-U(1,J-1,K,L))/DY2
      VOR(NI,J,K,L)=(V(NI,J,K,L)-V(MI,J,K,L))/(0.5*DX2(J))
     1-(U(NI,J+1,K,L)-U(NI,J-1,K,L))/DY2
   12 CONTINUE
C
C     FIGURE FOR EACH OF FOUR CORNERS
C
C     FOR CORNER (1,1)
      VOR(1,1,K,L)=(V(2,1,K,L)-V(1,1,K,L))/(0.5*DX2(1))
     1-(U(1,2,K,L)-U(1,1,K,L))/(0.5*DY2)
C
C     FOR CORNER (1,NJ)
      VOR(1,NJ,K,L)=(V(2,NJ,K,L)-V(1,NJ,K,L))/(0.5*DX2(NJ))
     1-(U(1,NJ,K,L)-U(1,MJ,K,L))/(0.5*DY2)
C
C     FOR CORNER (NI,NJ)
      VOR(NI,NJ,K,L)=(V(NI,NJ,K,L)-V(MI,NJ,K,L))/(0.5*DX2(NJ))
     1-(U(NI,NJ,K,L)-U(NI,MJ,K,L))/(0.5*DY2)
C
C     FOR CORNER (NI,1)
      VOR(NI,1,K,L)=(V(NI,1,K,L)-V(MI,1,K,L))/(0.5*DX2(1))
     1-(U(NI,2,K,L)-U(NI,1,K,L))/(0.5*DY2)
   15 CONTINUE
C
C     HORIZONTALLY SMOOTH THE VORTICITY FIELD
C
```

```
      DO16L=1,NL
      DO16K=1,NK
      DO16I=2,MI
      DO16J=2,MJ
      VOR(I,J,K,L)=.4*VOR(I,J,K,L)+.15*VOR(I+1,J,K,L)+
     1.15*VOR(I-1,J,K,L)+.15*VOR(I,J+1,K,L)+.15*VOR(I,J-1,K,L)
   16 CONTINUE
C
C     NOW SMOOTH IN THE VERTICAL
C
      DO17L=1,NL
      DO17I=1,NI
      DO17J=1,NJ
      DO17K=2,NKM1
      VOR(I,J,K,L)=.6*VOR(I,J,K,L)+.20*VOR(I,J,K-1,L)
     1+.20*VOR(I,J,K+1,L)
   17 CONTINUE
C
C     DETERMINE ABSOLUTE VORTICITY AT ALL GRID POINTS.
C
      DO20L=1,NL
      DO20K=1,NK
      DO20I=1,NI
      DO20J=1,NJ
      ABSVOR(I,J,K,L)=VOR(I,J,K,L)+CF(J)
      IF(ABS(ABSVOR(I,J,K,L)).LT.3.E-5) ABSVOR(I,J,K,L)=3.E-5
   20 CONTINUE
      RETURN
      END



      SUBROUTINE DIVERG
C
C     THE PURPOSE OF THIS SUBROUTINE IS TO COMPUTE THE DIVERGENCE
C     (DIV) PER SECOND AT THE INTERIOR GRID POINTS FOR ALL
C     THE LEVELS AND ALL THE TIMES REQUIRED.
C     DY2=TWICE THE LATITUDE INTERVAL IN NAUTICAL MILES
C     DX2(J) = TWICE THE LONGITUDE INTERVAL IN NAUTICAL MILES.
C
      COMMON NI, NJ, NK, NL, BL, BLI, PIE,
     1DX(11),U(13,11,17,3),V(13,11,17,3),DY2,CF(11),VOR(13,11,17,3),
     2MJ,MI,DIV(13,11,17,3),ABSVOR(13,11,17,3),OMEGK(13,11,17,3),
     3NKM1,NKM2,DP,DX2(11),PSFC(13,11),P(17),DP1,DT,NIM2,NIM3,NJM2,
     4NJM3,FUN1(13,11,17,1),FUN2(13,11,17,1),WN(13,11,17,1),
     5WNPLS1(13,11,17,1),EPS,T(9,2)
C
```

```
      DO10L=1,NL
      DO10K=1,NK
      DO10J=2,MJ
      DO10I=2,MI
      DIV(I,J,K,L)=((U(I+1,J,K,L)-U(I-1,J,K,L))/DX2(J)
     1+(V(I,J+1,K,L)-V(I,J-1,K,L))/DY2)
   10 CONTINUE
C
C     HORIZONTALLY SMOOTH THE DIVERGENCE FIELD
C
C     FIRST, ALL INTERIOR POINTS.
      DO50L=1,NL
      DO50K=1,NK
      DO50I=3,NIM2
      DO50J=3,NJM2
      DIV(I,J,K,L)=.4*DIV(I,J,K,L)+.15*DIV(I-1,J,K,L)+.15*DIV(I+1,J,K,L)
     1+.15*DIV(I,J+1,K,L)+.15*DIV(I,J-1,K,L)
   50 CONTINUE
C
C     NOW, SMOOTH THE BOUNDARIES.
C
      DO60L=1,NL
      DO60K=1,NK
      DO65I=3,NIM2
      DIV(I,2,K,L)=DIV(I,2,K,L)*.5+.15*DIV(I+1,2,K,L)+.15*DIV(I-1,2,K,L)
     1+.2*DIV(I,3,K,L)
      DIV(I,MJ,K,L)=.5*DIV(I,MJ,K,L)+.15*DIV(I+1,MJ,K,L)
     1+.15*DIV(I-1,MJ,K,L)+.2*DIV(I,NJM2,K,L)
   65 CONTINUE
      DO70J=3,NJM2
      DIV(2,J,K,L)=.5*DIV(2,J,K,L)+.15*DIV(2,J+1,K,L)+.15*DIV(2,J-1,K,L)
     1+.2*DIV(3,J,K,L)
      DIV(MI,J,K,L)=.5*DIV(MI,J,K,L)+.15*DIV(MI,J+1,K,L)
     1+.15*DIV(MI,J-1,K,L)+.2*DIV(NIM2,J,K,L)
   70 CONTINUE
C
C     SAME FOR CORNERS
C
      DIV(2,2,K,L)=.5*DIV(2,2,K,L)+.25*DIV(2,3,K,L)+.25*DIV(3,2,K,L)
      DIV(2,MJ,K,L)=.5*DIV(2,MJ,K,L)+.25*DIV(2,NJM2,K,L)
     1+.25*DIV(3,MJ,K,L)
      DIV(MI,MJ,K,L)=.5*DIV(MI,MJ,K,L)+.25*DIV(MI,NJM2,K,L)
     1+.25*DIV(NIM2,MJ,K,L)
      DIV(MI,2,K,L)=DIV(MI,2,K,L)*.5+.25*DIV(MI,3,K,L)
     1+.25*DIV(NIM2,2,K,L)
   60 CONTINUE
C
C     NOW SMOOTH IN THE VERTICAL
```

```
C
      DO75L=1,NL
      DO75K=2,NKM1
      DO75I=2,MI
      DO75J=2,MJ
      DIV(I,J,K,L)=.6*DIV(I,J,K,L)+.20*DIV(I,J,K-1,L)+.20*DIV(I,J,K+1,L)
   75 CONTINUE
      RETURN
      END



      SUBROUTINE KINOMG
C
C     THE PURPOSE OF THIS SUBROUTINE IS TO COMPUTE INSTANTANEOUS
C     VERTICAL VELOCITIES IN MBS/HR USING THE KINEMATIC-CORRECTED
C     METHOD. ASSUME THAT OMEGA AT 150 MBS IS ZERO. ASSUME THAT
C     OMEGA AT THE SURFACE IS DETERMINED BY TERRAIN EFFECTS ONLY.
C     THE METHOD CONSISTS OF VERTICALLY INTEGRATING THE CONTINUITY
C     EQUATION.
C
      COMMON NI, NJ, NK, NL, BL, BLI, PIE,
     1DX(11),U(13,11,17,3),V(13,11,17,3),DY2,CF(11),VOR(13,11,17,3),
     2MJ,MI,DIV(13,11,17,3),ABSVOR(13,11,17,3),OMEGK(13,11,17,3),
     3NKM1,NKM2,DP,DX2(11),PSFC(13,11),P(17),DP1,DT,NIM2,NIM3,NJM2,
     4NJM3,FUN1(13,11,17,1),FUN2(13,11,17,1),WN(13,11,17,1),
     5WNPLS1(13,11,17,1),EPS,T(9,2)
C
C     DETERMINE OMEGA AT THE SURFACE DUE TO TERRAIN EFFECT, USING
C     950 MB WIND DATA TO REPRESENT THE SURFACE. UNITS ARE MBS/HR.
C
      DO25L=1,NL
      DO25I=2,MI
      DO25J=2,MJ
      OMEGK(I,J,1,L)=(U(I,J,1,L)*(PSFC(I+1,J)-PSFC(I-1,J))/DX2(J)
     *+V(I,J,1,L)*(PSFC(I,J+1)-PSFC(I,J-1))/DY2)*3600.0
   25 CONTINUE
C
C     DEFINE THE PARAMETER P(K) AS THE PRESSURE FOR EACH LEVEL IN
C     MBS FROM LEVEL 2 TO NK.
C
      DP1=1000.0
      IF(DP.GE.99.0) DP1=1100.0
      DO27K=2,NK
      P(K)=DP1-DP*K
   27 CONTINUE
C
```

```
C       FIGURE THE VERTICALLY AVERAGED DIVERGENCES FOR EACH VERTICAL
C       COLUMN. COMPARE EACH OF THESE TO THE AVERAGE DIVERGENCE THAT
C       SATISFIES THE INTEGRAL CONSTRAINT FOR EACH COLUMN. THE DIFFERENCE,
C       CORK, IS THE CORRECTION WHICH MUST BE MADE IN THE COMPUTATION OF
C       OMEGA TO SATISFY THE INTEGRAL CONSTRAINT. THIS SHOULD GIVE A
C       COMPUTED VERTICAL MOTION FIELD AT 150 MB EVERYWHERE EQUAL TO
C       ZERO. THIS WILL BE PRINTED OUT FOR CHECKING PURPOSES.
        DO30L=1,NL
        DO30J=2,MJ
        DO30I=2,MI
        CORK=0.0
        SUM=0.0
        P(1)=PSFC(I,J)
C
C       FIGURE ACTUAL COMPUTED AVERAGE DIVERGENCE.
        DO5K=1,NKM1
        SUM=SUM+(DIV(I,J,K,L)+DIV(I,J,K+1,L))*(P(K)-P(K+1))/2.0
      5 CONTINUE
        AVGDIV=SUM/(P(1)-P(NK))
C
        WRITE(6,90) AVGDIV
     90 FORMAT(/' AVGDIV = ',E15.5/)
C
C       FIGURE THE AVERAGE DIVERGENCE THAT SATISFIES THE INTEGRAL
C       CONSTRAINT.
C
        AICDIV=-OMEGK(I,J,1,L)/((PSFC(I,J)-150.0)*3600.0)
C
        WRITE(6,95) AICDIV
     95 FORMAT(/' AICDIV = ',E15.5/)
C
C       SUBTRACT AVGDIV FROM AICDIV TO GET CORRECTION CORK.
        CORK=AICDIV-AVGDIV
C
        WRITE(6,100) CORK
    100 FORMAT(/' CORK = ',E15.5/)
C
C       CORRECT DIVERGENCES TO MEET INTEGRAL CONSTRAINT
C
        DO96K=3,NK
        DIV(I,J,K,L)=DIV(I,J,K,L)+CORK*K/9.
     96 CONTINUE
C
C       FIRST TWO LEVELS MUST BE CORRECTED SEPARATELY FOR MASS CONSIDER-
C       ATIONS SINCE THEY ARE NOT REPRESENTATIVE OF 50 MB INCREMENTS.
C
        DIV(I,J,1,L)=DIV(I,J,1,L)+CORK*(1./9.)*((PSFC(I,J)-P(2))/50.)
        DIV(I,J,2,L)=DIV(I,J,2,L)+CORK*(2./9.)*.01*(PSFC(I,J)-P(3))
```

```
C
C       NOW COMPUTE VERTICAL MOTIONS AT EACH LEVEL IN THE VERTICAL FOR
C       ALL GRID POINTS AND TIME INTERVALS. SET P(1) = SURFACE PRESSURE
C       AT EACH GRID POINT REPRESENTED BY THE STANDARD ATMOSPHERE
C       PRESSURE FOR EACH ELEVATION. MULTIPLY BY 3600 TO CONVERT MB/SEC
C       TO MB/HR.
C
        DO28K=1,NKM1
        OMEGK(I,J,K+1,L)=OMEGK(I,J,K,L)+((DIV(I,J,K,L)+DIV(I,J,K+1,L))/
       12.0)*(P(K)-P(K+1))*3600.
   28 CONTINUE
   30 CONTINUE
      RETURN
      END



      SUBROUTINE VOROMG
C
C       THE PURPOSE OF THIS SUBROUTINE IS TO COMPUTE INSTANTANEOUS
C       VERTICAL VELOCITIES IN MBS/HR USING THE COMPLETE VORTICITY METHOD
C       (INCLUDING THE TWISTING TERM). ASSUME THAT OMEGA AT 150 MBS IS
C       ZERO. ASSUME THAT OMEGA AT THE SURFACE IS DETERMINED BY TERRAIN
C       EFFECTS ONLY. THE METHOD CONSISTS OF:(1) EVALUATING THE TERM FUN1
C       (THE FIRST HALF OF THE EQUATION=((DABSVOR/DT)/(ABSVOR SQUARED)))
C       AT ALL GRID POINTS AND LEVELS FOR THE TIME CONSIDERED. (2)
C       VERTICALLY INTEGRATE THESE TERMS AND COMPARE TO BOUNDARY
C       CONDITIONS. (3) THEN COMPUTE CORRECTIONS SO THAT THE INTEGRAL
C       CONSTRAINT IS SATISFIED. (4) NOW COMPUTE FIRST APPROXIMATION FOR
C       OMEGA FIELD WN(I,J,K) USING CORRECTIONS. (5) PLUG WN(I,J,K) INTO
C       SECOND HALF OF THE EQUATION AND COMPUTE FUN2(OR(((DWN/DX)(DV/DP)
C       -(DWN/DY)(DU/DP))/(ABSVOR SQUARED)) AT EACH GRID POINT AND LEVELS
C       FOR THE TIME CONSIDERED. (6) REPEAT STEP 2. (7) REPEAT STEP 3 FOR
C       FUN2. (8) NOW COMPUTE SECOND APPROXIMATION FOR OMEGA FIELD WNPLS1
C       (I,J,K) BY SOLVING COMPLETE EQUATION FOR OMEGA WITH CORRECTIONS.
C       (9) CHECK WNPLS1 - WN, IF DIFFERENCE LESS THAN SOME EPS, GOOD: IF
C       NOT, MAKE A RUNNING COUNT OF POINTS THAT ARE NO GOOD. THEN, WHEN
C       THRU FIELD, CHECK COUNT. IF COUNT NOT ZERO, SET WN=WNPLS1, AND
C       REPEAT FROM STEP 5 ON.
C
C       ALSO TO PRINT THE VERTICAL MOTION DETERMINED BY VOROMG.
C
        COMMON NI, NJ, NK, NL, BL, BLI, PIE,
      1DX(11),U(13,11,17,3),V(13,11,17,3),DY2,CF(11),VOR(13,11,17,3),
      2MJ,MI,DIV(13,11,17,3),ABSVOR(13,11,17,3),OMEGK(13,11,17,3),
      3NKM1,NKM2,DP,DX2(11),PSFC(13,11),P(17),DP1,DT,NIM2,NIM3,NJM2,
      4NJM3,FUN1(13,11,17,1),FUN2(13,11,17,1),WN(13,11,17,1),
```

```
     5WNPLS1(13,11,17,1),EPS,T(9,2)
C
C
      ALPHA=1.0
C
C     FIRST, COMPUTE WN(I,J,1,2) OMEGA AT THE SURFACE DUE TO TERRAIN
C     EFFECTS(USING 950 MB WIND DATA TO REPRESENT THE SURFACE). UNITS
C     ARE MB/SEC.
C
      DO5I=2,MI
      DO5J=2,MJ
      WN(I,J,1,1)=U(I,J,1,2)*(PSFC(I+1,J)-PSFC(I-1,J))/DX2(J)
     2+V(I,J,1,2)*(PSFC(I,J+1)-PSFC(I,J-1))/DY2
    5 CONTINUE
C
C     NOW CALL FUNCT1 TO GET FIRST APPROXIMATIONS TO FUN1 TERM AT
C     ALL POINTS AND LEVELS.
C
      CALL FUNCT1
C
C     DEFINE THE PARAMETER P(K) AS THE PRESSURE FOR EACH LEVEL IN
C     MBS FROM LEVEL 1 TO NK. SET P(1) = SURFACE PRESSURE AT EACH GRID
C     POINT REPRESENTED BY THE STANDARD ATMOSPHERE PRESSURE FOR EACH
C     ELEVATION. THIS MUST BE DONE DURING EACH INDIVIDUAL LOOP AS
C     P(1)=PSFC(I,J). HOWEVER, P(2) THRU P(NK) DO NOT CHANGE.
C
      DP1=1000.0
      IF(DP.GE.99.0)DP1=1100.0
C     DETERMINE P(K) FOR LEVELS 2 THRU NK.
      DO7K=2,NK
      P(K)=DP1-DP*K
    7 CONTINUE
C
C     NOW DETERMINE CORRECTION FOR VERTICALLY AVERAGED FUN1 TO
C     SATISFY THE INTEGRAL CONSTRAINT. THEN CORRECT FIRST APPROXIMATION
C     TO OMEGA(WN) PROPORTIONATELY (AS IN KINOMG). CORRECT FUN1 SO
C     THAT EACH VERTICAL COLUMN SATISFIES THE INTEGRAL CONSTRAINT.
C
      DO14I=2,MI
      DO14J=2,MJ
      TOTF=0.0
C     SET P(1) EQUAL THE SURFACE PRESSURE
C
      P(1)=950.
      PSFC(I,J)=P(1)
C
C
      DO11K=1,NKM1
```

```
      TOTF= TOTF+(FUN1(I,J,K,1)+FUN1(I,J,K+1,1))*(P(K)-P(K+1))/2.0
   11 CONTINUE
C     AVEFUN = AVERAGE FUN1 COMPUTED
      AVEFUN=TOTF/(P(1)-P(NK))
C
      WRITE(6,60) AVEFUN
   60 FORMAT(/' AVEFUN = ',E15.5/)
C
C     AVFNSB = AVERAGE FUN1 SATISFYING THE INTEGRAL CONSTRAINT
      AVFNSB=WN(I,J,1,1)/(ABSVOR(I,J,1,2)*(PSFC(I,J)-150.0))
C
      WRITE(6,65) AVFNSB
   65 FORMAT(/' AVFNSB = ',E15.5/)
C
C     COMPUTE THE TOTAL CORRECTION CORVF1.
      CORVF1=AVFNSB-AVEFUN
C
      WRITE(6,70) CORVF1
   70 FORMAT(' CORVF1 = ',E15.5/)
C
C     CORRECT FUN1 TO SATISFY THE INTEGRAL CONSTRAINT.
C
      DO97K=3,NK
   97 FUN1(I,J,K,1)=FUN1(I,J,K,1)+CORVF1*K/9.
C
C     AS IN KINOMG, FIRST TWO LEVELS MUST BE CORRECTED SEPARATELY FOR
C     MASS CONSIDERATIONS SINCE THEY ARE NOT REPRESENTATIVE OF 50 MB
C     INCREMENTS.
C
      FUN1(I,J,1,1)=FUN1(I,J,1,1)+CORVF1*(1./9.)*((PSFC(I,J)-P(2))/50.)
      FUN1(I,J,2,1)=FUN1(I,J,2,1)+CORVF1*(2./9.)*.01*(PSFC(I,J)-P(3))
C
C
C
C     NOW COMPUTE A FIRST APPROXIMATION WN(I,J,K,2) TO OMEGA AT ALL
C     LEVELS FOR THIS PARTICULAR (I,J,2) LOCATION. UNITS ARE MBS/SEC.
      DO13K=1,NKM1
      WN(I,J,K+1,1)=(WN(I,J,K,1)/ABSVOR(I,J,K,2)-(((FUN1(I,J,K,1)+
     1FUN1(I,J,K+1,1))/2.0))*
     2(P(K)-P(K+1)))*ABSVOR(I,J,K+1,2)
   13 CONTINUE
   14 CONTINUE
C
C     PRINT CORRECTED FUN1 FIELD
C
      DO130K=1,NK
      LEV=1000-K*50
      WRITE(6,131)   LEV
```

```
  131 FORMAT('1',5X,' THIS IS THE FIELD OF CORRECTED FUN1 '
     1' (UNITLESS) AT LEVEL K = ',I3///)
      DO132JK=2,MJ
      J=(NJ+1)-JK
  132 WRITE(6,133)  ((FUN1(I,J,K,1),I=2,MI))
  133 FORMAT(11E10.2////////)
  130 CONTINUE
C
C     NOW WE HAVE A FIRST APPROXIMATION (WN) TO OMEGA. WANT TO PRINT
C     THIS TO SEE IF INTEGRAL CONSTRAINT IS SATISFIED (OP WN AT 150 MBS
C     IS EQUAL TO ZERO EVEPYWHERE). UNITS ARE MBS/SEC.
C
C     CONVERT TO MB/HOUR
C
      DO116K=1,NK
      DO116I=2,MI
      DO116J=2,MJ
  116 WN(I,J,K,1)=WN(I,J,K,1)*3600.
C
C
      DO19K=1,NK
      LEV=1000-K*50
      WRITE(6,17) LEV
   17 FORMAT('1',5X,'FIRST APPROXIMATION TO OMEGA BY THE VORTICITY'
     1' METHOD IN MB/HR AT LEVEL K=',I3///)
      DO16JK=2,MJ
      J=(NJ+1)-JK
   16 WRITE(6,18)     ((WN(I,J,K,1),I=2,MI))
   18 FORMAT(11E10.2////////)
   19 CONTINUE
C
C     CONVERT BACK TO MB/SEC.
C
      DO117K=1,NK
      DO117I=2,MI
      DO117J=2,MJ
  117 WN(I,J,K,1)=WN(I,J,K,1)/3600.
C
C
C
      DO99I=2,MI
      DO99J=2,MJ
   99 WNPLS1(I,J,1,1)=WN(I,J,1,1)
C
C
C     SET COUNTER LOOPCT=0. THIS IS TO BE USED TO INDICATE NUMBER OF
C     CYCLES REQUIRED TO GET A SATISFACTORY OMEGA FIELD FROM THIS
C     SUBROUTINE
```

```
      LOCPCT=0
C     NOW, CALL FUNCT2 TO GET FIRST APPROXIMATION TO FUN2 TERM AT ALL
C     POINTS AND LEVELS.
C
   20 CALL FUNCT2
C
C     SET COUNTER KOUNT=0 FOR USE, AS STATED, IN FINAL APPROXIMATION.
      KOUNT=0
      LOCPCT=LOOPCT+1
C
C     NOW, AS FOR FUN1, MUST VERTICALLY INTEGRATE THESE FUN2 TERMS.
C     COMPARE TO BOUNDARY CONDITIONS FOR INTEGRAL CONSTRAINT. DETERMINE
C     CORRECTION SO THAT EACH VERTICAL COLUMN SATISFIES THE INTEGRAL
C     CONSTRAINT. CORRECT THE FUN2 VALUES IN A MANNER SIMILAR TO THE
C     FUN1 CORRECTIONS. FIGURE SECOND APPROXIMATION FOR OMEGA
C     (WNPLS1). NOW COMPARE THIS NEW FIELD TO THE FIRST APPROXIMATION.
C     IF ALL AGREE WITHIN AN EPS WE HAVE FOUND FINAL OMEGA FIELD. IF
C     NOT, RETURN TO STATEMENT 20 AND RECYCLE. CONTINUE IN THIS FASHION
C     UNTIL A SATISFACTORY OMEGA FIELD IS REACHED.
C     SINCE FUN1 HAS SATISFIED THE INTEGRAL, THEN FUN2 MUST AVERAGE
C     TO ZERO, BECAUSE INTEGRAL CONSTRAINT = FUN1 + FUN2
C
C
      DO25I=3,NIM2
      DO25J=3,NJM2
      TOTF=0.0
      DO26K=1,NKM1
      TOTF=TOTF+(FUN2(I,J,K,1)+FUN2(I,J,K+1,1))*(P(K)-P(K+1))/2.0
   26 CONTINUE
C
      AVEFUN=TOTF/(P(1)-P(NK))
C
      AVFNSB=0.0
C
C     COMPUTE THE TOTAL CORRECTION CORVF2 AS BEFORE.
C
      CORVF2=AVFNSB-AVEFUN
C
C     IN ORDER TO KEEP THE TOTAL OMEGA AT THE TOP OF THE ATMOSPHERE
C     (K=NK) EQUAL TO ZERO, AND SINCE OMEGA AT THE SURFACE (K=1) IS
C     DETERMINED BY THE TERRAIN, CORRECT ONLY THOSE VALUES OF FUN2
C     FROM K=2 TO K=NKM1.
C
      DO98K=2,NKM1
   98 FUN2(I,J,K,1)=FUN2(I,J,K,1)+CORVF2*(PSFC(I,J)-150.)/
     1(((PSFC(I,J)+900.)/2.)-175.)
C
C     COMPUTE THE NEXT APPROXIMATION. USING THE COUNTER KOUNT, COUNT THE
```

```
C       NUMBER OF TIMES THE DIFFERENCE BETWEEN WNPLS1 AND WN IS GREATER
C       THAN THE SET EPS=EPSILON(SEE SUBROUTINE CONSTANT). IF KOUNT
C       GREATER THAN ZERO WHEN FINISHED, RECYCLE, AGAIN MEETING INTEGRAL
C       CONSTRAINT FOR FUN2 FOR NEW WN. CONTINUE UNTIL ALL WNPLS1 SATISFY
C       EPSILON, THEN WE HAVE A GOOD, FINAL FIELD OF OMEGA AT TIME 2
C       READY FOR PRINTING.
C
        DO30K=1,NKM1
        WNPLS1(I,J,K+1,1)=(WNPLS1(I,J,K,1)/ABSVOR(I,J,K,2)-
       1.5*(FUN1(I,J,K,1)+FUN1(I,J,K+1,1)+FUN2(I,J,K,1)+
       2FUN2(I,J,K+1,1))*(P(K)-P(K+1)))*ABSVOR(I,J,K+1,2)
C
C       DETERMINE DIFFERENCE IN 2 OMEGAS.
        RES=WNPLS1(I,J,K+1,1)-WN(I,J,K+1,1)
        IF(ABS(RES).LT.1.E-40)RES=0.0
        IF(ABS(RES).GT.EPS)KOUNT=KOUNT+1
        WNPLS1(I,J,K+1,1)=WN(I,J,K+1,1)+ALPHA*RES
   30 CONTINUE
   25 CONTINUE
C
C       NOW CHECK KOUNT FOR NUMBER OF UNSATISFIED GRID POINTS, AND LOOPCT
C       FOR NUMBER OF TIMES RECYCLED. PRINT THESE.
C
        WRITE(6,35) LOOPCT, KOUNT
   35 FORMAT(2X,'AFTER ',I3,' CYCLES THROUGH THE FIELD THERE ARE STILL'
     1' ',I4,' OMEGAS THAT DO NOT SATISFY THE EPSILON REQUIREMENT'/)
C
        DO40I=3,NIM2
        DO40J=3,NJM2
        DO40K=2,NK
        WN(I,J,K,1)=WNPLS1(I,J,K,1)
   40 CONTINUE
        IF(LOOPCT.GT.200) GO TO 50
        IF(KOUNT.GT.0) GO TO 20
C
C
C       FIRST, MULTIPLY THE FIELD BY 3600 TO CONVERT UNITS FROM MB/SECOND
C       TO MB/HOUR.
C
  110 DO115I=2,MI
        DO115J=2,MJ
        DO115K=1,NK
        WN(I,J,K,1)=WN(I,J,K,1)*3600.0
  115 CONTINUE
C
C       NOW WRITE OUT THE FIELD
C
        DO120K=1,NK
```

```
      LEV=1000-K*50
      WRITE(6,135)  LEV
  135 FORMAT('1',2X,'VERTICAL MOTION (OMEGA) BY THE COMPLETE VORTICITY'
     1' METHOD IN MB/HR AT LEVEL K=',I3,' (NOTE: BOUNDARY VALUES ARE'
     2' FIRST APPROXIMATIONS)'///)
      DO120JK=2,MJ
      J=(NJ+1)-JK
  120 WRITE(6,125)  (((WN(I,J,K,1),I=2,MI)))
  125 FORMAT(11F10.2////////)
C
CC
C
   50 RETURN
      END



      SUBROUTINE FUNCT1
C
CC    THE PURPOSE OF THIS SUBROUTINE IS TO COMPUTE THE FUNCTION
CC    FUN1 =(DVOR/DT + V DOT DEL ABSVOR)/ABSVOR SQUARED  AT EACH
CC    GRID POINT FOR ONE TIME PERIOD (TIME 2). THIS IS A UNITLESS
CC    FUNCTION.
C
      COMMON NI, NJ, NK, NL, BL, BLI, PIE,
     1DX(11),U(13,11,17,3),V(13,11,17,3),DY2,CF(11),VOR(13,11,17,3),
     2MJ,MI,DIV(13,11,17,3),ABSVOR(13,11,17,3),OMEGK(13,11,17,3),
     3NKM1,NKM2,DP,DX2(11),PSFC(13,11),P(17),DP1,DT,NIM2,NIM3,NJM2,
     4NJM3,FUN1(13,11,17,1),FUN2(13,11,17,1),WN(13,11,17,1),
     5WNPLS1(13,11,17,1),EPS,T(9,2)
C
CC
C
      DO 10J=2,MJ
      DO 10I=2,MI
      DO10K=1,NK
      FUN1(I,J,K,1)=((VOR(I,J,K,3)-VOR(I,J,K,1))/(2.*DT)+
     1U(I,J,K,2)*(ABSVOR(I+1,J,K,2)-ABSVOR(I-1,J,K,2))/DX2(J)+
     2V(I,J,K,2)*(ABSVOR(I,J+1,K,2)-ABSVOR(I,J-1,K,2))/DY2)
     3/(ABSVOR(I,J,K,2)**2)
   10 CONTINUE
C
CC    APPLY A SMOOTHER TO FUN1
C
      ALFA=.6
      ALFA1=(1.-ALFA)/4.
C
```

```
      DO 11K=1,NK
      DO11J=3,NJM2
      DO11I=3,NIM2
   11 FUN1(I,J,K,1)=ALFA*FUN1(I,J,K,1)+ALFA1*FUN1(I+1,J,K,1)+
     1ALFA1*FUN1(I-1,J,K,1)+ALFA1*FUN1(I,J+1,K,1)+ALFA1*FUN1(I,J-1,K,1)
C
      RETURN
      END



      SUBROUTINE FUNCT2
C
CCC   THE PURPOSE OF THIS SUBROUTINE IS TO COMPUTE THE FUNCTION
CCC   FUN2 = ((DWN/DX)(DV/DP)-(DWN/DY)(DU/DP))/ABSVOR SQUARED AT
CCC   EACH GRID POINT FOR ONE TIME PERIOD (TIME 2). THIS IS A UNITLESS
CCC   FUNCTION.
C
      COMMON NI, NJ, NK, NL, BL, BLI, PIS,
     1DX(11),U(13,11,17,3),V(13,11,17,3),DY2,CF(11),VOR(13,11,17,3),
     2MJ,MI,DIV(13,11,17,3),ABSVOR(13,11,17,3),OMEGK(13,11,17,3),
     3NKM1,NKM2,DP,DX2(11),PSFC(13,11),P(17),DP1,DT,NIM2,NIM3,NJM2,
     4NJM3,FUN1(13,11,17,1),FUN2(13,11,17,1),WN(13,11,17,1),
     5WNPLS1(13,11,17,1),EPS,T(9,2)
C
CCC   THE FUNCTION MUST BE EVALUATED IN THREE STEPS. FIRST, AT THE
CCC   SURFACE USING A BACKWARD FINITE DIFFERENCING PROCEDURE FOR
CCC   D(-)/DP; THEN,AT ALL INTERIOR LEVELS USING CENTERED DIFFERENCES:
CCC   AND AT 150 MB (LEVEL NK) BY A FORWARD DIFFERENCE. ALL OTHER
CCC   DERIVATIVES ARE ESTIMATED BY CENTRAL DIFFERENCES.
CCC
CCC   COMPUTE FUN2(I,J,1,1) AT THE SURFACE
CCC
C
      DO 10 I=3,NIM2
      DO 10 J=3,NJM2
      FUN2(I,J,1,1)=(((WN(I+1,J,1,1)-WN(I-1,J,1,1))/DX2(J))*
     1(V(I,J,1,2)-V(I,J,2,2))/(PSFC(I,J)-P(2))-((WN(I,J+1,1,1)-
     2WN(I,J-1,1,1))/DY2)*(U(I,J,1,2)-U(I,J,2,2))/(PSFC(I,J)-P(2)))/
     3(ABSVOR(I,J,1,2)**2)
      P(1)=PSFC(I,J)
C
CC    COMPUTE FUN2 FOR ALL LEVELS 2 THROUGH NKM1.
C
      DO 5K=2,NKM1
      FUN2(I,J,K,1)=(((WN(I+1,J,K,1)-WN(I-1,J,K,1))/DX2(J))*
     1(V(I,J,K-1,2)-V(I,J,K+1,2))/(P(K-1)-P(K+1))-((WN(I,J+1,K,1)-
```

```
     2WN(I,J-1,K,1))/DY2)*(U(I,J,K-1,2)-U(I,J,K+1,2))/(P(K-1)-P(K+1)))/
     3(ABSVOR(I,J,K,2)**2)
   5 CONTINUE
C
C      COMPUTE FUN2(I,J,NK,2) AT 150 MBS(LEVEL NK). THESE SHOULD ALL
C      BE ZERO IF INTEGRAL CONSTRAINT FOR FIRST APPROXIMATION OF OMEGA
C      (WN) HAS BEEN MET. COMPUTE ANYWAY AS A CHECK.
C
      FUN2(I,J,NK,1)=(((WN(I+1,J,NK,1)-WN(I-1,J,NK,1))/DX2(J))*
     1(V(I,J,NKM1,2)-V(I,J,NK,2))/(P(NKM1)-P(NK))-((WN(I,J+1,NK,1)-
     2WN(I,J-1,NK,1))/DY2)*(U(I,J,NKM1,2)-U(I,J,NK,2))/(P(NKM1)-P(NK)))/
     3(ABSVOR(I,J,NK,2)**2)
  10 CONTINUE
     RETURN
     END



     SUBROUTINE PRINT1
C
C      THE PURPOSE OF THIS SUBROUTINE IS TO PRINT THE RELATIVE VORTICITY,
C      DIVERGENCE, AND OMEGA(FROM THE KINEMATIC METHOD) FIELDS IN A
C      USEFUL FORM.
C
      COMMON NI, NJ, NK, NL, BL, BLI, PIE,
     1DX(11),U(13,11,17,3),V(13,11,17,3),DY2,CF(11),VOR(13,11,17,3),
     2MJ,MI,DIV(13,11,17,3),ABSVOR(13,11,17,3),OMEGK(13,11,17,3),
     3NKM1,NKM2,DP,DX2(11),PSFC(13,11),P(17),DP1,DT,NIM2,NIM3,NJM2,
     4NJM3,FUN1(13,11,17,1),FUN2(13,11,17,1),WN(13,11,17,1),
     5WNPLS1(13,11,17,1),EPS,T(9,2)
C
      DIMENSION  VT(24), DV(24), VM(24), X1(17), T1(3), DIVMS(11,9),
     *VORS(13,11)
C
      DATA X1/' SFC',' 900',' 850',' 800',' 750',' 700',' 650',' 600',
     *' 550',' 500',' 450',' 400',' 350',' 300',' 250',' 200',' 150'/
      DATA  T1/'1700','1830','2000'/
C
C      READ TITLES
C
      READ(5,3) VT
      READ(5,3) DV
      READ(5,3) VM
    3 FORMAT(20A4)
C
C      CONVERT TO SMALLER FIELD AND PRINT VORTICITIES. THIS MUST BE
C      DONE TO ALL FIELDS TO MEET THE REQUIREMENTS OF SUBROUTINE
```

```
C       MTMPII. THIS IS A SUBROUTINE IN THE POSTGRADUATE SCHOOL
C       LIBRARY WHICH WAS DEVELOPED TO ANALYZE ANY MATRIX FIELD. IT
C       PRINTS OUT AN EASILY READ, CONTOURED FIELD.
C
        DO5L=1,NL
        DO5K=1,NK
        DO6I=1,NI
        DO6J=1,NJ
      6 VORS(I,J)=VOR(I,J,K,L)
        VT(12)=X1(K)
        VT(18)=T1(L)
      5 CALL MTMPII(VORS,NI,NJ,VT,10.E-05,100.,0.0,-90.E-05,0,1)
C
C       CONVERT TO SMALLER FIELD AND PRINT DIVERGENCES
C
      8 DO15L=1,NL
        DO15K=1,NK
        DO10I=1,NIM2
        DO10J=1,NJM2
     10 DIVMS(I,J)=DIV(I+1,J+1,K,L)
        DV(10)=X1(K)
        DV(16)=T1(L)
     15 CALL MTMPII(DIVMS,NIM2,NJM2,DV,10.E-05,100.,0.0,-90.E-05,0,1)
C
C       CONVERT TO A SMALLER FIELD AND PRINT CORRECTED KINEMATIC
C       METHOD VERTICAL MOTIONS
C
        DO25L=1,NL
        DO25K=1,NK
        DO20I=1,NIM2
        DO20J=1,NJM2
     20 DIVMS(I,J)=OMEGK(I+1,J+1,K,L)
        VM(16)=X1(K)
        VM(22)=T1(L)
     25 CALL MTMPII(DIVMS,NIM2,NJM2,VM,20.,0.001,0.0,-300.,0,1)
C
    100 RETURN
        END
```

LIST OF REFERENCES

Alberty, R. L., 1969: Dynamic pressure effects in organized convection, Monthly Weather Review, 97, 590-596.

Asai, T., 1964: Cumulus convection in the atmosphere with vertical wind shear; numerical experiment. Journal of the Meteorological Society of Japan, 42, 245-259.

Ballenzweig, E. M., 1955: A critique of methods of estimating large-scale vertical motions in the atmosphere. Unpublished Manuscript, Technical Report No. 36, Office of Naval Research, 40 pp.

Byers, H. R., and R. R. Braham, 1949: The Thunderstorm. U. S. Department of Commerce, 287 pp.

Carlson, T. N., and F. H. Ludlum, 1968: Conditions for the occurrence of severe local storms. Tellus, 2, 203-226.

Clark, B. A., 1969: Rawinsonde errors and their application to a mesoscale study. Unpublished Master's Thesis, U. S. Naval Post-graduate School, Monterey, 50 pp.

Dirks, R. A., 1969: A climatology of central great plains mesoscale convective systems. National Environmental Satellite Center, Technical Report, Contract E-10-68G, 50 pp.

_____, J. D. Mahlman, and E. R. Reiter, 1967: Evidence of a meso-scale wave phenomenon in the lee of the Rocky Mountains. Atmospheric Science Paper No. 115, Colorado State University, 29 pp.

Doroshenko, F. T., 1960: The causes of squall development. Meteorologiia i Gidrologii., 4, (AD-253 559), 28-31.

Endlich, R. M., and R. L. Mancuso, 1968: Objective analysis of environmental conditions associated with severe thunderstorms and tornadoes. Monthly Weather Review, 96, 342-350.

Fankhauser, J. C., 1968: Thunderstorm-environment interactions revealed by chaff trajectories in the mid-troposphere. National Severe Storms Laboratory Report No. 39, 14 pp.

_____, 1969: The use of mesoscale rawinsonde observations for defining convective processes. Journal of Applied Meteorology, (to be published).

Fujita, T., 1955: Results of detailed synoptic studies of squall lines. Tellus, 7, 405-436.

_____, 1957: Recent studies in mesometeorology. 75th Anniversary Volume of the Journal of the Meteorological Society of Japan, 256-261.

_____, 1963: Analytical mesometeorology. Meteorological Monographs, 5, 77-125.

_____, and M. Brown, 1958: A study of mesosystems and their radar echoes. Bulletin of the American Meteorological Society, 39, 538-554.

House, D. C., 1963: Forecasting tornadoes and severe thunderstorms. Meteorological Monographs, 5, 141-155.

Koscielski, A., 1965: 110 tornado forecasts and reasons why they did or did not verify. Unpublished Manuscript, Severe Local Storms Forecast Center, ESSA, 20 pp.

Mahlman, J. D., 1968: Unpublished Class Notes. U. S. Naval Postgraduate School, Monterey.

Matsumoto, S., 1967: Orographic edge effect on the downstream cumulus activity. Journal of the Meteorological Society of Japan, 45, 500-503.

_____, and K. Ninomiya, 1963: Errors in numerical analysis using three observing stations. Journal of the Meteorological Society of Japan, 41, 299-304.

_____, K. Ninomiya, and T. Akiyama, 1967a: A synoptic and dynamic study on the three dimensional structure of mesoscale disturbances observed in the vicinity of a cold vortex center. Journal of the Meteorological Society of Japan, 45, 64-81.

_____, K. Ninomiya, and T. Akiyama, 1967b: Cumulus activities in relation to the mesoscale convergence field. Journal of the Meteorological Society of Japan, 45, 292-304.

Newton, C. W., 1966: Circulations in large sheared cumulonimbus. Tellus, 18, 699-713.

NSSP Staff, 1961: Environmental and thunderstorm structures as shown by national severe storms project observations in spring 1960 and 1961. Monthly Weather Review, 91, 271-291.

O'Brien, J. J., 1969: Alternative solutions to the classical vertical velocity problem. Journal of Applied Meteorology, (to be published).

Panofsky, H. A., P. Hanna, and A. L. Morris, 1959: Vertical Motion and Weather, Research Report NWRF 30-0359-024, Navy Weather Research Facility, 46 pp.

Reiter, E. R., 1963: Jet-Stream Meteorology, Chicago and London, University of Chicago Press, 515 pp.

Senshu, T., 1961: Analysis of a mesoscale disturbance on 30 January 1955 in western Japan. Journal of the Meteorological Society of Japan, 39, 55-81.

Takedo, T., 1965: The downdraft in convective shower-cloud under the vertical wind shear and its significance for the maintenance of convective system. Journal of the Meteorological Society of Japan, 43, 302-309.

Tepper, M., 1959: Mesometeorology - the link between macroscale synoptic weather and local weather. Bulletin of the American Meteorological Society, 40, 56-72.

Van Sickle, K. L., 1969: An isentropic trajectory study of a severe storm. Unpublished Research Paper, U. S. Naval Postgraduate School, Monterey, 132 pp.

Yanai, M., and T. Nitta, 1967: Computation of vertical motion and vorticity budget in a Caribbean easterly wave. Journal of the Meteorological Society of Japan, 45, 444-466.

INITIAL DISTRIBUTION LIST

		No. Copies
1.	Lieutenant Randy J. Coleman, USN U.S.S. TRIPOLI (LPH-10) FPO San Francisco 96601	3
2.	Dr. Jerry D. Mahlman Department of Meteorology Naval Postgraduate School Monterey, California 93940	5
3.	Dr. Ronnie L. Alberty Department of Meteorology Naval Postgraduate School Monterey, California 93940	5
4.	Dr. Kenneth C. Brundidge Texas A&M University College Station, Texas 77840	1
5.	Department of Meteorology Naval Postgraduate School Monterey, California 93940	3
6.	Library Naval Postgraduate School Monterey, California 93940	2
7.	Office of the Naval Weather Service Naval Station (Washington Navy Yard Annex) Washington, D. C. 20390	1
8.	Defense Documentation Center Cameron Station Alexandria, Virginia 22314	20
9.	Officer in Charge Navy Weather Research Facility Naval Air Station, Building R-48 Norfolk, Virginia 23511	2

Security Classification

DOCUMENT CONTROL DATA - R & D

(Security classification of title, body of abstract and indexing annotation must be entered when the overall report is classified)

1. ORIGINATING ACTIVITY (Corporate author)	2a. REPORT SECURITY CLASSIFICATION
Naval Postgraduate School Monterey, California 93940	Unclassified
	2b. GROUP

3. REPORT TITLE

A Diagnostic Analysis of the 30 May 1967 Squall Line in Central Oklahoma

4. DESCRIPTIVE NOTES *(Type of report and, inclusive dates)*

Master's Thesis; October 1969

5. AUTHOR(S) *(First name, middle initial, last name)*

Randy J. Coleman

6. REPORT DATE	7a. TOTAL NO. OF PAGES	7b. NO. OF REFS
October 1969	138	33

8a. CONTRACT OR GRANT NO.	9a. ORIGINATOR'S REPORT NUMBER(S)
b. PROJECT NO.	
c.	9b. OTHER REPORT NO(S) *(Any other numbers that may be assigned this report)*
d.	

10. DISTRIBUTION STATEMENT

This document has been approved for public release and sale; its distribution is unlimited.

11. SUPPLEMENTARY NOTES	12. SPONSORING MILITARY ACTIVITY
	Naval Postgraduate School Monterey, California 93940

13. ABSTRACT

A squall line is investigated during a 3-hour period of its mature life. Upper air data from the mesonetwork in Oklahoma at 1700, 1830, and 2000 GMT is used to determine vorticity, divergence, and vertical motion at 50 mb intervals. These and other fields are computed and investigated in detail, and possible problems associated with them are discussed. Two methods of computing vertical motion are described in detail.

A mesoscale wave with a wavelength of approximately 90 n.m. is found at 700 mb. It moves faster than the wind at 700 mb but slower than the squall line. This wave is investigated in detail and is hypothesized to be the cause and the terminator of the squall line.

The kinematic vertical motion technique presented appears to give realistic fields. Appendix B describes the problems found in the vorticity method and how it can be used on the synoptic scale.

DD FORM 1 NOV 65 1473 (PAGE 1)

S/N 0101-807-6811

Security Classification

A-31408

14 KEY WORDS	LINK A		LINK B		LINK C	
	ROLE	WT	ROLE	WT	ROLE	WT
Squall line						
Mesoscale						
Rawinsonde mesonetwork						